Two-Loop Controller for Maximizing Performance of a Grid-Connected Photovoltaic-Fuel Cell Hybrid Power Plant

Kyoungsoo Ro

Dissertation submitted to the Faculty of the Virginia Polytechnic Institute and State University in partial fulfillment of the requirements for the degree of

Doctor of Philosophy
in
Electrical Engineering

Saifur Rahman, Chairperson
Hugh F. VanLandingham
Robert P. Broadwater
Yilu Liu
John W. Roach

April 14, 1997
Blacksburg, Virginia

Keywords: Photovoltaics, Fuel Cells, Batteries, Neural Networks, Maximum Power Point Tracking Controller, Real and Reactive Power Control, Environmental Evaluation.

Two-Loop Controller for Maximizing Performance of a Grid-Connected Photovoltaic-Fuel Cell Hybrid Power Plant

Kyoungsoo Ro

(ABSTRACT)

The study started with the requirement that a photovoltaic (PV) power source should be integrated with other supplementary power sources whether it operates in a stand-alone or grid-connected mode. First, fuel cells for a backup of varying PV power were compared in detail with batteries and were found to have more operational benefits. Next, maximizing performance of a grid-connected PV-fuel cell hybrid system by use of a two-loop controller was discussed. One loop is a neural network controller for maximum power point tracking, which extracts maximum available solar power from PV arrays under varying conditions of insolation, temperature, and system load. A real/reactive power controller (RRPC) is the other loop. The RRPC meets the system's requirement for real and reactive powers by controlling incoming fuel to fuel cell stacks as well as switching control signals to a power conditioning subsystem. The RRPC is able to achieve more versatile control of real/reactive powers than the conventional power sources since the hybrid power plant does not contain any rotating mass. Results of time-domain simulations prove not only effectiveness of the proposed computer models of the two-loop controller, but also their applicability for use in transient stability analysis of the hybrid power plant. Finally, environmental evaluation of the proposed hybrid plant was made in terms of plant's land requirement and lifetime CO_2 emissions, and then compared with that of the conventional fossil-fuel power generating forms.

ACKNOWLEDGEMENTS

First of all, I would like to express my sincere gratitude to my advisor, Dr. Saifur Rahman. His kind guidance, thorough comments and constant support have made it possible for me to make my dissertation complete. His teaching of the course "Alternate Energy Systems" had a great influence on my idea for this dissertation. I would also like to thank Dr. Hugh F. VanLandingham, Dr. Robert P. Broadwater, Dr. Yilu Liu and Dr. John W. Roach for their time and advice as my advisory committee.

During my Ph.D. program, I have been associated with my colleagues at the Center for Energy and the Global Environment. I would like to list here some of them to memorize and thank them: Yonael Teklu, Jiuping Pan, Majid Roghanizad, Concha Callwood, Irislav Drezga, Arnie de Castro, Joseph Wolete and Murat Dilek. I would like to specially thank Mr. Teklu for his support to capture solar data from the photovoltaic test facility located on the roof of Whittemore Hall in the Virginia Tech campus.

I would like to show my great appreciation to my wonderful parents, brothers and sister for their encouragement and support until I obtain a doctorate degree. I want to dedicate this dissertation to my wife, Jeannie, and my daughter, Erin. My daughter was born just early this year on February 5, 1997 and she is very special to me because I have waited for her for seven years. It is my mother-in-law that I must thank for her hard and lovely labor for feeding my daughter at night.

TABLE OF CONTENTS

page

LIST OF FIGURES ---------- **vii**

LIST OF TABLES ---------- **xi**

CHAPTER 1. INTRODUCTION ---------- **1**
1.1 Purpose ---------- 1
1.2 Problem Statement ---------- 3

CHAPTER 2. LITERATURE REVIEW ---------- **6**
2.1 Photovoltaic (PV) Systems ---------- 6
2.1.1 Background Information ---------- 6
2.1.2 State of The Art in PV Power Generation ---------- 9
2.2 Batteries ---------- 11
2.2.1 Introduction (Lead-Acid Battery) ---------- 11
2.2.2 Nickel-Cadmium Battery ---------- 12
2.2.3 Sodium-Sulfur Battery ---------- 14
2.2.4 Zinc-Bromine Battery ---------- 15
2.2.5 Battery Applications to Power Systems ---------- 15
2.3 Fuel Cells ---------- 17
2.3.1 Fuel Cell Background ---------- 17
2.3.2 Phosphoric Acid Fuel Cell (PAFC) ---------- 20
2.3.3 Molten Carbonate Fuel Cell (MCFC) ---------- 22
2.3.4 Solid Oxide Fuel Cell (SOFC) ---------- 23
2.3.5 Fuel Cell Power Systems ---------- 24
2.4 Neural Networks (NNs) ---------- 25
2.4.1 Neural Network Background ---------- 25
2.4.2 NN Applications to Power Systems ---------- 27
2.5 Power Conditioning Subsystems (PCUs) ---------- 29
2.5.1 Background Information ---------- 29
2.5.2 PCU Applications to Renewable Power Sources ---------- 32

CHAPTER 3. BATTERIES OR FUEL CELLS FOR PV POWER BACKUP ------- **34**
3.1 Common Attributes ---------- 34

3.2 Different Attributes ---------- 36
3.2.1 Efficiency ---------- 36
3.2.2 Capacity Variation ---------- 36
3.2.3 Flexibility in Operation ---------- 38
3.2.4 Cost ---------- 42
3.2.5 Environmental Externality ---------- 42
3.3 Summary ---------- 43

CHAPTER 4. DESCRIPTION OF PV-FUEL CELL HYBRID SYSTEM ---------- 45
4.1 Overall View of the PV-Fuel Cell Power Plant ---------- 45
4.2 Detailed Description of the Grid-Connected Hybrid System ---------- 46

CHAPTER 5. NEURAL NETWORK CONTROLLER FOR MPPT ---------- 50
5.1 Neural Network (NN) Controller of the PV Power Plant ---------- 50
5.2 Computer Model of the MPPT Control System ---------- 53

CHAPTER 6. REAL/REACTIVE POWER CONTROLLER (RRPC) ---------- 56
6.1 Real/Reactive Power Controller of the PV-Fuel Cell Hybrid System ---------- 56
6.2 Computer Model of the RRPC System ---------- 58

CHAPTER 7. CASE STUDIES ---------- 61
7.1 Sudden Decrease of Insolation with Constant Cell Temperature ---------- 62
7.2 Slow Decrease of Insolation with Constant Cell Temperature ---------- 68
7.3 Sudden Increase of Insolation with Constant Cell Temperature ---------- 74
7.4 Slow Increase of Insolation with Constant Cell Temperature ---------- 80
7.5 Variable Insolation and Cell Temperature ---------- 86
7.6 Change of Power Commands with Variable Insolation and Cell Temperature ---- 91

CHAPTER 8. ENVIRONMENTAL EVALUATION ---------- 97
8.1 Introduction ---------- 97
8.2 Land Requirement ---------- 97
8.3 CO_2 Emissions ---------- 99
8.4 Evaluation of the PV-Fuel Cell Hybrid Plant ---------- 100

CHAPTER 9. CONCLUSIONS AND RECOMMENDATIONS ---------- 102

NOMENCLATURE ---------- 105

REFERENCES ---------- 107

APPENDIX A. CO_2 EMISSIONS FROM CONVENTIONAL FOSSIL FUEL POWER PLANTS ---------- 116

APPENDIX B. CO_2 EMISSIONS FROM PV POWER PLANTS ---------- 119

APPENDIX C. CO_2 EMISSIONS FROM FUEL CELL POWER PLANTS --------- 121

VITA ---------- 122

LIST OF FIGURES

page
Figure 1.1 Samples of PV power output variations ---------- 2
Figure 2.1 I-V characteristics of solar cells. (a) Influence of solar insolation. (b) Influence of cell temperature ---------- 7
Figure 2.2 Equivalent circuit for a solar cell ---------- 8
Figure 2.3 Equivalent circuit for a battery ---------- 13
Figure 2.4 Typical plot of cell voltage vs. current density for a fuel cell ---------- 18
Figure 2.5 Equivalent circuit for a fuel cell ---------- 19
Figure 2.6 A typical neural network ---------- 25
Figure 2.7 (a) A variable-frequency full bridge inverter. (b) Waveforms of the ac voltage and current ---------- 31
Figure 3.1 Comparison of energy conversion processes ---------- 37
Figure 3.2 Voltage characteristics of a battery at various discharge rates ---------- 38
Figure 3.3 Equally high efficiency of fuel cells at partial and full loads ---------- 39
Figure 3.4 Energy densities for fuel cells and batteries ---------- 40
Figure 3.5 PV power variations requiring different battery capacities ---------- 41
Figure 4.1 Simplified overall diagram of the PV-fuel cell hybrid system ---------- 46
Figure 4.2 Diagram of the grid-connected PV system ---------- 47
Figure 4.3 Diagram of the grid-connected fuel cell system ---------- 48
Figure 5.1 Neural network controller for MPPT in the PV array ---------- 51
Figure 5.2 Computer model of the PV and MPPT control system ---------- 53
Figure 6.1 Voltage notations for the PV-fuel cell hybrid system ---------- 57
Figure 6.2 Real/reactive power control system of the fuel cell power plant ---------- 58
Figure 6.3 Computer model of the fuel cell plant and RRPC system ---------- 59
Figure 7.1 Sudden decrease of insolation from 100 mW/cm^2 to 30 mW/cm^2 ---------- 62
Figure 7.2 (a) Transient response of the PV array voltage (V_{pv}) for sudden insolation decrease from 100mW/cm^2 to 30mW/cm^2 ---------- 63
Figure 7.2 (b) Transient response of the PV array current (I_{pv}) for sudden insolation decrease from 100mW/cm^2 to 30mW/cm^2 ---------- 64
Figure 7.2 (c) Transient response of the PV array DC power (P_{pv}) for sudden insolation decrease from 100mW/cm^2 to 30mW/cm^2 ---------- 64
Figure 7.2 (d) Transient response of the PV array power (P_{ac1}, Q_{ac1}) supplied to the grid for sudden insolation decrease from 100mW/cm^2 to 30mW/cm^2 ---------- 65
Figure 7.2 (e) Transient response of the fuel cell voltage (V_{fc}) for sudden insolation

decrease from 100mW/cm^2 to 30mW/cm^2 ---------- 65
Figure 7.2 (f) Transient response of the fuel cell current (I_{fc}) for sudden insolation decrease from 100mW/cm^2 to 30mW/cm^2 ---------- 66
Figure 7.2 (g) Transient response of the fuel cell DC power (P_{fc}) for sudden insolation decrease from 100mW/cm^2 to 30mW/cm^2 ---------- 66
Figure 7.2 (h) Transient response of the fuel cell power (P_{ac2}, Q_{ac2}) supplied to the grid for sudden insolation decrease from 100mW/cm^2 to 30mW/cm^2 ---------- 67
Figure 7.2 (i) Transient response of the total power (P_{ac}, Q_{ac}) supplied to the grid for sudden insolation decrease from 100mW/cm^2 to 30mW/cm^2 ---------- 67
Figure 7.3 Slow decrease of insolation from 100 mW/cm^2 to 30 mW/cm^2 ---------- 68
Figure 7.4 (a) Transient response of the PV array voltage (V_{pv}) for slow insolation decrease from 100mW/cm^2 to 30mW/cm^2 ---------- 69
Figure 7.4 (b) Transient response of the PV array current (I_{pv}) for slow insolation decrease from 100mW/cm^2 to 30mW/cm^2 ---------- 70
Figure 7.4 (c) Transient response of the PV array DC power (P_{pv}) for slow insolation decrease from 100mW/cm^2 to 30mW/cm^2 ---------- 70
Figure 7.4 (d) Transient response of the PV array power (P_{ac1}, Q_{ac1}) supplied to the grid for slow insolation decrease from 100mW/cm^2 to 30mW/cm^2 ---------- 71
Figure 7.4 (e) Transient response of the fuel cell voltage (V_{fc}) for slow insolation decrease from 100mW/cm^2 to 30mW/cm^2 ---------- 71
Figure 7.4 (f) Transient response of the fuel cell current (I_{fc}) for slow insolation decrease from 100mW/cm^2 to 30mW/cm^2 ---------- 72
Figure 7.4 (g) Transient response of the fuel cell DC power (P_{fc}) for slow insolation decrease from 100mW/cm^2 to 30mW/cm^2 ---------- 72
Figure 7.4 (h) Transient response of the fuel cell power (P_{ac2}, Q_{ac2}) supplied to the grid for slow insolation decrease from 100mW/cm^2 to 30mW/cm^2 ---------- 73
Figure 7.4 (i) Transient response of the total power (P_{ac}, Q_{ac}) supplied to the grid for slow insolation decrease from 100mW/cm^2 to 30mW/cm^2 ---------- 73
Figure 7.5 Sudden increase of insolation from 30 mW/cm^2 to 100 mW/cm^2 ---------- 74
Figure 7.6 (a) Transient response of the PV array voltage (V_{pv}) for sudden insolation increase from 30mW/cm^2 to 100mW/cm^2 ---------- 75
Figure 7.6 (b) Transient response of the PV array current (I_{pv}) for sudden insolation increase from 30mW/cm^2 to 100mW/cm^2 ---------- 76
Figure 7.6 (c) Transient response of the PV array DC power (P_{pv}) for sudden insolation increase from 30mW/cm^2 to 100mW/cm^2 ---------- 76
Figure 7.6 (d) Transient response of the PV array power (P_{ac1}, Q_{ac1}) supplied to the grid for sudden insolation increase from 30mW/cm^2 to 100mW/cm^2 ---------- 77
Figure 7.6 (e) Transient response of the fuel cell voltage (V_{fc}) for sudden insolation increase from 30mW/cm^2 to 100mW/cm^2 ---------- 77
Figure 7.6 (f) Transient response of the fuel cell current (I_{fc}) for sudden insolation increase from 30mW/cm^2 to 100mW/cm^2 ---------- 78
Figure 7.6 (g) Transient response of the fuel cell DC power (P_{fc}) for sudden insolation increase from 30mW/cm^2 to 100mW/cm^2 ---------- 78

Figure 7.6 (h) Transient response of the fuel cell power (P_{ac2}, Q_{ac2}) supplied to the grid for sudden insolation increase from 30mW/cm^2 to 100mW/cm^2 ---------- 79
Figure 7.6 (i) Transient response of the total power (P_{ac}, Q_{ac}) supplied to the grid for sudden insolation increase from 30mW/cm^2 to 100mW/cm^2 ---------- 79
Figure 7.7 Slow increase of insolation from 30 mW/cm^2 to 100 mW/cm^2 ---------- 80
Figure 7.8 (a) Transient response of the PV array voltage (V_{pv}) for slow insolation increase from 30mW/cm^2 to 100mW/cm^2 ---------- 81
Figure 7.8 (b) Transient response of the PV array current (I_{pv}) for slow insolation increase from 30mW/cm^2 to 100mW/cm^2 ---------- 82
Figure 7.8 (c) Transient response of the PV array DC power (P_{pv}) for slow insolation increase from 30mW/cm^2 to 100mW/cm^2 ---------- 82
Figure 7.8 (d) Transient response of the PV array power (P_{ac1}, Q_{ac1}) supplied to the grid for slow insolation increase from 30mW/cm^2 to 100mW/cm^2 ---------- 83
Figure 7.8 (e) Transient response of the fuel cell voltage (V_{fc}) for slow insolation increase from 30mW/cm^2 to 100mW/cm^2 ---------- 83
Figure 7.8 (f) Transient response of the fuel cell current (I_{fc}) for slow insolation increase from 30mW/cm^2 to 100mW/cm^2 ---------- 84
Figure 7.8 (g) Transient response of the fuel cell DC power (P_{fc}) for slow insolation increase from 30mW/cm^2 to 100mW/cm^2 ---------- 84
Figure 7.8 (h) Transient response of the fuel cell power (P_{ac2}, Q_{ac2}) supplied to the grid for slow insolation increase from 30mW/cm^2 to 100mW/cm^2 ---------- 85
Figure 7.8 (i) Transient response of the total power (P_{ac}, Q_{ac}) supplied to the grid for slow insolation increase from 30mW/cm^2 to 100mW/cm^2 ---------- 85
Figure 7.9 Variations of insolation and cell temperature ---------- 86
Figure 7.10 (a) Transient response of the PV array voltage (V_{pv}) for real-time variations of insolation and cell temperature ---------- 87
Figure 7.10 (b) Transient response of the PV array current (I_{pv}) for real-time variations of insolation and cell temperature ---------- 87
Figure 7.10 (c) Transient response of the PV array DC power (P_{pv}) for real-time variations of insolation and cell temperature ---------- 88
Figure 7.10 (d) Transient response of the PV array power (P_{ac1},Q_{ac1}) supplied to the grid for real-time variations of insolation and cell temperature ---------- 88
Figure 7.10 (e) Transient response of the fuel cell voltage (V_{fc}) for real-time variations of insolation and cell temperature ---------- 89
Figure 7.10 (f) Transient response of the fuel cell current (I_{fc}) for real-time variations of insolation and cell temperature ---------- 89
Figure 7.10 (g) Transient response of the fuel cell DC power (P_{fc}) for real-time variations of insolation and cell temperature ---------- 90
Figure 7.10 (h) Transient response of the fuel cell power (P_{ac2}, Q_{ac2}) supplied to the grid for real-time variations of insolation and cell temperature ---------- 90
Figure 7.10 (i) Transient response of the total power (P_{ac}, Q_{ac}) supplied to the grid for real-time variations of insolation and cell temperature ---------- 91
Figure 7.11 (a) Transient response of the PV array voltage (V_{pv}) for change of power

commands with variable insolation and cell temperature ---------- 92
Figure 7.11 (b) Transient response of the PV array current (I_{pv}) for change of power commands with variable insolation and cell temperature ---------- 92
Figure 7.11 (c) Transient response of the PV array power (P_{pv}) for change of power commands with variable insolation and cell temperature ---------- 93
Figure 7.11 (d) Transient response of the PV array power (P_{ac1}, Q_{ac1}) supplied to the grid for change of power commands with variable insolation and cell temperature --- 93
Figure 7.11 (e) Transient response of the fuel cell voltage (V_{fc}) for change of power commands with variable insolation and cell temperature ---------- 94
Figure 7.11 (f) Transient response of the fuel cell current (I_{fc}) for change of power commands with variable insolation and cell temperature ---------- 94
Figure 7.11 (g) Transient response of the fuel cell DC power (P_{fc}) for change of power commands with variable insolation and cell temperature ---------- 95
Figure 7.11 (h) Transient response of the fuel cell power (P_{ac2}, Q_{ac2}) supplied to the grid for change of power commands with variable insolation and cell temperature --- 95
Figure 7.11 (i) Transient response of the total power (P_{ac}, Q_{ac}) supplied to the grid for change of power commands with variable insolation and cell temperature ------- 96
Figure 8.1 Land requirement and lifetime CO_2 emissions for electric power plants ------- 101

LIST OF TABLES

page
Table 2.1 Comparison of three types of fuel cells ---------- 21
Table 2.2 Key attributes of the principal learning procedures ---------- 27
Table 3.1 Capacity variations of a battery at various discharge rates ---------- 39
Table 4.1 Power specifications of the single M55 PV module ---------- 48
Table 4.2 Specifications of the single 260-kW PAFC stack ---------- 49
Table 8.1 Land requirement for electric power plants ---------- 98
Table 8.2 CO_2 emissions for electric power plants with a 30-year lifetime ---------- 99
Table A.1 CO_2 productions from fossil fuel power plants with fuel treatment ---------- 118
Table B.1 Accumulated energy requirements for PV power plants ---------- 119
Table B.2 CO_2 emissions of PV power plants ---------- 120

CHAPTER 1

INTRODUCTION

1.1 Purpose

As conventional fossil-fuel energy sources diminish and the world's environmental concern about acid deposition and global warming increases, renewable energy sources (solar, wind, tidal, and geothermal, etc.) are attracting more attention as alternative energy sources. Among the renewable energy sources solar photovoltaic (PV) energy has been widely utilized in small-size applications. It is also the most promising candidate for research and development for large-scale uses as the fabrication of less-costly photovoltaic devices becomes a reality.

PV power generation, which directly converts solar radiation into electricity, contains a lot of significant advantages such as inexhaustible and pollution-free, silent and with no rotating parts, and size-independent electricity conversion efficiency. Positive environmental effect of photovoltaics is replacing electricity generated in more polluting way or providing electricity where none was available before. With increasing penetration of solar photovoltaic devices, various anti-pollution apparatuses can be operated by solar PV power; for example, water purification by electrochemical processing or stopping desert expansion by photovoltaic water pumping with tree implantation [17].

From an operational point of view, a photovoltaic array experiences large variations of its output power under intermittent weather conditions. Those phenomena may cause operational problems at a central control center in a power utility, such as excessive frequency deviations, spinning reserve increase, etc. Figure 1.1 illustrates two samples of PV power variations for one day. The data was measured at a time interval of 10 minutes from the PV test facility in the Virginia Tech campus on July 10 and July 18, 1993. When photovoltaic power penetration approaches about 10% of the system load, it is difficult for the conventional power generation system to keep track of the rapid PV power output changes [10].

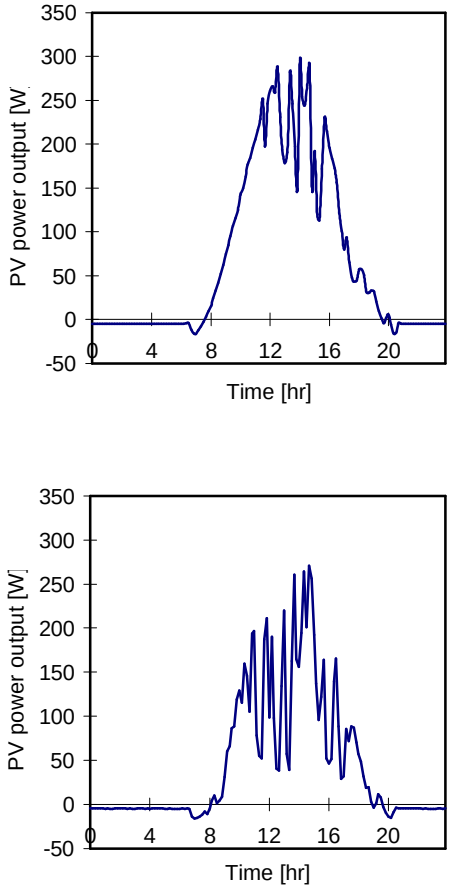

Figure 1.1 Samples of PV power output variations.

One method to overcome the above problem is to integrate the PV power plant with other power sources such as diesel backup [20], fuel cell backup [1,2], battery backup [7,13,18], and superconductive magnetic energy storage (SMES) backup [15]. The diesel backup for PV power is able to make a continuous 24-hour power supply be possible. However, it has a couple of severe drawbacks. Its electricity efficiency decreases significantly at a low level of power output, and the diesel power generation is environmentally detrimental as well. The SMES technology is many years from commercialization, and there is a significant potential health risk associated with the technology because of its strong magnetic field generation. Both the battery backup and the fuel cell backup are the most likely technologies to provide backup power for the PV power system in the near future. Thus, a detailed comparison between those two backup powers will be made later in Chapter 3.

A fuel cell power is a very attractive option being used with an intermittent power generation source like the PV power because the fuel cell power system contains lots of great features such as high efficiency, fast load-response, modular production and fuel flexibility. Its feasibility in coordination with a photovoltaic power system has been successfully demonstrated for both grid-connected and stand-alone applications [1]. Due to the fast ramping capability of the fuel cell power system, a PV-fuel cell hybrid system may be able to solve the PV's inherent problem of intermittent power generation. Unlike a storage battery, which also contains attractive attributes such as fast response rate, modular construction and flexibility for site selection, the fuel cell power can produce electricity continuously to support the PV power. Therefore, the quality of overall power generated from the PV-fuel cell hybrid power plant may be improved. The combination of the photovoltaic and fuel cell power plants is now a viable technology to commercial applications.

Environmental impacts of the fuel cell power generation are relatively small in contrast to other fossil-fuel power sources. Since chemical reactions inside the fuel cell stack are accomplished by catalysts, it must require a low sulfur-content fuel. Since the fuel cell stack operates electrochemically at lower temperature than other thermomechanical power plants, it generates very little amount of NO_x. NO_x forms mainly from nitrogen contained in the combustion air if fuels used have low nitrogen content. Low-emission characteristics of the fuel cell power plant may allow some utilities to offset the costs of installing additional emission control equipment. Moreover, their high efficiency is able to result in lower fossil-fuel CO_2 emissions, which will help reduce the rate of global warming. Therefore, the fuel cell power system has a great potential for being coordinated with the PV array to smooth out the PV power's fluctuations.

One purpose of this study is to prove that the fuel cell power has the best potential for the PV power backup. Designing an efficient controller for a PV-fuel cell hybrid power plant is another purpose. The controller consists of two loops; one loop is a neural network controller for MPPT (Maximum Power Point Tracking) and the other is a real/reactive power controller. The two-loop controller is able not only to achieve maximum utilization of the available solar power but also to satisfy the hybrid power plant's operational requirement for real and reactive power control. Thus, such a hybrid power plant can be used as a reliable power generation source either on a stand-alone or a grid-interactive mode. The other purpose is to establish simplified computer models of the two-loop controller. Those computer models might be useful for use in transient stability analysis of a power system that includes the PV-fuel cell hybrid system.

1.2 Problem Statement

It has been well-proven that a photovoltaic power source should be integrated with other power sources, whether used in either a stand-alone or grid-connected mode. This study starts with a comparison between batteries and fuel cells for PV power backup since these two power sources are the most likely technologies for PV power supplement. Then it will be proven that fuel cells have more benefits when they are applied to support a PV power varying severely on inclement weather days.

A technique for maximizing performance of a grid-connected PV-fuel cell hybrid power plant by using a two-loop controller is discussed. One loop is the neural network controller for maximum power point tracking (MPPT) in the PV array, which extracts maximum available solar power at varying weather conditions. A centralized PV power plant requires much larger initial capital investment compared to other power generation sources. Thus, it is imperative to extract as much available solar energy as possible from the PV array; if not, the photovoltaic power system might lose some of the valuable solar energy. Nonlinear current-voltage (I-V) characteristics of a PV module match well to a neural network application. In order that the PV array keep track of its maximum power points, the outputs of the neural network controller should generate optimal switching signals to the power conditioning subsystem (PCS) of the PV array. The PCS usually consists of a full-bridge dc to ac inverter.

A real/reactive power controller (RRPC) installed at the fuel cell power plant is the other loop. The RRPC is going to achieve the utility grid's requirement for real and reactive powers by controlling the fuel cell stacks and the PCS. Real power control is made by regulating both the incoming fuel (mostly natural gas) to the fuel cell stacks and the switching control signals to the PCS of the fuel cell power plant. Reactive power is controlled only by generating appropriate switching scheme to the PCS. Simplified computer models of the two-loop controller are developed. Time-domain simulations prove an applicability of the two-loop controller for use in a transient stability analysis of the hybrid power plant.

I continue to discuss an environmental evaluation of the proposed PV-fuel cell hybrid power plant compared with the conventional power generation forms. Two categories through which the evaluation is accomplished are land area requirement for the hybrid power plant construction and its lifetime CO_2 emissions. The CO_2 emissions of the hybrid power plant are caused by fuel consumption during its life-long period, and construction, operation and maintenance (O&M) of the hybrid power plant.

The major contributions that are made in this dissertation are summarized below:

(i) Compare batteries with fuel cells for a backup of a PV power that fluctuates on inclement weather days, and verify that the fuel cells have more benefits for that purpose. It will be discussed in Chapter 3.

(ii) Apply a neural network controller to always extract maximum available solar power from the PV array under changing conditions of solar insolation, cell

temperature and utility system load. Chapter 5 will describe the neural network controller for the PV array.

(iii) Design a real/reactive power controller for the fuel cell power plant so that the PV-fuel cell hybrid system satisfies the utility system's requirement for real and reactive powers. Real power control is achieved by effectively controlling both the fuel injected to the fuel cell stacks and the switching scheme of the full-bridge dc-ac inverter. Reactive power is controlled by generating appropriate switching signals to the inverter. Chapter 6 will give the method to design the RRPC.

(iv) Present simplified computer models of the neural network controller for MPPT and the RRPC system in the grid-connected PV-fuel cell hybrid power plant. Chapter 5 and 6 explain these computer models. Then Chapter 7 verifies the performance of the computer models by time-domain computer simulations.

(v) Evaluate environmental impacts of the proposed PV-fuel cell hybrid system in terms of land requirement for the plant construction and its lifetime CO_2 emissions. They will be discussed in Chapter 8.

The other chapters will support to better-understand this dissertation. Chapter 2 covers a broad range of background information on photovoltaics, batteries, fuel cells, neural networks and power conditioning subsystems. Chapter 4 describes the PV-fuel cell hybrid power plant in the overall view and detailed view. Conclusions and Recommendations will be given in Chapter 9, which is followed by Nomenclature and References. Appendix A gives calculations of CO_2 emissions from conventional fossil fuel power plants. CO_2 emissions from PV power plants and fuel cell power plants are computed in Appendix B and Appendix C, respectively.

CHAPTER 2

LITERATURE REVIEW

A comprehensive literature search has been made in the areas that would get together to constitute the proposed PV-fuel cell hybrid power plant and control systems. This chapter consists of five sections and discusses photovoltaic systems, batteries, fuel cells, neural networks and power conditioning subsystems in that order. The objective of this discussion is to make it easy to understand this dissertation.

2.1 Photovoltaic (PV) Systems

2.1.1 Background Information

Figure 2.1 illustrates typical current-voltage (I-V) curves of an ARCO M55 solar cell module according to the variations of insolation level and cell temperature. The figure also includes the loci of maximum power points and equivalent resistive load lines. Open-circuit voltage of the solar cell module, a crosspoint of the curve to the vertical axis, varies little with insolation changes. It is inversely proportional to temperature, or a rise in temperature produces a decrease in voltage. Short-circuit current, a crosspoint of the curve to the horizontal axis, is directly proportional to insolation and is relatively steady in changing temperature.

The solar cell module acts like a constant current source for most part of its I-V curve. It can provide a constant current from zero to around 15V despite a changing resistive load. As the resistance continues to increase, the curve reaches a breakdown point and starts to drop to zero.

As demonstrated in Figure 2.1, an increase in solar insolation causes the output current to increase and the vertical part of the curve to move rightward. An increase in cell temperature

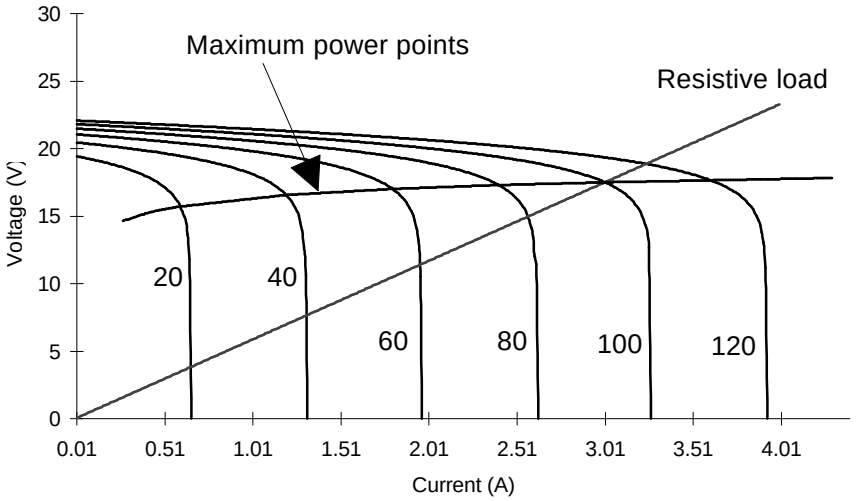

(a) Influence of solar insolation [mW/cm^2] (Temperature = 25^{o}C).

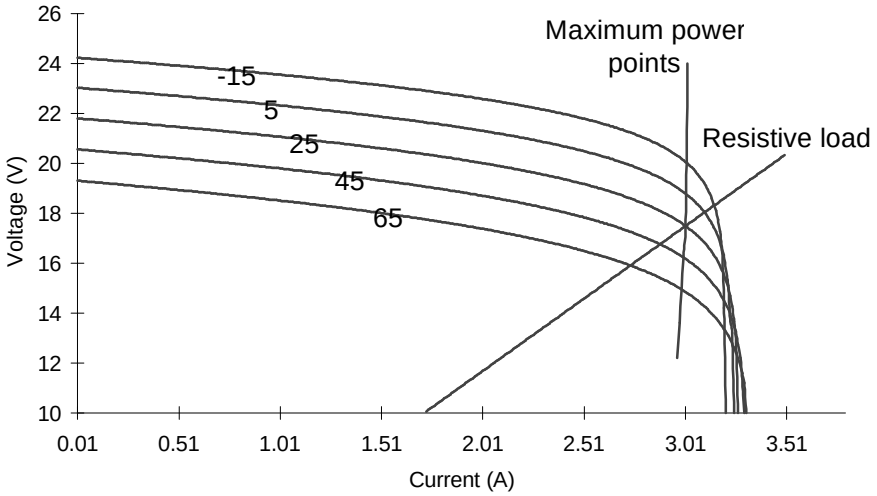

(b) Influence of cell temperature [^{o}C] (Insolation = 100 mW/cm^2).

Figure 2.1 I-V characteristics of solar cells.

causes the voltage to drop, while decreasing temperature produces the opposite effect. Thus the I-V curves display how a solar cell responds to all possible loads under a certain set of insolation and cell temperature conditions.

An operating point of a solar cell will move by varying insolation, cell temperature, and load values. For a given insolation and operating temperature, the output power depends on the value of a load resistance. As the load increases (or the resistance decreases), the operating point moves along the curve forward the right. So only one load value makes the PV generator produce maximum power. A maximum power point trajectory, which is positioned at the knee of the I-V curve, represents the nearly constant output voltage of the PV generator at varying solar insolation condition. When the temperature varies, the maximum power points are generated in such a manner that the output current stays approximately constant.

A solar cell usually uses a p-n junction diode in a physical configuration to produce photovoltaic electricity. As the I-V curve demonstrates, a solar cell acts like a constant current source under low load conditions and the current drops to zero at high loads. Thus it can be represented as an ideal current source. Its equivalent circuit shown in Figure 2.2 precisely explains what occurs in a solar cell [11]. The circuit consists of a light-dependent current source and a group of resistances, including internal shunt resistance, R_{sh}, and series resistance, R_s. The series resistance should be as low as possible and its shunt resistance should be very high, so that most of the available current can be delivered to the load. Considering this assumption, the characteristics of a solar cell can be expressed by the following equations [3].

$$V = \frac{AKT}{q} ln(\frac{I_{ph} - I + I_o}{I_o}) - IR_s \qquad (2.1)$$

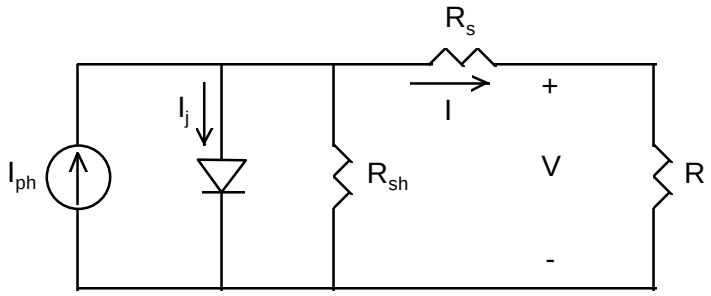

Figure 2.2 Equivalent circuit for a solar cell [11].

or

$$I = I_{ph} - I_o [exp\{\frac{q(V + IR_s)}{AKT}\} - 1] \quad (2.2)$$

where

$$I_{ph} = [I_{scr} + K_i(T - 298)]\lambda/100 \quad (2.3)$$

$$I_o = I_{or}(\frac{T}{T_r})^3 exp[\frac{qE_{G0}}{BK}(\frac{1}{T_r} - \frac{1}{T})] \quad (2.4)$$

From the above equations, we can conclude that the output current and voltage of a PV module are affected by solar insolation and operating cell temperature.

The *fill factor* of a silicon solar cell is defined as the ratio of peak power to the power computed by multiplying the open-circuit voltage by the short-circuit current. That reflects how much series resistance and how little shunt resistance there is in the solar cell. A good fill factor ranges from 0.6 to 0.8. As the solar cell degrades with age, its series resistance tends to increase resulting in a lower fill factor.

2.1.2 State of The Art in PV Power Generation

As solar cell manufacturing technologies improve steadily, commercial applications of PV power generation have increased from stand-alone to utility-connected generating systems. Interconnection and operation of a PV power unit are not same as electric utilities have been doing for the conventional power plants. It requires specific PV interface, protection schemes, storage devices, and control mechanisms. Especially because the PV power output is directly affected by the changes of weather (solar intensity, temperature, etc.), it becomes considerably complicated to efficiently control the PV power plant.

Kalaitzakis and Vachtsevanos [7] proposed a methodology for the effective integration of photovoltaic devices into the electric utility distribution network operations. They focused on the storage requirements for control and stability purposes, power flow control, and power modulating device contributing to the improvement of system stability. System stability can be improved by monitoring the variations in system frequency, utility grid bus voltage, and the real power at the inverter output bus. Finally, their simulation studies indicate that an application of the proposed control approach may result in reduced load following requirements for conventional power generating units, and better power quality and stability of the interconnected system.

Khallat and Rahman [49] presented the concept of adding fuel cells to provide operational support to a PV system. They determined the capacity credit of the PV system when these are included in the utility generation mix. The study indicated that the capacity credit of the PV system continues to rise with increasing penetration up to 16.8% and then it decreases. By the comparison of the capacity credit available and the fuel cell requirements, their net difference increases from 4.2% to 16.8% penetration. It was concluded that there is an upper limit for PV penetration with fuel cell support for a power system.

Rahman and Kroposki [52] discussed a performance evaluation of crystalline and amorphous silicon PV modules in the light of their capability to operate as a demand side management (DSM) tool. The analysis of collected data showed a significant difference in the cell efficiency, which is 10% for the single crystalline cells and around 3% for the amorphous cells. The authors compared the plane-of-array insolations under different tilt conditions; the largest gain in insolation due to 2-axis tracking over a semi-annual tilt change is 12.2% while the smallest gain is 4.9%.

Hiyama et al. [21, 22] presented a neural network application to the identification of the optimal operating point of PV modules and designed a PI-type controller for real-time maximum power tracking. Optimal operating voltages are identified through the proposed neural network by using the open-circuit voltages measured from monitoring cells and optimal operating currents are calculated from the measured short-circuit currents. The output of the neural network goes through the PI controller to the voltage control loop of the inverter to change the terminal voltage of the PV system to the identified optimal one.

Ohnishi et al. [17] described applications of solar cells especially to residential areas such as solar-powered air conditioners and grid-connected PV power generating systems. Concerned about the disadvantages of solar cells, namely that they cannot generate power at night and their output fluctuates dramatically depending on solar intensities, they proposed a Global Energy Network Equipped with Solar cells and International Superconductor grids (GENESIS) for resolving these problems. They forecasted that in the year 2000 the world energy demand will be the equivalent of 14 billion kilo-liter of crude oil per year. To meet that requirements, $800 km^2$ of solar cells would be needed, assuming a conversion efficiency of 10%. The study concluded that that plan is quite feasible because about 4% of the world's desert area would suffice for that purpose.

Schaefer and Hagedorn [16] compared PV power generation with the conventional power generation forms in terms of some environmental characteristics. Solar power is the most surface intensive power generation form due to its low efficiency and low energy density of solar radiation. They calculated the accumulated energy consumption in the fabrication of solar cells and the construction of PV power plants, and, for single-crystalline solar cells, those values are 11,000kWh/kWp and 12,200kWh/kWp, respectively. The accumulated energy consumption in the solar cell fabrication and PV power plant construction involves CO_2 emissions, which can

be estimated using emission factors within a given energy supply structure. In the case of Germany, equivalent CO_2 emissions of PV power plants for a lifetime of 20 years are 70 gCO_2/kWh for single-crystalline solar cells.

2.2 Batteries

2.2.1 Introduction (Lead-Acid Battery)

A storage battery is a chemical device reversible in its action, which stores chemical energy for use later as electrical energy. The chemical energy stored in electrodes of a battery cell is converted to electrical energy when the cell is discharging. Electrical energy is applied to the battery during the operation of charging, so the electric current produces chemical changes in the battery.

The most commonly used storage battery for utility applications is the lead-acid type. The fundamental parts of a lead-acid battery cell are two dissimilar electrodes immersed in an electrolyte, namely

Anode(-) : Spongy lead (Pb)
Cathode(+) : Lead dioxide (PbO_2)
Electrolyte : Dilute solution of sulfuric acid (H_2SO_4)

When a battery cell is connected to a circuit, it allows charge to flow around the circuit. In its external part, the charge flow is electrons resulting in electrical current. Within the cell, the charge flows in the form of ions that are transported from one electrode to the other. The cathode, highly oxidized lead dioxide, receives electrons from the external circuit on discharge. These electrons react with the cathode material, which leaves some lead free to combine with sulphate ions to form lead sulphate. Hydrogen ions move in to the cathode and combine with oxygen to form water. At the anode, reactions between the anode material and the sulphate ions result in excessive electrons that can be donated to the external circuit. In this way the chemical energy stored in the battery is converted to electrical energy.

The chemical reaction occurred at the anode is

$$Pb + SO_4^{2-} \underset{\text{Charge}}{\overset{\text{Discharge}}{\rightleftharpoons}} PbSO_4 + 2e^- \qquad (2.5)$$

and that at the cathode is

$$PbO_2 + SO_4^{2-} + 4H^+ + 2e^- \underset{\text{Charge}}{\overset{\text{Discharge}}{\rightleftharpoons}} PbSO_4 + 2H_2O \quad (2.6)$$

Therefore, the net reaction can be expressed as follows

$$PbO_2 + Pb + 2H_2SO_4 \underset{\text{Charge}}{\overset{\text{Discharge}}{\rightleftharpoons}} 2PbSO_4 + 2H_2O \quad (2.7)$$

A battery system is a group of battery cells that supply dc power at a nominal voltage to an electrical load. The number of cells connected in series determines the nominal voltage of the battery system, and the capacity of the battery system is the basic factor in determining the discharge rate. The voltage is the force enforcing each of the electrons coming out of the battery and the capacity is the number of electrons that can be obtained from the battery. While the voltage is fixed by cell chemistry, the capacity is variable depending on the quantity of active materials. The discharge rate of a battery is given in terms of ampere-hours (Ah) to a particular discharge voltage level. For the lead-acid battery, its nominal cell voltage is 2V and the nominal discharge voltage level is 1.75V/cell, or approximately 87.5% of the nominal cell voltage rating.

The equivalent circuit for a battery is shown in Figure 2.3. The internal resistance is due to the resistance of electrolyte and electrode. Self-discharge resistance is a result of electrolysis of water at high voltages and slow leakage across the battery terminals at low voltages. The overvoltage is modeled as an RC circuit with a time constant in the order of minutes [36, 37].

Lead-acid battery systems are a near-term solution to power regulation needs for electric utilities. However, the technology has suffered from a slow acceptance into power markets due to such factors as uncertain return on investment and difficulty in quantifying benefits. Recently, there is worldwide interest to develop alternatives to lead-acid batteries that are able to produce high performance at low cost. Advanced batteries such as nickel-cadmium, sodium-sulfur and zinc-bromine are likely to emerge in the next decade.

2.2.2 Nickel-Cadmium Battery

As the nickel-cadmium battery promoters claim its superiority over the lead-acid batteries in spite of the high capital cost, there are several tries to adopt the nickel-cadmium batteries for use in PV applications. One major reason for that is its longer life and operational reliability. It is undamaged by complete discharge and overcharge.

The active material of the cathode is nickel hydrate with graphite and that of the anode is cadmium sponge, with additives to aid conductivity. The electrolyte is a solution of potassium

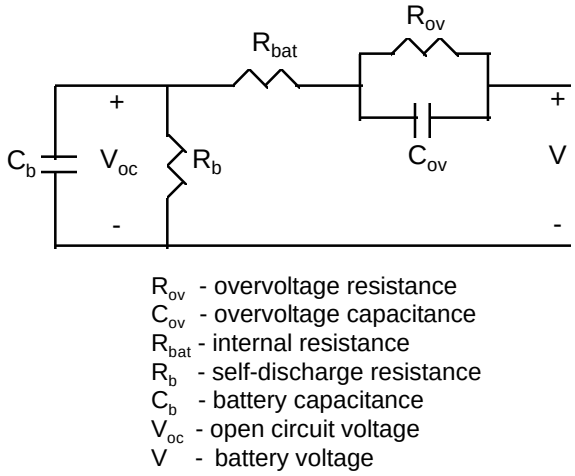

Figure 2.3 Equivalent circuit for a battery [36].

hydroxide (KOH), including a small amount of lithium hydroxide (LiOH) to improve capacity. The charge-discharge reaction may be written as

$$2Ni(OH)_3 + Cd \underset{\text{Charge}}{\overset{\text{Discharge}}{\rightleftharpoons}} 2Ni(OH)_2 + Cd(OH)_2 \qquad (2.8)$$

The nominal voltage of a nickel-cadmium battery on discharge is 1.2V. When the battery is connected to an external load, its voltage falls to a value depending on discharge rate and state of charge. The normal final discharge voltage is 1.05V/cell. The battery is characterized by a low self-discharge rate; its capacity drops to about 80% in a year under open circuit conditions. Its operating temperature range is between -50 to 60^{o}C and the battery capacity drops to half of the nominal capacity at -50^{o}C.

Nickel-cadmium battery system contains its significant features for PV applications. With respect to charging conditions, the nickel-cadmium battery offers more than 80% charging efficiency, as high as a lead-acid battery does. It does not suffer from complete discharge or overcharge in contrast to the lead-acid battery and its annual maintenance is less costly that that of the lead-acid battery. At low temperatures there is a need for the lead-acid battery to be kept in a high state of charge to avoid freezing, which would make it less cost effective over the nickel-cadmium battery.

A disadvantage associated with the nickel-cadmium battery is its memory effect and high capital cost. Repeated use in the same way causes the battery to adjust itself to a certain capacity in relation to its load. Its cost per ampere-hour of capacity is considered as another disadvantage for wide use although the battery is promoted as an alternative to the lead-acid battery in PV applications.

2.2.3 Sodium-Sulfur Battery

The sodium-sulfur battery operates at relatively high temperature ranging from $300^{o}C$ to $380^{o}C$ in order to maintain the sodium, sulfur and reaction products in liquid forms and to obtain adequate electrolyte conductivity. Unlike conventional battery systems that consist of solid electrodes and liquid electrolytes for the reaction medium, the sodium-sulfur battery is based on liquid electrodes and a β-alumina (Al_2O_3) solid electrolyte. The battery uses molten sodium and molten sulfur as active materials for the anode and the cathode, respectively. Its operation relies on the property of β-alumina, which combines very low electronic conductivity with an unusually high ionic conductivity, specially to sodium ions. The overall chemical reaction can be written as

$$2Na + 3S \underset{\text{Charge}}{\overset{\text{Discharge}}{\rightleftharpoons}} Na_2S_3 \qquad (2.9)$$

The operating discharge voltage characteristics are somewhat lower than those of lead-acid batteries. The sodium-sulfur battery would start at around 1.9V and finish at about 1.4V.

The sodium-sulfur battery possesses several potential advantages for energy storage applications. It is capable of quick responses to sudden changes from charge to discharge conditions and vice versa, as well as sudden changes in load demand. Its capital cost is projected to be low compared to other advanced battery systems because the battery component materials are relatively abundant and inexpensive. A projected installation cost of $100/kWh is believed achievable [34]. Energy efficiency of the sodium-sulfur battery is high at approximately 80% and it does not self-discharge. It possesses high volumetric energy density. The projected energy density of the battery is about 200Wh/kg compared to 35Wh/kg for lead-acid batteries.

There are a number of technical issues including cell reliability that must be addressed before the technology is ready for commercial introduction. Because sodium and sulfur are hazardous materials, safety and environmental concerns must be considered in its fabrication, operation and disposal.

2.2.4 Zinc-Bromine Battery

The zinc-bromine battery is another promising system for PV power applications due to inherent chemical simplicity, good electrochemical reversibility of the electrodes and low-cost material. It is a near-ambient temperature, flowing electrolyte system. Its active materials are stored externally in anolyte and catholyte reservoirs. Upon charging the battery, an electrolyte solution of zinc bromine ($ZnBr_2$) is passed through the battery with the aid of a circulator. As dc electricity is passed through the battery, zinc metal is deposited on the anode, and bromine gas is generated at the cathode and then is carried away with the circulating electrolyte stream. Upon discharge, circulation of the aqueous zinc bromine electrolyte carries bromine to the cathode of the stack and current may be withdrawn from the battery. Microporous polyethylene separators are used to slow the direct reaction of the bromine-rich stream with zinc. The overall cell reaction is written as

$$Zn\ (s) + Br_2\ (g) \underset{\text{Charge}}{\overset{\text{Discharge}}{\rightleftharpoons}} ZnBr_2\ (aq) \qquad (2.10)$$

where s, g, and aq denote solid-, gas-, and aqueous-states, respectively.

There are several attributes of the zinc-bromine battery for applications of future energy storage. The majority of the battery's components are made of low-cost, plastic materials. Inexpensive construction materials coupled with low fabrication expenses result in favorable capital cost projections. It can be assembled in modular fashion using standard cell stacks, allowing the user to increase capacity to meet future requirements. The near-ambient temperature operation does not require the complex thermal management necessary in some high-temperature systems. It can be repeatedly deep discharged without performance deterioration. Its energy efficiency is not as high as that of the competitors, roughly 60-70%.

However, there are a number of key technical issues related to the reliability and performance of the battery. The efficiency of the battery system is somewhat lower than other systems, due to resistive losses in the separators, electrolyte, and electrodes. The system's mechanical complexity creates a good deal of maintenance requirements including pump repair and stack replacement. Additionally, the safe handling, storage and disposal of zinc-bromine batteries must be considered because bromine is a toxic material.

2.2.5 Battery Applications to Power Systems

The future electric power system is estimated to be uncertain and potential capacity shortages, competitive power markets and increasing environmental regulations will create further stresses on the interconnected power network. The roles of storage facilities, especially a

battery energy storage (BES) system as power regulation and energy management are being recognized as a practical solution to future operating uncertainty.

BES systems have been interesting power utilities as an option to supply power at peak-time to achieve load leveling. For example, Southern California Edison's Chino battery plant has demonstrated the capability of lead-acid batteries to satisfy the utility's operational and performance requirements for load leveling. Recently, other dynamic benefits of BES have been identified, such as load following, spinning reserve, power factor correction, long line stabilization, and voltage and frequency regulation, etc. [34, 38]. The BES system is predicted to become an economically attractive option for utilities in the future due to those benefits coupled with the ability to provide peak power.

Abraham et al. [32] presented the major types of batteries being developed for load leveling and a generic description of the balance of plant (BOP). It is used to define the components needed to integrate the battery facility with an electric system. Four different battery types considered are lead-acid, zinc-bromine, zinc-chloride and sodium-sulfur. The major BOP subsystems for load-leveling batteries include dc-ac interface equipment, converter, battery enclosures, control and safety systems. The technical considerations are protection against faults on the ac and dc side of converter, selection of the proper size and type of converter, and master site controller to safely monitor and control the battery facility, etc.

Ball et al. [39] developed and tested a prototype 250kVA modular BES system for utility peak shaving applications. The modules contain forty-eight 12V Delco-Remy 2000 batteries, which are lead-calcium batteries constructed for deep cycling. The battery system was demonstrated for four quadrant, full real and reactive power control in either charge or discharge mode, and energy capacity grew when discharging at lower power levels. Batteries and electronic power converters inherently respond quickly to changes in power command, so full power is reached from standby power within four 60Hz cycles. Thus the transition time lag (from pressing a key on the PC keyboard to the transition ended) was typically about 2 seconds.

Jung et al. [86] proposed a method of determining the installation site and optimal capacity of the BES system for load leveling by comparing the load pattern of the main transformer in a distribution subsystem with the load pattern of the power system. If the load factor improves, the location is considered to be a BES installation site. Then its optimal capacity is determined by the given operation pattern, the charging and discharging characteristics, and efficiency. They estimate that the load shifting amount be 300-400MW and the improvement of daily load factor be 5%.

Kottick et al. [38] demonstrated the impact of a 30MW BES facility on the frequency regulation in the Israeli isolated power system by utilizing its quick response time. The operation of the BES unit is modeled as a first order transfer function. The BES facility is designed to operate at an average energy level of 70% of its energy capacity. It should not be discharged to a level below 40% of its capacity and should be able to supply 30MW for a period

of 15 minutes. This requires the BES with an energy capacity of 25MWh. The simulation conditions are that the maximum load disturbance is 30MW, its power gradient is 10MW/sec, and the time constant of the BES facility is 0.5 seconds. The computer simulation indicated that the BES facility reduces drastically the frequency deviations resulting from sudden demand variations.

Lu et al. [40] proposed an incremental model of BES system for investigation of its application to load-frequency control. A computer model of a two-area interconnected power system including governor deadband and generation rate restraint is employed for a realistic response. Taking as the feedback signals the frequency deviations and area control errors, the BES system is effective in damping the oscillations caused by load disturbances. The analysis illustrated that, for an area of 2000MW capacity, a 5MW/20MWh BES is sufficient if the maximum load disturbance is 0.005 p.u.

Salameh et al. [36, 37] presented a mathematical model of a lead-acid battery, which take into account self-discharge, battery storage capacity, internal resistance, overvoltage and ambient temperature, and evaluated the ampere-hour capacity of a lead-acid battery using that mathematical model. Change in end voltages, rates of charge and discharge, and temperature all do not affect the battery model to represent the behavior of a lead-acid battery. They also found that the capacity decreases with a decrease in temperature, and an increase in rate of charge and discharge.

Kunisch et al. [31] presented an interesting paper, saying that load leveling operation of BES plants is not economical in Europe but it can show operational and economical advantages for load-frequency control and instantaneous reserve operation. The economy of a load leveling BES is largely depending on the prevailing load curve characteristics. Relying on the shape of the load peaks reasonable load reductions range from 5% to 15% of the peak load for peaking periods shorter than 3 hours. For most European utilities, the system load exceeds 90% of the daily peak load for at least 8 hours. Under these conditions, it was said that gas-turbines with or without compressed air storage and pumped hydro plants are more economical for peaking load than BES units.

2.3 Fuel Cells

2.3.1 Background Information

It looks exceptional that fuel cells have not been widely commercialized for power utility applications since sulfuric acid fuel cells were invented 150 years ago by an Englishman, William Grove. The great promise of fuel cells as a means for efficient production of electricity from the oxidation of a fuel has been recognized again due to the growing interest in

environmental concern about global warming and decreasing conventional power generating sources.

The fuel cell is an electrochemical device that converts the free-energy change of an electrochemical reaction into electrical energy. The simplest overall fuel cell reaction is

$$H_2 + \tfrac{1}{2} O_2 \rightarrow H_2O + electricity \qquad (2.11)$$

The free-energy change of this reaction under standard conditions of temperature and pressure ($25^{\circ}C$, 1 atm) is 56.32kCal/mole. The number of electrons transferred in this reaction is 2 and the reversible potential is 1.229V. Even if there were no efficiency losses in $H_2 - O_2$ fuel cells, heat would still be rejected from a fuel cell. Thus, the theoretical efficiency of the fuel cells at $25^{\circ}C$ is 83%.

The performance of a fuel cell that operates at low and intermediate temperatures of 25-200 $^{\circ}$C is illustrated in Figure 2.4 [19]. That figure, a typical cell voltage versus current density plot, explains the important role of electrode kinetics on its performance. The following relation may represent the performance equations when the current density varies from zero to the end of the linear region.

$$E_f = E_{f0} - b \log I_f - RI_f \qquad (2.12)$$

where

$$E_{f0} = E_r + b \log I_{f0} \qquad (2.13)$$

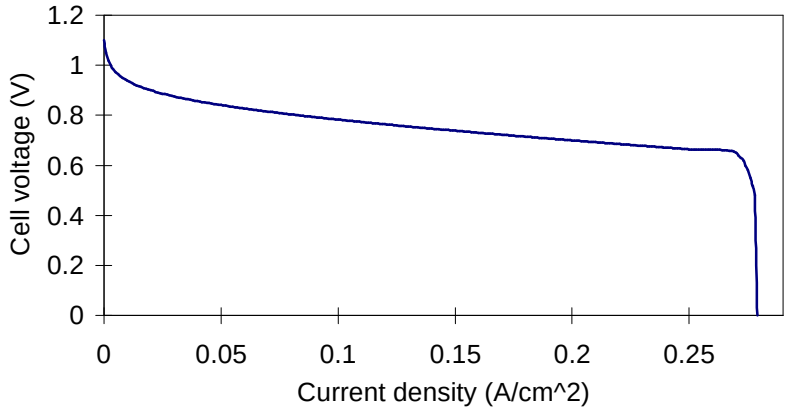

Figure 2.4 Typical plot of cell voltage vs. current density for a fuel cell [19].

The low electrocatalytic activity of most electrode materials for the oxygen electrode reaction causes the difficulties in attaining high energy efficiencies and high power densities in low- to medium-temperature fuel cells. Fuel cell performance can be increased by increasing cell temperature and reactant pressure.

The equivalent circuit for a fuel cell is depicted in Figure 2.5 [24]. The equivalent steady state dc resistance is high but the transient impedance is low. The low transient impedance will make fuel cell response much faster than any conventional generating system.

It should be remembered that fuel cells will use the same primary fuels as conventional power generation forms, and fuel cells must be economically competitive with these conventional systems. Therefore, fuel cells do not offer a real energy alternative but contribute to energy savings because of their intrinsic high efficiency.

The reliability of fuel cells for steady power generation has been proven in the U.S. aerospace program. Design reliability (mean time to failure) greater than 95% has been achieved consistently under the stringent conditions of space flight. The design reliability required for most terrestrial uses is lower than those needed for aerospace applications. However, terrestrial units require reliability during much longer total operating periods. It is expected that the first generation of commercial fuel cell power generation systems will have an on-stream availability of 90%. Ultimately, fuel cell power plants can have on-stream availability of 98-99%.

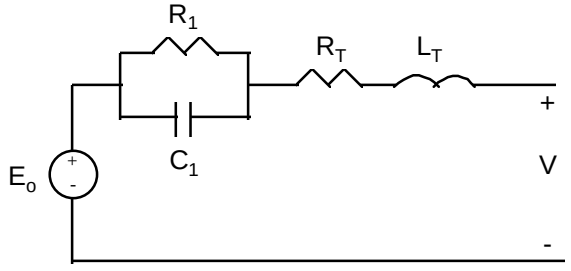

E_0 - open circuit voltage
R_1 - charge transfer resistance
C_1 - cell capacitance
R_T - electrolyte resistance
L_T - equivalent inductance

Figure 2.5 Equivalent circuit of a fuel cell [24].

The high reliability of a fuel cell system will largely result not only from the modularity of the stacks and stack components, but from their lack of highly stressed moving parts operating under extreme conditions. It operates under relatively benign conditions, so it can be designed such that maintenance is required only at infrequent intervals. A plant could be operated at full power during periods of routine maintenance by replacing spare modules. Without spare parts, plants could be designed so that only partial shutdown will be necessary in the event of failure.

Any low-temperature fuel cell system must take several fuel-processing steps to produce hydrogen that will be consumed inside the fuel cell stacks. The most effective way to produce the hydrogen is by steam-reforming of hydrocarbon fuels. First, fuel purification to avoid poisoning of the steam-reforming catalyst is required, which is done by hydrodesulfurization. This is followed by reforming and carbon monoxide (CO) shift reaction to reduce any residual CO values to acceptable levels. The above reactions are endothermic, so they need a net heat input from the fuel used or from any available heat. High-temperature heat is required for the reforming, typically 750 - 800^{o}C. Unless this heat can be given directly by the waste heat from a high-temperature fuel cell, it must be provided by burning excess fuel.

Since the energy crisis of 1973, which was instrumental in the renaissance of fuel cells, it has been customary to classify fuel cells by the types of electrolyte: alkaline, phosphoric acid, molten carbonate, solid oxide, and solid polymer. The alkaline fuel cell system being used in space shuttle flights is a strong contender for NASA's lunar and Mars missions, and the solid polymer fuel cells are being developed for applications to transportation. Table 2.1 summarizes the characteristics of three major fuel cell systems that contain great potentials for power utility applications.

2.3.2 Phosphoric Acid Fuel Cell (PAFC)

Phosphoric acid technology has moved from the laboratory research and development to commercial application. The principal obstacle against widespread commercial acceptance is cost. Capital costs of about $2500 - $4000/kW must be reduced to $1000 - $1500/kW if the technology is to be accepted in the electric power markets.

The basic cell structure is similar to that of a battery. It consists of an anode, a cathode and an electrolyte. The anode and cathode are made of a porous graphite substrate treated with a platinum catalyst, having the surface adjacent to the electrolyte. The electrolyte matrix retains the concentrated phosphoric acid and its thickness is in the range between 0.01 and 0.03 cm. The electrolyte matrix has minimum ionic resistance while separating the fuel and oxidant gas streams.

The PAFC system operates at 180 to 210^{o}C. At lower temperatures, phosphoric acid is a poor ionic conductor. At higher temperatures, material (carbon and platinum) stability becomes limiting. The chemical reactions occurred at two electrodes are written as follows:

Table 2.1 Comparison of three types of fuel cells.

Characteristics	First generation	Second generation	Third generation
Fuel cell	PAFC	MCFC	SOFC
Electrolyte	Phosphoric acid (H_3PO_4)	Lithium carbonate (Li_2CO_3) Potassium carbonate (K_2CO_3)	Yttria-stabilized zirconia (ZrO_2)
Working temp.	180 - 210 ^oC	600 - 700 ^oC	900 - 1000 ^oC
Efficiency	40 - 45 %	50 - 60 %	>60 % (projected)
Current density	150 - 350 mA/cm^2	100 - 250 mA/cm^2	100 - 300 mA/cm^2
Cell voltage	0.6 - 0.7 V	0.7 - 0.85 V	0.6 - 0.7 V
Fuel	H_2	H_2 and CO	H_2 and CO
Advantages	- Tolerant to CO_2 - Most advanced	- No noble catalysts required - CO is usable fuel - Internal reforming in cells is feasible - High-grade heat is available	- No noble catalysts required - CO is usable fuel - Internal reforming in cells is feasible - CO_2 recycling not required
Disadvantages	- Catalysts require noble metals - CO is an anode poison - Low conductivity electrolyte	- CO_2 source required for cathode	- Relatively high electrolyte resistivity

At anode: $2H_2 \rightarrow 4H^+ + 4e^-$ (2.14)

At cathode: $O_2 + 4H^+ + 4e^- \rightarrow 2H_2O$ (2.15)

Overall: $2H_2 + O_2 \rightarrow 2H_2O$ (2.16)

PAFCs can today meet the environmental, efficiency and endurance characteristics that are required for utility service. Projected costs for building PAFC systems appear marginal

when compared with costs for alternative power plants. The first utility application would be as a dispersed power generator fueled by a natural gas. However, PAFCs may find applications in coal-fired central-station power plants with coal gasifiers. With the current emphasis on cogeneration, it is also possible that the PAFC's unique environmental character will lead to its early use in applications where its electric and thermal energy can be employed.

2.3.3 Molten Carbonate Fuel Cell (MCFC)

Molten carbonate technology is attractive because it offers several potential advantages over PAFCs. Carbon monoxide, which poisons the PAFCs, is indirectly used as a fuel in MCFCs. The higher operating temperature of approximately 650°C makes the MCFCs a better candidate for combined cycle applications. This technology is on the stage of prototype commercial demonstrations and main development efforts are focused on large multi-MW central-station power plants with a coal gasifier. This is partially due to their high operating temperature and the problems inherent in starting (heating) and stopping (cooling) MCFC power plants. Their capital costs are expected to be lower than those of PAFCs.

The MCFC structure is geometrically very similar to that of the PAFC, but the materials used are very different from those used in the PAFC. The anode consists of a porous nickel treated with an insoluble oxide to reduce sintering. The cathode is similar to the anode except that it uses nickel oxide doped with lithium to give electronic conductivity. MCFCs use an alkali metal (lithium or potassium) carbonate as the electrolyte. Since these carbonates can function as electrolytes only when in the liquid form, the operating temperature should be maintained above the melting points of the carbonates. The following equations illustrate the chemical reactions that take place inside the cell.

At anode: $$2H_2 + 2CO_3^{2-} \rightarrow 2H_2O + 2CO_2 + 4e^- \quad (2.17)$$

and $$2CO + 2CO_3^{2-} \rightarrow 4CO_2 + 4e^- \quad (2.18)$$

At cathode: $$O_2 + 2CO_2 + 4e^- \rightarrow 2CO_3^{2-} \quad (2.19)$$

Overall: $$2H_2 + O_2 \rightarrow 2H_2O \quad (2.20)$$

$$2CO + O_2 \rightarrow 2CO_2 \quad (2.21)$$

A consequence of these reactions is that CO_2 must be recycled from the anode to cathode. Waste heat from the fuel cell can be available at a relatively high temperature (greater than 500°C), which enables its use in bottoming or industrial heating cycles.

A fuel cell system must include fuel conversion process by external or internal reforming from sulfur-free hydrocarbon gas to hydrogen-rich gas. For large central MCFC power plants, efficient external reforming may be recommended because of the effects of scale and high-energy efficiency. However, for smaller dispersed units, internal reforming has the advantages of simplicity and direct use of part of heat generated in the cells.

2.3.4 Solid Oxide Fuel Cell (SOFC)

Solid oxide technology requires very significant changes in the structure of the cell. SOFCs employ a tubular stack configuration. As the name implies, SOFCs use a solid, nonporous metal oxide electrolyte such as stabilized zirconia, so the electrolyte does not need to be replenished during the operational life of the cells. This simplifies design, operation and maintenance as well as having the potential to reduce costs. This offers the stability and reliability of all solid-state construction and allows higher temperature operation. The ceramic make-up of the cell lends itself to cost-effective fabrication techniques.

The anode is typically a porous nickel-zirconia cermet that serves as the electrocatalyst, which can be electronically conductive, allow fuel gas to reach the electrolyte interface, and catalyze the fuel oxidation reaction. The cathode consists of a discontinuous catalyst layer coated with a porous, doped indium oxide. The cathode must conduct electrons, allow oxygen to reach the electrolyte interface, and catalyze the reduction of oxygen to oxide ions. The chemical reactions inside the cell may be written as follows:

At anode: $$2H_2 + 2O^{2-} \rightarrow 2H_2O + 4e^- \quad (2.22)$$

and $$2CO + 2O^{2-} \rightarrow 2CO_2 + 4e^- \quad (2.23)$$

At cathode: $$O_2 + 4e^- \rightarrow 2O^{2-} \quad (2.24)$$

Overall: $$2H_2 + O_2 \rightarrow 2H_2O \quad (2.25)$$

$$2CO + O_2 \rightarrow 2CO_2 \quad (2.26)$$

SOFCs offer advantages similar to those of MCFCs, such as good performance on fuels containing hydrogen and carbon monoxide, no need of noble-metal catalysts, and the availability of high-grade waste heat. The tolerance to impure fuel streams makes SOFC systems especially attractive for utilizing H_2 and CO from natural gas steam-reforming and coal gasfication plants. Additionally, they do not suffer the constraint of MCFCs that require a carbon dioxide recycle to the cathode.

2.3.5 Fuel Cell Power Systems

Fuel cells are known to possess a great number of attributes that make them attractive for the purpose of power generation. The inherent modularity in their production contains the feature less sensitive to size. It enables them to be added successively. Fuel cells have high efficiency and relatively flat efficiency characteristics that make them useful for part-load operation. Fuel cells can utilize a variety of fuels such as natural gas, coal-derived gas, biogas and methanol, and they are able to respond very fast to load changes. Their low noise and emissions and negligible water requirements allow them much more flexibility in siting. Because of those benefits, fuel cells have continuously been under research and development despite their high initial cost right now.

Bell and Hayman [26] reviewed the electric utilities' efforts to develop fuel cell technology including the siting and construction of the 4.5MW phosphoric-acid fuel cell (PAFC) demonstrator in New York City. The study suggested that if PAFCs were available with a cost of about $400/kW and a heat rate of 9300Btu/kWh, they would be attractive for intermediate duty generation. These fuel cell units would capture about 27% of capacity additions competing against nuclear, oil-fired intermediate, and gas turbine units.

Rahman and Tam [1] presented to use fuel cells in coordination with PV systems. Through simulation using actual data from a PV test facility, it was shown that it is feasible to use the PV-fuel cell hybrid system to meet variable loads for either utility or stand-alone applications. Operation of the hybrid system overcomes the intermittence problem inherent in PV and makes photovoltaic electric power generation more attractive.

Tam and Rahman [2] proposed an augmented power conditioning subsystem (APCS) applied at central station photovoltaic-fuel cell power plant in order to improve the power system performance. By using phase shift control, real and reactive power can be controlled independently and a variety of operation and control modes are developed for different system situations.

Matsumoto et al. [28] discussed a performance model of a molten carbonate fuel cell (MCFC) for any cathode gas composition by single-cell experimental data. The study investigated three different systems (that is, external reforming (ER), direct internal reforming (DIR), and indirect internal reforming (IIR) system) and compared their performances. A DIR system can achieve about 6% higher electric power generation efficiency than an ER system, and about 5% higher than a IIR system.

Hsu et al. [79] is proceeding on development of a hybrid system of a SOFC with a gas turbine, which utilizes the high temperature exhaust gas from the fuel cell system. The hybrid system is potentially capable of reaching electrical efficiencies around 70% assuming the fuel cell efficiencies from 50 to 55%. They plan to provide the products to customers at a system price below $1000/kW.

Ruhl et al. [80] have completed preliminary designs and tests for 20 kW SOFC modules for stationary distributed generation applications using pipeline natural gas. The system's NO_x emission level is less than 3 lb/GWh while its efficiencies range from 45 to 50%. Its dynamic response capability is less than 4 sec at a load increase from 1 to 100% output, and less than 2 msec at a load decrease from 100 to 1%.

2.4 Neural Networks (NNs)

2.4.1 Neural Network Background

Artificial neural networks (ANNs) are information processing systems. Neural networks can generally be thought of as " black box" devices that accept inputs and produce outputs. Some of the characteristics that NNs perform include

(i) Classification
(ii) Pattern matching
(iii) Pattern completion
(iv) Noise removal
(v) Optimization
(vi) Control

Figure 2.6 shows a typical neural network that consists of processing elements (PEs or neurons) and weighted connections. The connection weights which store the information are

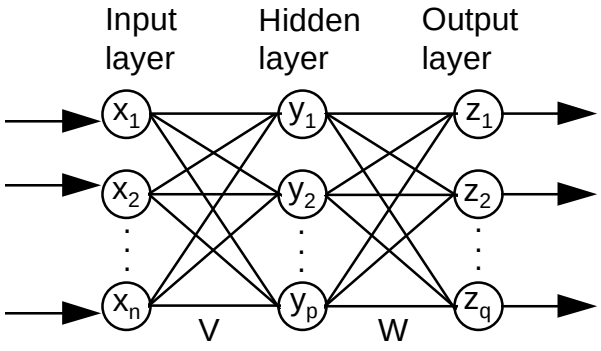

Figure 2.6 A typical neural network.

often determined by a NN learning procedure. The neural network illustrates several important features such as (i) each PE acts independently of all others, (ii) each PE relies only on local information, and (iii) the large number of connections provides a large amount of redundancy and facilitates a distributed representation of information. The first two features allow NNs to operate efficiently in parallel. The last feature provides NNs with inherent fault-tolerance and generalization qualities that are very difficult to obtain from typical computing systems. In addition to these features, NNs are able to learn arbitrary nonlinear mappings through introduction of nonlinearity in PEs.

PE activation functions map a processing element's infinite domain to a prespecified range. Although abundant activation functions are possible, the following five functions are usually employed by the majority of NNs:

(i) Linear function
(ii) Step function
(iii) Ramp function
(iv) Sigmoid function
(v) Gaussian function

Except for the linear function, all of the functions introduce a nonlinearity in the network dynamics by limiting the output values within a fixed range.

NNs consist of layer(s) of processing elements interconnected by weighted connections. The arrangement of the PEs, connections, and patterns into a NN is referred to as a topology. Four common NN topologies may be written as

(i) Instars, outstars, and the ADALINE
(ii) Single-layer networks
(iii) Two-layer networks
(iv) Multilayer networks

The instar is the minimal pattern encoding network. The outstar is the dual of the instar and is the minimal pattern recall NN. The ADALINE (ADAptive LInear NEuron) has the same topology as the instar, but the weights are adjusted by using the least-mean-square algorithm. One-layer NNs are used to perform pattern processing tasks such as pattern completion, noise removal, and optimization and two-layer NNs are used for pattern matching and pattern classification. Application fields of multilayer NNs are pattern classification, pattern matching, and function approximation. For the question of how many layers are enough for a given problem, it was proven that three layers (one hidden layer) are sufficient to perform any nonlinear mapping to any desired degree of accuracy. Although this is a very important result, it still does not indicate the proper number of PEs in hidden layers.

The most appealing quality of NNs is their ability to learn. Learning is defined as a change in connection weight values that results in capture of information. All learning methods can be classified into two categories: supervised and unsupervised learning. Supervised learning is a process that requires an external teacher whereas unsupervised learning is a process that incorporates no external teacher and relies upon only local information during the entire learning process. The six most famous learning methods are listed as

(i) Hebbian learning
(ii) Differential Hebbian learning
(iii) Competitive learning
(iv) Two-layer error correction learning
(v) Multilayer error backpropagation learning
(vi) Stochastic learning

Table 2.2 describes five key attributes of the neural network learning algorithms mentioned above.

2.4.2 NN Applications to Power Systems

Applications of artificial neural networks to power systems have advanced rapidly in recent years. NNs have been widely applied for solving various power system problems including security assessment [60, 63, 68], stability analysis [61, 64, 67], tuning of power system stabilizers [62, 72], generator shedding problem [65], fault identification [66, 71], unit commitment [69], subsynchronous resonance oscillation [70], VAR control [73], load forecasting [74], economic/

Table 2.2 Key attributes of the principal learning procedures [59].

Learning algorithm	Learning Time	On-line/ Off-line	Supervised/ Unsupervised	Linear/ Nonlinear	Structural/ Temporal
Hebbian learning	Fast	On-line	Unsupervised	Linear	Structural
Differential Hebbian learning	Fast	On-line	Unsupervised	Linear	Structural
Competitive learning	Slow	On-line	Unsupervised	Linear	Structural
Two-layer error correction	Slow	Off-line	Supervised	Linear	Both
Error backpropagation	Very slow	Off-line	Supervised	Nonlinear	Both
Stochastic learning	Extremely slow	Off-line	Supervised	Nonlinear	Structural

environmental dispatch [75], and voltage stability assessment [76]. The success of these works results from the fact that NNs are capable of solving a complicated problem in an efficient way by performing parallel processing on the information distributed over a number of neurons (processing elements).

Chen and Hsu [61] developed a new learning method of multilayer NNs (one hidden layer) for the steady-state stability analysis of a synchronous generator. The inputs of the NN are the real power output and power factor of the generator and power system stabilizer (PSS) parameters. The output of the network provides the information on steady-state stability. Their learning algorithm is that the outputs of hidden layer neurons are binary-valued (0 or 1) depending upon the inputs, and then the value of the output neuron is decided as the " Boolean AND" operation of the binary hidden-layer outputs. By the computer simulation, it is found that the proposed learning method converges faster and its misclassification rate is lower than the error backpropagation method. The misclassification rate of the proposed method is 3.5% on 10 minutes of learning time.

Ikenono and Iwamoto [64] presented a generalized online technique for transient stability analysis using the backpropagation algorithm. The NN consists of one input layer, one hidden layer and one output layer. The numbers of neurons in the input, hidden and output layers are 32, 15, and 1 respectively. The output neuron denotes the critical breaker clearing time and the input neurons include magnitude of bus voltage, angle of bus voltage, generator output power, load power, inertia constant of generator and existence of alteration in system configuration. Simulation results indicate that the proposed technique gives desirable solution if critical clearing time is short, but when critical clearing time is rather long, the proposed method gives some results requiring a longer time.

Hsu and Chen [62] proposed a new approach using an ANN for adapting PSS parameters. It is desirable to adapt the PSS parameters in real time based on generator loading conditions in order to have good damping characteristics over a wide range of operating conditions. They used a multilayer feedforward NN (two hidden layers) with the error backpropagation learning rule. The inputs to the NN contain generator real power output and power factor, which characterize generator operating conditions. The outputs of the network are the desired PSS parameters. It is concluded from the simulation results that the generator can maintain good damping features over a wide range of operating conditions when the PSS parameters are adapted by the ANN. The generator with fixed PSS parameters does not yield satisfactory dynamic responses when the operating condition is severely perturbed.

El-Keib and Ma [76] investigated voltage stability problem resulting from system heavy loading and proposed a multilayer feedforward ANN with error backpropagation learning for calculation of voltage stability margins. The proposed method uses an energy function, derived from a vector integration of the real and reactive power mismatch equations between a stable equilibrium point and an unstable equilibrium point, to provide a quantitative measure of system

vulnerability to voltage instability. Sensitivity of the energy margin with respect to system variables provides information regarding the most effective direction to steer the system to maximize voltage stability. As input candidates to the NN, real and reactive powers at all buses as well as real and reactive power outputs of all generators are applied. Then a reasonable number of inputs are selected by the sensitivity method. The analysis reveals that the system exhibits quite different response scenarios as system loading conditions vary. Moreover, the sensitivity method causes the NN to produce less accurate estimation of voltage stability margin when operating states are near the collapse point.

Sidhu and Ao [77] proposed an adaptive loss evaluation algorithm based on NN using backpropagation for power transmission systems. A three-layer feedforward network is employed because it can model complex mapping functions reasonably well. Real and reactive powers of generators and loads, as well as voltage magnitudes at voltage-controlled buses are chosen as inputs to the NN, and total system losses are the output. The computed capacity losses from the NN are as close as those obtained by load flow studies; the maximum error is 1.8%. The proposed network can be used to predict capacity and energy losses as a part of off-line load forecasting. For on-line applications, it can be used to monitor the actual capacity losses in the system.

King et al. [75] applied the Hopfield neural network to optimal economic/environmental dispatch of thermal generating units in an electric power system. A multi-objective function is adopted to minimize both the total fuel cost and NO_x/SO_2 emissions of thermal units. They introduced an energy function of state variables that maps the economic/environmental dispatch problem to the Hopfield domain. The Hopfield model, a single layer recursive NN, is created with N neurons, one for each generating unit. The output value of each neuron represents the generation value of each unit. Computation results indicated that the cost of generation increases as emission levels decrease and including transmission losses in the dispatch problem complicates obtaining the optimal solution.

2.5 Power Conditioning Subsystems (PCSs)

2.5.1 Background Information

Photovoltaic or fuel cell power systems, which generate power as dc electricity, require power conversion devices from dc to ac in order to provide power to the transmission and distribution network of a utility grid. There are other applications, where it is necessary to be able to control power flow in both directions between the ac and dc sides. Examples of such applications are converters in battery and supermagnetic energy storage or high-voltage dc power transmission.

The dc to ac power conversion is accomplished in phase-controlled (uncontrollable frequency) converters by means of thyristors (sometimes termed SCRs). This device is one member of controllable switches. SCRs have the following distinct characteristics.

* Turning on an SCR requires applying a positive signal to its gate while its anode-cathode voltage is positive.

* Once the SCR is on, it remains on independent of a signal at its gate until its anode current goes to zero. That means that once the SCR is on, it behaves like a diode.

* When the anode current goes to zero, a small amount of time, called turn-off time, must elapse before a positive anode-cathode voltage can be reapplied to the SCR.

A phase-controlled converter requires that the external ac system be a voltage source, typically ac utility line. This condition is necessary because the phase-controlled converter uses the reversal of the ac voltage to drive the commutation process. Therefore the ac frequency in the converter is constrained to be that of the ac source.

In the past these phase-controlled converters were used for controlling the flow of electric power in a number of applications such as high voltage dc transmission, even though they contain a major drawback that they cannot be turned off by a gate signal. Owing to the availability of controllable switches such as bipolar junction transistors (BJTs), metal-oxide-semiconductor field effect transistors (MOSFETs), gate-turn-off thyristors (GTOs), etc., usage of the early thyristors is nowadays restricted to a specific application. This is because these controllable switches can control both the ac voltage and frequency, and these circuits are called variable-frequency dc-ac converters. The progress in semiconductor technology will undoubtedly lead to higher power ratings, faster switching speeds, and low costs. Of the many controllable switches, GTOs show a great capability for high voltages and large currents.

Figure 2.7 shows a basic single-phase variable-frequency full bridge inverter [87]. If L/R is greater than π/ω, the third harmonic component of i_a is on the order of 10% of its fundamental and the current is written as

$$i_a(t) \cong I_{a_1} \sin(\omega t - \theta) \tag{2.27}$$

where

$$I_{a_1} = \frac{V_{a_1}}{\sqrt{(\omega L)^2 + R^2}} \tag{2.28}$$

$$V_{a_1} = \frac{2V_{dc}}{\pi}\int_{\delta}^{\pi-\delta} \sin(\omega t)\, d(\omega t) = \frac{4V_{dc}}{\pi}\cos\delta \tag{2.29}$$

and

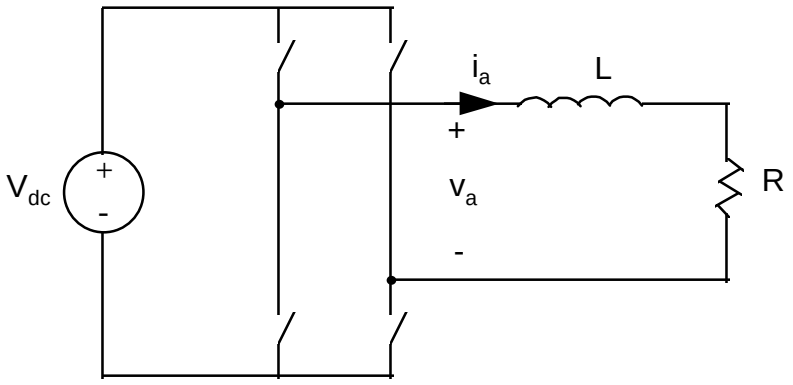

(a)

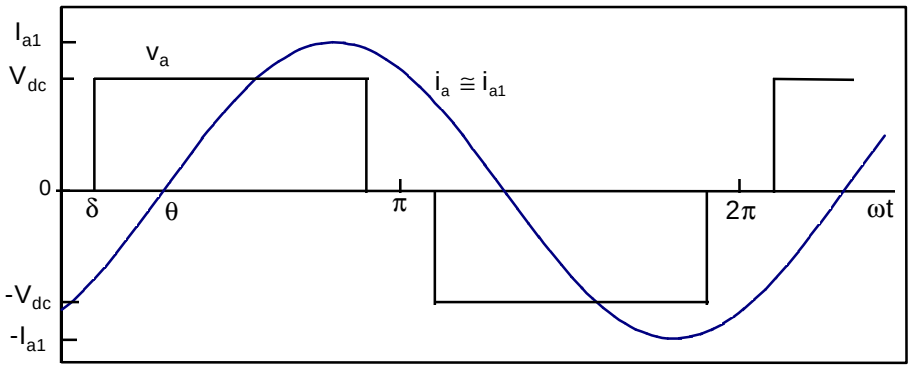

(b)

Figure 2.7 (a) A variable-frequency full bridge inverter. (b) Waveforms of the ac voltage and current [87].

$$\theta = tan^{-1}\left(\frac{\omega L}{R}\right) \tag{2.30}$$

The average power P delivered to the resistor R is

$$P = \frac{V_{a_1} I_{a_1}}{2} cos\theta = \frac{8V_{dc}^{\ 2}}{\pi^2 \sqrt{(\omega L)^2 + R^2}} cos^2 \delta \, cos\theta \tag{2.31}$$

From this analysis the power depends on δ, and therefore the power can be controlled only by varying δ or V_{dc}. This is because the power factor is fixed in the passive load of Figure 2.7 (a). If the resistive load in Figure 2.7 is replaced with an ac voltage source, θ in addition to δ can be used as a control variable.

2.5.2 PCU Applications to Renewable Power Sources

Large scale grid-connected photovoltaic or fuel cell power plants require power conversion from the dc generated from the power plants to the ac of a three-phase power utility network. Efficient control of dc to ac power conversion devices, design of a new inverter circuit for photovoltaic energy feedback into a utility grid, and modeling of an inverter with different types of commutation are discussed. Michaels et al. [55] presented simulation techniques for line-commutated and self-commutated three-phase bridge inverters. They represented the system by different sets of differential equations depending upon the states of the switches in the circuit. As a result, they have found that the self-commutated inverter is more suitable for the application to a fuel cell system than the line-commutated inverter. They, finally, proposed that this kind of inversion device should have features such as high conversion efficiency, low capital and operating costs, compatibility with utility system interface, and operating flexibility for control of voltage and real/reactive power.

Dugan et al. [44] studied harmonic distortions in voltage and reactive power correction from 6.6kW line-commutated inverters in 100 photovoltaic house subdivision, which is equivalent to approximately 7% penetration on the 10MVA distribution feeder. Under common conditions the total harmonic distortion (THD) caused by the inverters is around 2-3%, and under the worst conditions it reaches 6.2% on one feeder and 4.8% on the other. The study indicated that the THD levels are strongly influenced by the power factor correction capacitors on the distribution feeder, and each line-commutated inverter consumes up to 4kVar of reactive power at peak output.

Boegli and Ulmi [8] realized a new regulated utility interactive inverter for direct residential photovoltaic energy feedback to a public utility grid. A modulated buck converter converts the photovoltaic dc current to a rectified 50-Hz sine wave current and the following self-commutated half-bridge inverter generates a 50-Hz sine wave current. It is, then, fed into one phase of the public utility grid. The new inverter needs only three power transistor switches and a transformer for isolation between the PV array and the grid. The yearly overall efficiency of the 1-kW prototype is 88% and the total harmonic distortion is 1% at 1kW.

Wasynczuk [5, 6] described simplified computer models of three-phase line-commutated and self-commutated utility interactive photovoltaic inverter systems for applications to transient stability analysis. The computer simulation indicated that the simplified models are reasonably

accurate when used to predict the PV system response following step changes in the inverter delay angle, rapid decreases or increases in solar insolation and step changes in ac voltage magnitude or phase.

R. Naik [89] presented a new topology for interfacing of PV, wind-electric and fuel-cell systems with a utility grid. The interface consists of a 3-phase dc-ac line-commutated inverter and dc-dc converter. The firing angle of the 3-phase inverter is kept at a constant value and the power flow from the dc source to the utility is controlled by the dc-dc converter. A constant-extinction angle control scheme is used, which is common in converters for the HVDC transmission systems. The total harmonic distortion (THD) in line currents is 3.9% at simulation and that is 5.9% at experiment results.

W. Shireen and M.S. Arefeen [90] proposed a modified inverter switching technique for the interface with a utility grid such that the ac output of the 3-phase pulse-width modulation (PWM) inverter becomes immune to fluctuations in the unregulated dc input, such as battery, fuel cells, PV cells, etc. The proposed method is a feedforward approach to suitably alter the modulating function for inverter switching control to counter the fluctuation in the input dc voltage. If the input voltage increases, the width of the PWM pulses decrease and if the input voltage decreases, the width of the PWM pulses increase. The response time for accommodating input voltage variation is limited by the delay of the control circuit. The experiment results reveal that the lower order harmonics of the output voltage are effectively canceled.

CHAPTER 3

BATTERIES OR FUEL CELLS FOR PV POWER BACKUP

As energy storage devices, batteries continue to be applied to electric power utilities for drawing benefits of peak shaving and load leveling. Battery energy storage facilities provide the utilities additional dynamic benefits such as voltage and frequency regulation, load following, spinning reserve, and power factor correction [34, 38]. Applications of the storage batteries to power systems are predicted to grow in the future due to those benefits coupled with the ability to provide peak power.

Fuel cell power generation is another attractive option for providing power for electric utilities and commercial buildings because of its high efficiency and environmentally benign feature. This type of power production is especially economical (i) where potential users are faced with high cost in electric power generation from coal or oil, (ii) where environmental constraints are stringent, or (iii) where load constraints of transmission and distribution systems are so tight that their new installations are not possible.

Both batteries and fuel cells have their own unique contributions to electric power systems as discussed above. Those two power sources also contain a great potential to back up severe PV power fluctuations under inclement weather conditions. In this chapter comparison between batteries and fuel cells is carried out in detail only for their PV power backup options, so their common attributes and different attributes will be discussed.

3.1 Common Attributes

Photovoltaic power outputs vary depending mainly upon solar insolation and cell temperature. Since control of the ambient weather conditions is beyond human beings' capability, it is almost impossible for human operators to control the PV power itself. Thus, a

PV power generator may sometimes experience sharp output power fluctuations owing to intermittent weather conditions, which causes control problems such as load frequency control, generator voltage control and even system stability analysis.

There is, therefore, a need for backup power facilities in the PV power generation. As mentioned in Chapter 1, batteries and fuel cells are the most likely technologies to provide the PV system with backup power because these two backup power sources contain some distinct features in common. Those characteristics are listed below.

- Fast load-response capability: Fuel cells and batteries are able to respond very fast to load changes because their electricity is generated by chemical reactions. A 14.4kW lead-acid battery running at 600A has maximum load gradient of 300 A/sec [31]. A phosphoric-acid fuel cell system can match a demand that varies by more than half its rated output within 0.1 second [78]. The dynamic response time of a 20kW solid-oxide fuel cell power plant is less than 4 second when a load increases from 1 to 100%, and it is less than 2 msec when a load decreases from 100 to 1% [80].

- Modularity in production: Factory assembly of standard cell units provides fuel cell and battery power plants with short lead-time from planning to installation. This modular production enables them to be added in discrete increments of capacity, which allows better matching of the power plant capacity to expected load growth. In contrast, the installation of a single large conventional power plant may produce excess capacity for several years, especially if the load growth rate is low.

- Highly reliable sources: Due to their multiple parallel modular units and absence of electromechanical rotating masses, fuel cell and battery power plants are more reliable than any other forms of power generation. Fuel cells are expected to attain a performance reliability near 85% [91]. Consequently, a utility that installs a number of fuel cell or battery power plants is able to reduce its reserve margin capacity while maintaining a constant level of the system reliability.

- Flexibility in site selection (Environmental acceptability): The electrochemical conversion processes of fuel cells and batteries are very quiet because they do not have any major rotating masses. External water requirement for their operation is, if any, very little while conventional power plants require massive amount of water for system cooling. Therefore, they can reduce or eliminate water quality problems created by the conventional plants' thermal discharges. Air pollutant emission levels of fuel cells and batteries are none or very little. Emissions of SO_2 and NO_x in the fuel cell power plant are 0.003 lb/MWh and 0.0004 lb/MWh respectively. Those values are projected to be about 1,000 times smaller than those of fossil-fuel power plants since fuel cells do not rely on a fuel-burning process [91]. These environmentally benign characteristics make it possible for those power plants to be located close to load centers in urban and suburban area. It can also reduce energy losses and costs associated with transmission

and distribution equipment. These siting near load centers may also reduce the likelihood of system blackouts.

3.2 Different Attributes

Electric current is produced in a storage battery by chemical reactions. The same chemical reactions take place in a fuel cell, but there is a difference between them with respect to fuel storage. In storage batteries chemical energy is stored in the positive/negative electrodes of the batteries. In fuel cells, however, the fuels are stored outside the cells and need to be fed into the electrodes continuously when the fuel cells are required to generate electricity. Other detailed comparison between battery backup and fuel cell backup for PV power supplement is made in the following sections.

3.2.1 Efficiency

Power generation in fuel cells is not limited by the Carnot Cycle in the view that they directly convert available chemical free energy to electrical energy rather than going through heat exchange processes. Thus, it can be said that fuel cells are a more efficient power conversion technology than the conventional steam-applying power generations. Figure 3.1 illustrates energy conversion processes for a conventional power generator and a fuel cell. Whereas the fuel cell is a one-step process to generate electricity, the conventional power generator has several steps for electricity generation and each step requires a certain amount of energy loss.

Fuel cell power systems have around 40-60% efficiencies depending on the type of electrolytes. For example, the efficiencies of phosphoric-acid fuel cells and molten-carbonate fuel cells are 40-45% and 50-60%, respectively. Furthermore, the fuel cell efficiency is usually independent of size; small power plants operate as efficiently as large ones.

Battery power systems themselves have high energy efficiencies of nearly 80%, but their overall system efficiencies from raw fuel (mostly coal or nuclear) through the batteries to converted ac power are reduced to below 30%. This is because energy losses take place whenever one energy form is converted to another. For this calculation, a 35% of efficiency was assumed for electricity generation from coal or nuclear power stations.

3.2.2 Capacity Variation

The capacity of a fuel cell is expressed in watts (W), whilst that of a storage battery is represented in ampere-hours (Ah) or watt-hours (Wh). A battery with a rated capacity of 100Ah

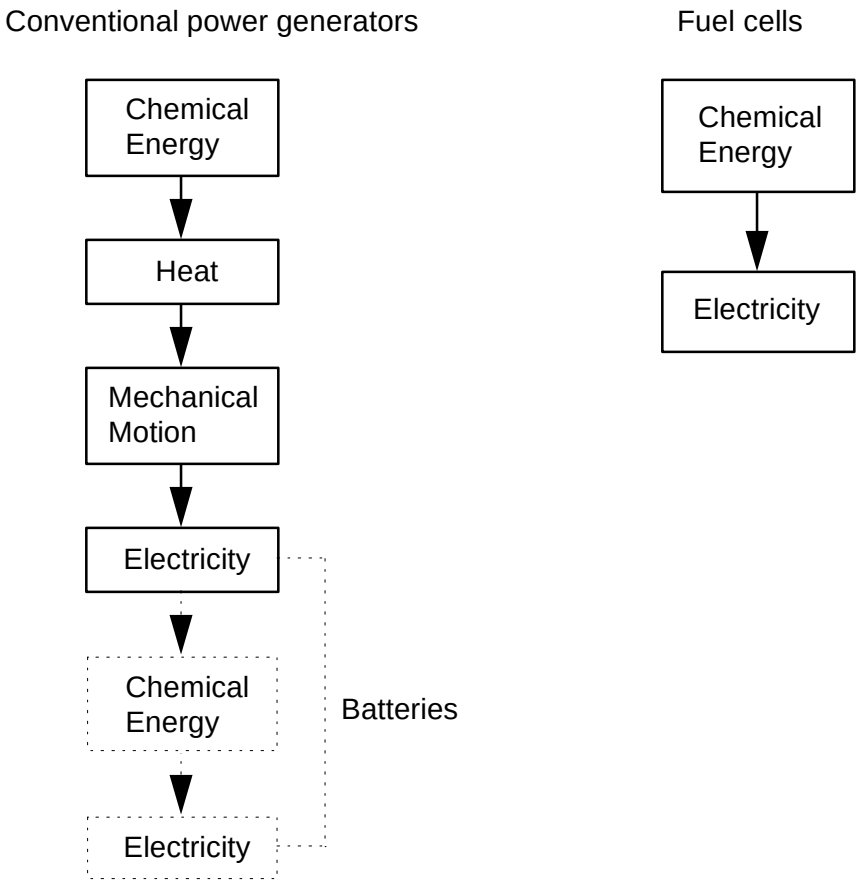

Figure 3.1 Comparison of energy conversion processes [78].

at a 10-hr discharge rate can supply 10A for 10 hours. At discharge rates in excess of 10A, the battery will provide less than 100 Ah. At less than 10A of discharge rates, the battery will provide more that 100 Ah. Thus, in specifying the capacity of a battery, it is necessary to note the time rate of discharge.

As the battery discharges, its terminal voltage, the product of the load current and the battery internal resistance (R_{bat}), gradually decreases. The fall of the terminal voltage on discharge is due to its internal resistance. When R_{bat} is constant at given cell temperature and state of discharge, the terminal voltage drop is directly proportional to the load current. However, the internal resistance of a battery varies with its cell temperature and state of discharge. The resistance increases with both fall in cell temperature and depth of discharge.

The decrease in battery voltages with increasing discharge currents is clearly seen in Figure 3.2 [14]. There is also a reduction in battery capacity with increasing rate of discharge. At 1-hr discharge rate, the available capacity is only 55% of that obtained at 20-hr rate. This is because there is insufficient time for the stronger acid to replace the weak acid inside the battery as the discharge proceeds. Capacity variations at different rates of discharge can be calculated from the curves in Figure 3.2, and is shown in Table 3.1 [14].

For fuel cell power systems, they have equally high efficiency at both partial and full loads as can be seen in Figure 3.3 [78]. The customer's demand for electrical energy is not always constant. So for a power utility to keep adjustment to this changing demand, either large base-load power plants must sometimes operate at part load, or smaller peaking units must be used during periods of high demand. Either way, efficiency suffers and pollution increases. Fuel cell systems have a greater efficiency at full load and this high efficiency is retained as load diminishes, so inefficient peaking generators may not be needed.

3.2.3 Flexibility in Operation

Fuel cells have an advantage over storage batteries in the respect of operational flexibility. Batteries need several hours to be taken for recharging after they are fully

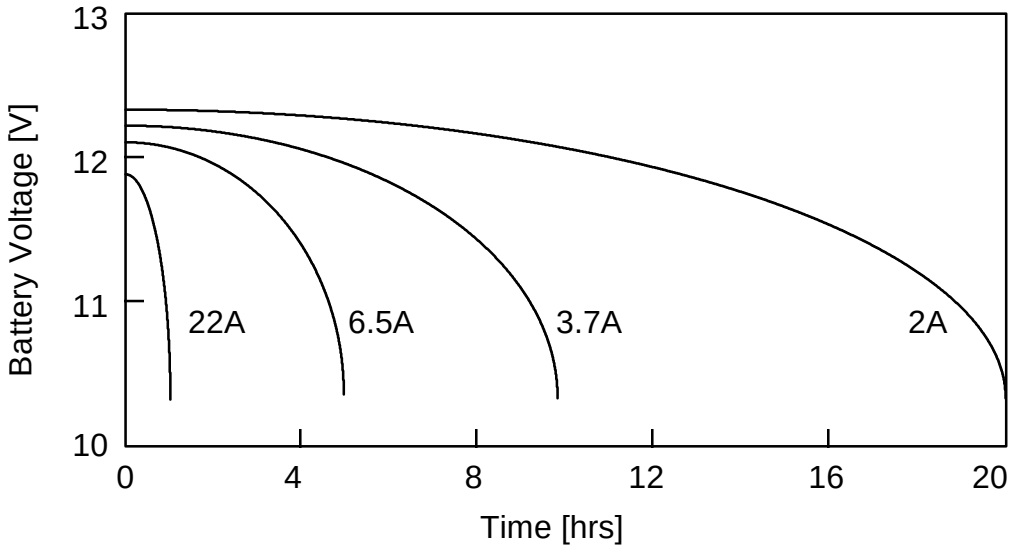

Figure 3.2 Voltage characteristics of a battery at various discharge rates [14].

Table 3.1. Capacity variations of a battery at various discharge rates [14].

Discharge rate	Mean voltage(V)	Current (A)	Wh capacity	% Wh capacity
20 hr	11.85	2	474	100
10 hr	11.75	3.7	435	92
5 hr	11.55	6.5	375	79
1 hr	11.40	22	251	53

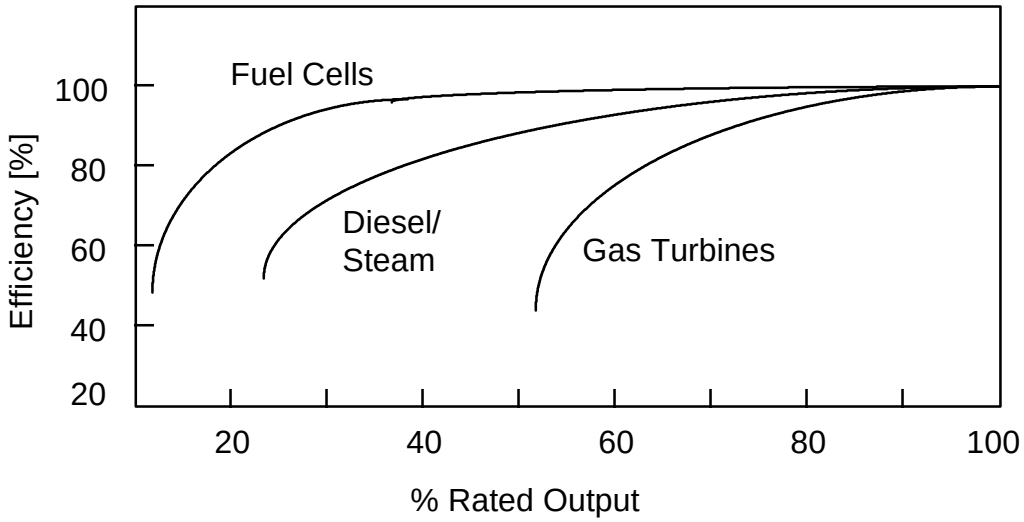

Figure 3.3 Equally high efficiency of fuel cells at partial and full loads [78].

discharged. During discharge the batteries' electrode materials are lost to the electrolyte, and the electrode materials can be recovered during the recharging process. Over time there is a net loss of such materials, which may be permanently lost when the battery goes through a deep

discharge. The limited storage capacity of the batteries implies that it is impossible for them to run beyond several hours.

Fuel cells, on the other hand, do not undergo such material changes. The fuel stored outside the cells can quickly be replenished, so they do not run down as long as the fuel can be supplied. Figure 3.4 illustrates the energy density of fuel cells compared with lead-acid batteries [14]. The fuel cells show higher energy density than the batteries when they operate for more than 2 hours. It means that fuel cell power systems with relatively small weight and volume can produce large energy outputs. That will provide the operators in central control centers for the flexibility needed for more efficient utilization of the capital-intensive fuel cell power plants. The fuel cell power plants can also be operated as intermediate power generation units during months when coal-fired or nuclear units are under forced outage or on maintenance.

Fuel cells use a hydrogen-rich gas to produce electricity. They can employ any fuel that can supply this gas, which includes petroleum, naphtha, natural gas, methanol and biomass. Medium-Btu (British thermal unit) gas from coal gasfication or other synthetic fuels may also become an acceptable fuel. In addition, where hydrogen storage is feasible, renewable power sources can drive an electrolysis process to produce hydrogen gas during off-peak periods that will be used to operate the fuel cells during peak demands.

The usage of storage batteries in an electric utility industry is expected to increase for the purposes of load leveling at peak loads, real-time frequency control, and stabilizing transmission lines. When integrated with photovoltaic systems, the batteries are required to do another duty.

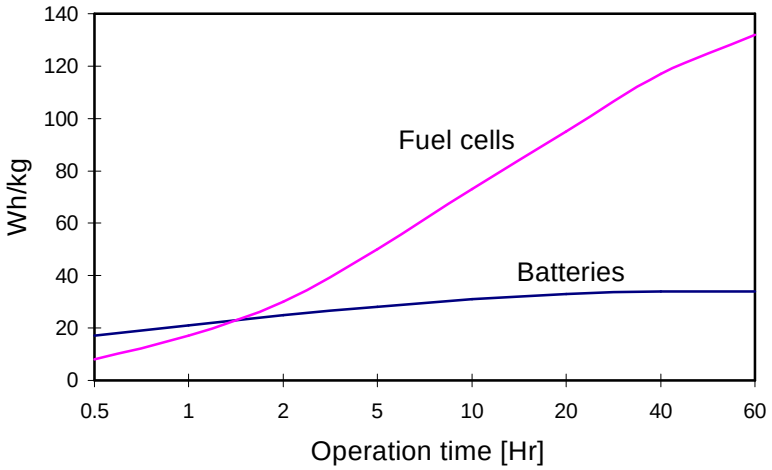

Figure 3.4 Energy densities for fuel cells and batteries [14].

It is to suppress the PV power fluctuations due to the changes of solar intensity and cell temperature. The fact that the PV power outputs change sharply under inclement weather conditions makes it hard to decide the capacity of the battery power plants since their discharging rates are not constant. For a lead-acid battery, the most applicable battery technology for photovoltaic applications to date, the depth of discharge should not exceed 80% because the deep discharge cycle reduces its effective lifetime. In order to prevent the deep discharge and to supplement varying the PV powers generated on inclement weather days, the battery capacity must be large. From Figure 3.5, that shows two different PV power variations, the dotted curve requires a larger battery capacity than the other curve. Moreover, the large battery capacity is usually not fully utilized, but for only several days.

Fuel cells integrated with photovoltaic systems can provide smoother operation. The fuel cell system is capable of responding quickly enough to level the combined power output of the hybrid PV-fuel cell system in case of severe changes in PV power output. Such a fast time-response capability allows a utility to lower its need for on-line spinning reserve. The flexibility of longer daily operation also makes it possible for the fuel cells to perform more than the roles of gas-fired power plants. Gas turbines are not economical for a purpose of load following because their efficiencies become lower and operating costs get higher at less than full load conditions.

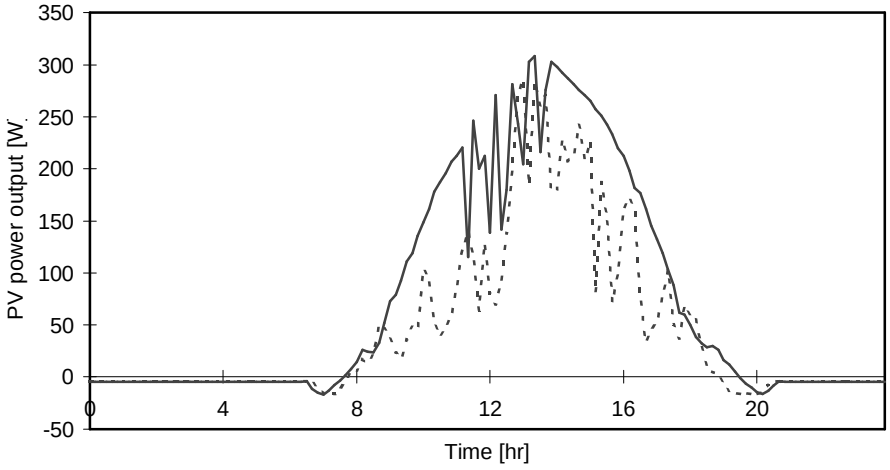

Figure 3.5 PV power variations requiring different battery capacities.

3.2.4 Cost

The history of fuel cell equipment costs has shown that the price of fuel cells has dropped significantly as the commercial market grows and the manufacturing technology becomes mature. Initial cost of phosphoric acid fuel cell power plants was $5,500/kW and the current system cost is about $3,000/kW [84]. This cost is expected to decrease further to around $1,500/kW by the turn of the century.

The cost of electricity to a utility customer who purchases a fuel cell power system at $1,500/kW is 9-10cents/kWh until the short-term loan is retired, and then it falls to about 5cents/kWh. Under longer-term financing that is typical of utility industries, the $1,500/kW electricity production cost of fuel cell power plants is approximately 7cents/kWh [85].

Batteries have a different cost notation since their capacity is represented in watt-hours. A lead-acid battery power plant has currently the lowest battery cost at around $150/kWh because it has been the longest and most fully developed battery technology. The battery cost is projected to reduce to $100/kWh in the future. Nickel-cadmium (NiCd) batteries are 4 to 5 times more expensive than the lead-acid types. Once the NiCd batteries are fully mature, their price will drop but they will not be as low as the lead-acid ones because of the raw material cost.

3.2.5 Environmental Externality

During their life cycle operation, fuel cell power plants produce environmental externalities in the process of fuel reforming. However, storage batteries themselves do not contain any environmental impacts even though the battery charging sources produce various emissions and solid wastes. A fuel cell power system emits by far less SO_2, NO_x and other particulates in the fuel reforming process compared to conventional fossil fuel power plants. The amount of CO_2 emissions from the fuel cell system is similar to that from conventional fossil-fuel power plants, but the fuel cell system's high efficiency ranging from 40% to 60% results in lower CO_2 emissions.

Batteries themselves do not produce any emissions during their operation period even if the power sources providing the batteries with charging power usually at off-peak time generate several chemical emissions and solid wastes. The batteries displace power generation rather than replace it. Therefore, the batteries' environmental impacts should be computed based on the baseload fuel mix used to charge the batteries.

For instance, the CO_2 emissions from fuel cell power plants were calculated as 376.43 $kgCO_2/MWh$ in Appendix C, where the efficiencies of the fuel reformer and the power plant are assumed to be 95% and 45% respectively. For batteries, the CO_2 emissions of the power sources that charge the batteries at off-peak should be computed. When the fuel mix during a charging

period of the batteries is supposed to be 40% of nuclear power and 60% of coal power, then the batteries' CO_2 emission rate would be 714.3 $kgCO_2$/MWh. The results in Appendix A are used in this calculation.

When fuel cell power plants are to be dismantled at the end of their commission, they do not exhibit any detrimental impacts on environment and no specific hazards are encountered. Component recovery rather than waste disposal is likely to be the issue. In phosphoric-acid fuel cells, nickel from the fuel reformer catalyst and platinum from the anode and cathode will require recovery. For molten-carbonate fuel cells, nickel from both the electrodes and the reforming catalysts can be recovered. In solid-oxide fuel cells, nickel and zirconium-containing ceramic components are likely to be recovered.

However, for battery power plants a significant amount of care is required to be taken of their disposal to prevent toxic materials from spreading around. All batteries that are commercially viable or under development for power system applications contain hazardous and toxic materials such as lead, cadmium, sodium, sulfur, bromine, etc. Since the batteries have no apparent salvage value and must be treated as hazardous wastes, disposal of spent batteries is an issue. Recycling batteries is encouraged rather than placing them in a landfill. One method favoring recycling of spent batteries is regulation. Thermal treatment for the lead-acid and cadmium-containing batteries is needed to recover lead and cadmium. Sodium-sulfur and zinc-bromine batteries are also required to be treated before disposal.

3.3 Summary

Both batteries and fuel cells are able to respond very fast to system load changes because they produce electricity by chemical reactions inside them. Their fast load-response capability can nicely support the sharp PV power variations resulted from ambient weather changes. These two PV power backup technologies also contain some excellent attributes in common, such as modular production, high reliability and flexibility in site selection.

However, there are subtle different attributes between batteries and fuel cells when they are applied to a PV power backup option. Power generation in fuel cell power plants is not limited by the Carnot Cycle, so they can achieve high power conversion efficiency. (Their theoretical maximum efficiency is 83%.) Even taking into account the losses due to activation overpotential and ohmic losses, the fuel cells still have high efficiencies from 40% to 60%. For example, efficiencies of PAFCs and MCFCs are 40-45% and 50-60% respectively. Battery power plants, on the other hand, themselves have high energy efficiency of nearly 80%, but the overall system efficiency from raw fuel through the batteries to the converted ac power is reduced to about 30%.

A battery's terminal voltage gradually decreases as the battery discharges due to a proportional decrease of its current. A battery capacity reduces with increasing rate of discharge, so its full capacity cannot be utilized when it discharges at high rates. On the other hand, fuel cell power plants have equally high efficiency at both partial and full loads. This feature allows the fuel cells to be able to follow a changing demand without losing efficiency.

The limited storage capacity of batteries indicates that it is impossible for them to run beyond several hours. The batteries when fully discharged need several hours to be recharged. For its use in PV power connections, it is as hard as forecasting the weather to compute the exact capacity of the batteries. In order to prevent the batteries' deep discharge and to supplement the varying PV powers on some inclement weather days, the battery capacity should be large, but that large capacity is not fully utilized on shiny days. For fuel cells, they do not contain such an operational time restriction as long as the fuel can be supplied. Thus, the fuel cell power plants can provide operational flexibility with the operators in central control centers by utilizing them efficiently. As intermediate power generation sources, fuel cell power plants may replace coal-fired or nuclear units under forced outage or on maintenance.

Storage batteries possess several benefits in peak shaving and load leveling for a power system operation. For those objectives, the batteries' discharge rate is nearly constant at rated value and their capacity can be fully utilized when designed optimally. The battery operation seems to be periodical every day; that is, it charges at system's off-peak and discharges at peak time. Therefore, the batteries can do a great job for those purposes. For the PV power backup the batteries' discharge rate is irregular and their full capacity may usually not be consumed. So, it is difficult to design an optimal capacity of the battery systems for support of the PV power variations and to economically operate them. Instead of batteries fuel cell power plants exhibit diverse operational flexibility for either a PV power backup or a support of power system operation.

CHAPTER 4

DESCRIPTION OF PV-FUEL CELL HYBRID SYSTEM

4.1 Overall View of the PV-Fuel Cell Power Plant

Figure 4.1 illustrates a simplified diagram of a grid-connected PV-fuel cell hybrid power plant including two loops of controllers; that is, a neural network controller for MPPT and a real/reactive power controller. The hybrid system consists of a photovoltaic array, a fuel cell plant and fuel reformer, and power conditioning subsystems (PCSs). The photovoltaic generator operates independently and is controlled to produce maximum available solar power. Power inverters in the PCS fulfill dc-ac power conversion by turning on and off switches according to a certain switching scheme. The neural network controller generates optimal switching signals to the power inverters for the PV array to always track the maximum power points.

The PV array, composed of a set of series-parallel connected solar cells, generates a dc power that is then converted to a useful ac power by the PCS. It acts as the interface between the photovoltaic power system and the ac utility grid. The output ac power of the PCS is provided to the utility grid through the transformer and interconnecting reactance. The neural network controller for MPPT receives as inputs the available insolation level and cell temperature. Then it sends out output switching signals to the inverters connected to the PVs, and therefore the photovoltaic generator always generates the maximum available solar power.

The fuel cell power generator is used as a supplement to the PV power plant. The fast ramping capability of the fuel cell power generation makes it be able to smooth out the PV power fluctuations owing to intermittent insolation changes. The other duty of the fuel cell power generator is to meet required real and reactive power demands of a power utility. That duty is performed in this study by the real/reactive power controller (RRPC), which consists of PI-type controllers. The fuel cell's capability for fast dynamic response is able to control real and reactive powers efficiently so that it would enhance power system stability.

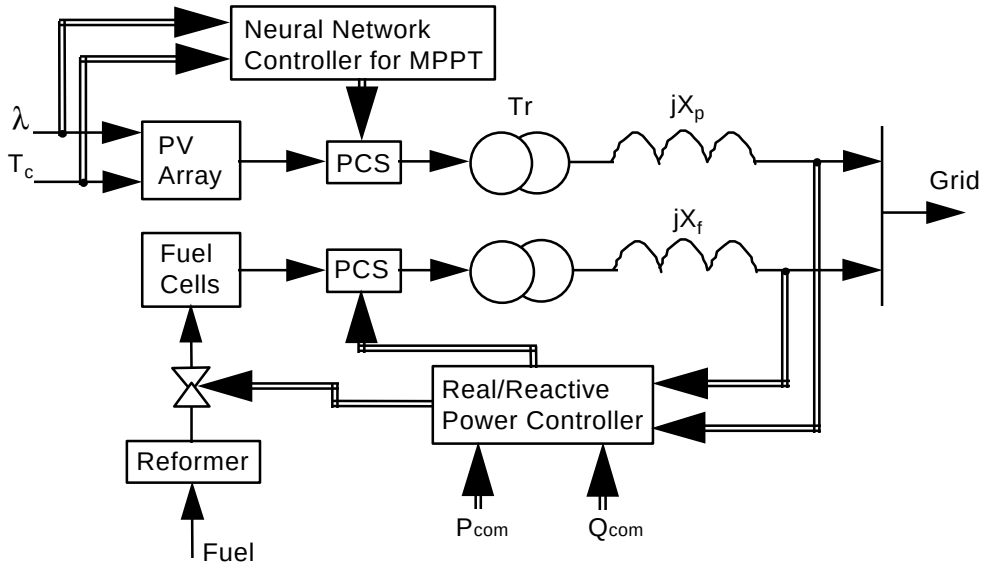

Figure 4.1. Simplified overall diagram of the PV-fuel cell hybrid system.

The fuel reformer of the fuel cell power plant processes a raw natural gas fuel through desulfurization, steam reforming and the CO shift process to produce a hydrogen-rich fuel. About 80% H_2, 20% CO_2 and a small amount of residuals are supplied to the fuel cell stacks. The reformed fuel and oxidant or O_2 provoke the electrochemical reaction inside the stacks to generate the dc power. The inputs to the RRPC are real and reactive power commands, output powers of the PV power and the fuel cell power plant.

In order to control real and reactive powers, the RRPC outputs are used as control signals to both the fuel cell stacks and the inverters. Real power control is performed by throttling the valve regulating the fuel fed into the fuel cell stacks and by adjusting the switching control scheme of the inverters connected to the fuel cell system. Reactive power is controlled by modulating the switching signals to the inverters. Effective control of reactive power in power system operation is important because it is strongly related to the transmission losses, voltage stability and control.

4.2 Detailed Descriptions of the Grid-Connected Hybrid System

A typical interconnection of the grid-connected PV power plant including two dc-ac inverters and transformers is shown in Figure 4.2. The PV array consists of ARCO solar M55 PV

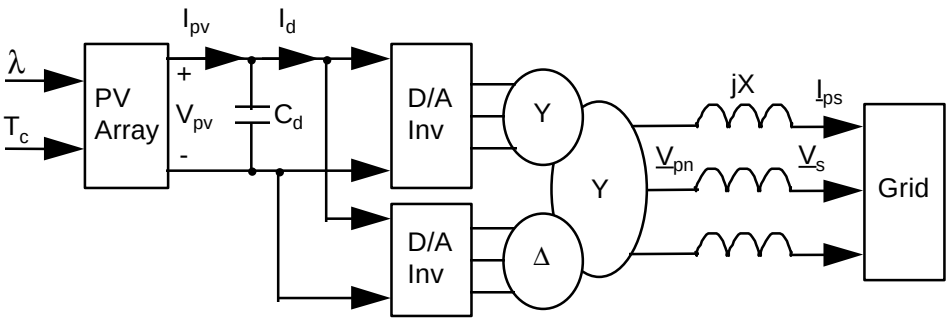

Figure 4.2. Diagram of the grid-connected PV system.

modules with 80 in series-connected and 480 in parallel-connected. It can produce 1.4MW at 700V when solar insolation is 100 mW/cm^2 and cell temperature is 25^{o}C. One M55 module composed of single-crystalline solar cells is capable of producing a maximum power of 53W at over 3A. Table 4.1 shows the power specifications of the PV module. The capacitor in parallel with the PV array operates to limit the change of the PV voltage, V_{pv}, supplied to the dc-ac inverters. The inverters comprise of two 6-switch 3-phase bridge converters. Switching signals for the inverters are generated by the neural network controller for MPPT in the PV array. The transformer setup shown in Figure 4.2 incurs the voltages behind the primary transformers phase-shifted each other by 30^o. The objective of that transformer setup is to reduce harmonics involved in the inverter output ac voltage.

A 2-MW grid-connected fuel cell power plant should accompany the PV power plant discussed above in order to satisfy the utility system's demands for real and reactive powers. Detailed diagram of the fuel cell power plant is illustrated in Figure 4.3. The fuel cell power plant consists of 8 sets (2 in series, 4 in parallel) of a 260-kW phosphoric acid fuel cell (PAFC) stack, which was developed by the Fuji and Mitsubishi companies in Japan. Each fuel cell stack is composed of 516 single cells connected in series. Key specifications of the single PAFC stack are listed in Table 4.2. The inverters, converting the fuel cell dc power to a useful ac power, have the same configuration as those in the PV system. Switching control scheme to the inverters is produced by the RRPC in the fuel cell power plant. Same as in the PV system, the phases of the voltage behind one primary transformer are shifted by 30^o from those behind the other primary transformer.

By adjusting the phases of the inverter ac voltage relative to the grid voltage, the fuel cell real power supplied to the utility grid can be controlled. In order to control the fuel cell reactive power, the magnitude of the inverter ac voltage should be manipulated.

Table 4.1 Power specifications of the single M55 PV module.*

Rated (Maximum) power	53.0 W
Optimal current	3.05 A
Optimal voltage	17.4 V
Short circuit current	3.27 A
Open circuit voltage	21.8 V
Normal operating cell temperature (NOCT)	47°C

* Whole values are at standard test conditions of:
100 mW/cm^2 insolation and 25°C cell temperature.

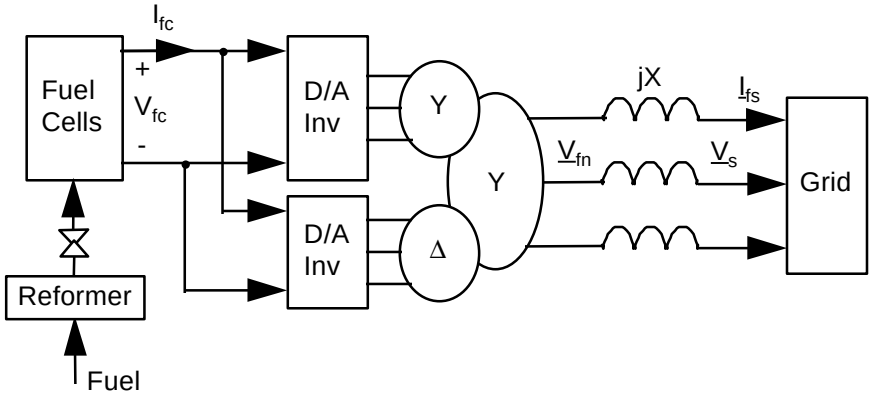

Figure 4.3 Diagram of the grid-connected fuel cell system.

When Figure 4.3 is connected with Figure 4.2 in the way shown in Figure 4.1, it will be the complete PV-fuel cell hybrid power plant. The neural network controller for MPPT will be

Table 4.2 Specifications of the single 260-kW PAFC stack.

DC output	260 kW
Rated current	200 mA/cm^2
Rated voltage	0.7 V
Operating temperature	190 ^oC
Operating pressure	4 kg/cm^2g
Cell size	3600 cm^2

applied to the PV power plant to produce its maximum available solar power and will be explained in detail in Chapter 5. To satisfy the utility system's demands for real and reactive powers, the real/reactive power controller is applied to the fuel cell power plant and will be explained in Chapter 6.

CHAPTER 5

NEURAL NETWORK CONTROLLER FOR MPPT

5.1 Neural Network (NN) Controller of the PV Power Plant

Photovoltaic power generation requires so much larger initial cost compared to other power generation sources that it is imperative to extract as much available solar energy as possible from the PV array. Otherwise, the system would lose valuable solar energy. Maximum power output of the PV array changes when solar insolation, temperature, and (or) load levels vary. Control is, therefore, needed for the PV generator to always keep track of the maximum power points. Trajectory of those maximum power points has been drawn in Figure 2.2 in Chapter 2. By controlling the switching scheme of the inverters connected to the PVs the maximum power points of the PV array can always be tracked.

Such a controller is implemented by a neural network approach in this study. Nonlinear I-V characteristics of a PV module match very well to a neural network application. In Figure 5.1, a multilayer feedforward perceptron-type NN is proposed for the MPPT control. The network consists of an input layer, one hidden layer and an output layer. The numbers of neurons in the input, hidden and output layers are two, four and two, respectively. The number of neurons in the hidden layer would be determined by trial and error. The neurons in the input layer of the neural network get the input signals from the measurement of insolation and cell temperature. The neurons in the hidden layer receive data from the input layer, calculate their outputs using the sigmoid activation function, and then pass them to the neurons in the output layer. The sigmoid function is written as

$$f(x) = \frac{1}{1+e^{-x}} \tag{5.1}$$

The neural network outputs are the data values of the neurons in the output layer.

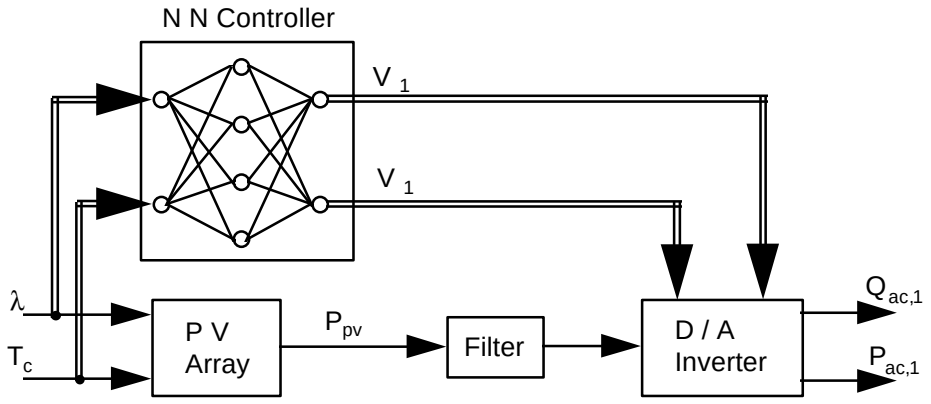

Figure 5.1. Neural network controller for MPPT in the PV array.

The neural network, using solar insolation and cell temperature as the inputs, generates switching control signals to the dc-ac inverters. The network outputs are used to adjust the inverters' switching scheme. Thus, the PV system not only provides its maximum available power to the utility grid but also maintains its reactive power transferred to the utility to be constant. In this study that reactive power reference value is set to be zero.

In the training process of the neural network, a set of input-output training data is needed. These training data can be obtained from the characteristics of the solar cells and the interconnected system values. The set of input-output training data consists of 595 patterns. Insolation values range from 10 mW/cm^2 to 112 mW/cm^2 by an increase of 3 mW/cm^2 and cell temperatures range from -20 ^{o}C to 60 ^{o}C by 5 ^{o}C.

Following are the derivations for the equations of the output training values ($V_{\delta 1}$ and $V_{\phi 1}$), which are the switching control signals to the inverters. From the condition that the PV reactive power supplied to the utility grid is zero and from Equation (5.22),

$$V_s = V_{pn} \cos\phi_{pn} \tag{5.2}$$

And from Equation (5.19), the magnitude of the line current injected into the grid is written as

$$I_{ps} = \frac{1}{\sqrt{3}X}\sqrt{V_{pn}{}^2 + V_s^2 - 2V_{pn}V_s \cos\phi_{pn}} \tag{5.3}$$

Substituting Equation (5.2) into Equation (5.3),

$$I_{ps} = \frac{1}{\sqrt{3}X}\sqrt{V_{pn}{}^2 - V_s^2} \tag{5.4}$$

From the condition that the power generated in the PV array, P_{pv}, is the same as the power behind the secondary transformer, and substituting Equation (5.4) into the following power equation,

$$\begin{aligned} P_{pv} &= \sqrt{3}V_{pn}I_{ps} \\ &= \frac{1}{X}V_{pn}\sqrt{V_{pn}{}^2 - V_s^2} \end{aligned} \tag{5.5}$$

When the equation for V_{pn} is derived from the above equation,

$$V_{pn} = \{\frac{V_s^2 + \sqrt{V_s^4 + 4X^2P_{pv}{}^2}}{2}\}^{\frac{1}{2}} \tag{5.6}$$

From Equation (5.15), one control variable, $V_{\delta 1}$, to the inverters is calculated as

$$V_{\delta 1} = cos\delta_1 = \frac{\pi V_{pn}}{4\sqrt{2}NV_{pv}\,cos15^o} \tag{5.7}$$

and from Equation (5.2), the other control variable, $V_{\phi 1}$, to the inverters can be written as

$$V_{\phi 1} = cos\phi_{pn} = \frac{V_s}{V_{pn}} \tag{5.8}$$

Updating the weights of the neural network is performed using the error backpropagation algorithm with the steepest descent method. That algorithm tries to minimize the sum of the mean squared errors represented in the following equation.

$$e = \tfrac{1}{2}\sum_{i=1}^{T}(v(i) - o(i))^2 \tag{5.9}$$

where $v(i)$: the i-th target output for the network.
$o(i)$: the computed output in the output layer.
T : the total number of training patterns.

5.2 Computer Model of the MPPT Control System

Overall dynamics of the grid-connected PV power plant are investigated via an appropriate computer model of the PV array and the MPPT control system, which is illustrated in Figure 5.2. The characteristic equations of a solar cell were expressed in Equation (2.1) - (2.4) in Chapter 2. The equations said that the voltage and current of the PV module are influenced by the changes of insolation, λ, and cell temperature, T_c. According to Figure 4.2, the variations of the PV voltage, V_{pv}, across the capacitor, C_d, depend mainly on the difference between the PV current, I_{pv}, and the dc inverter current, I_d. That relationship can be denoted as the following differential equation,

$$\frac{d}{dt}V_{pv} = \frac{1}{C_d}(I_{pv} - I_d) \tag{5.10}$$

The NN, which stores two sets of weighting values and thresholds, creates appropriate switching signals to the inverters so that the PV array can always generate the maximum available solar power.

The dc-ac inverters receive those NN outputs, and provide the utility grid with a certain amount of real and reactive powers. The following derivations will explain the calculations of those powers. The ac line-to-line voltage ahead the primary Y-connected transformer, $\underline{V}_{po,A}$, and that ahead the primary Δ-connected transformer, $\underline{V}_{po,B}$, in Figure 4.2 can be calculated respectively as

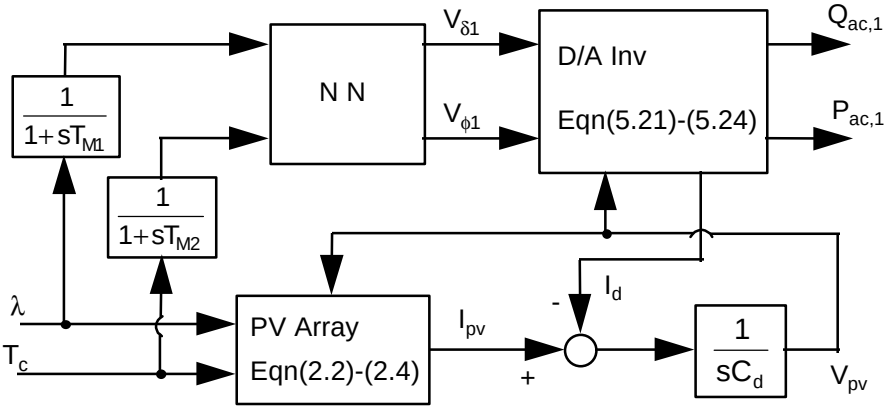

Figure 5.2 Computer model of the PV and MPPT control system.

$$\underline{V}_{po,A} = \frac{4}{\sqrt{2}\pi} V_{pv} \cos\delta_1 \angle\phi_{p1} \tag{5.11}$$

$$\underline{V}_{po,B} = \frac{4}{\sqrt{2}\pi} V_{pv} \cos\delta_1 \angle\phi_{p1} \tag{5.12}$$

where the angle δ_1 is able to control the magnitude of the above voltage and the angle ϕ_{p1} determines the phase between the above voltage and the grid reference voltage. Then, the ac line-to-line voltage behind the secondary transformer, $\underline{V}_{pn}$, is derived as

$$\underline{V}_{pn} = V_{pn} \angle\phi_{pn} \tag{5.13}$$

where

$$V_{pn} = \frac{4\sqrt{2}}{\pi} N V_{pv} \cos\delta_1 \cos 15^o \tag{5.14}$$

$$\phi_{pn} = \phi_{p1} + 15^o \tag{5.15}$$

N : turn ratio of the transformers

The angles of δ_1 and ϕ_{pn} are the control variables to the inverters behind the PV array and they are generated from the neural network controller for MPPT. The outputs of the NN are defined as

$$V_{\delta 1} = \cos\delta_1 \tag{5.16}$$

$$V_{\phi 1} = \cos\phi_{pn} \tag{5.17}$$

Next, the line current, $\underline{I}_{ps}$, injected into the utility grid is calculated as

$$\underline{I}_{ps} = \frac{\underline{V}_{pn} - \underline{V}_s}{jX} \tag{5.18}$$

$$= \frac{V_{pn}\sin(\phi_{pn} - 30^o) + V_s \sin 30^o}{\sqrt{3}X} - j\frac{V_{pn}\cos(\phi_{pn} - 30^o) - V_s \cos 30^o}{\sqrt{3}X} \tag{5.19}$$

From the following complex power equation, the real and reactive powers supplied to the utility grid from the PV power plant can be derived as

$$P_{ac,1} + jQ_{ac,1} = 3\underline{V}_s \underline{I}_{ps}^{\ *} \tag{5.20}$$

$$P_{ac,1} = \frac{1}{X}[V_s V_{pn} \sin\{\cos^{-1}(V_{\phi 1})\}] \tag{5.21}$$

$$Q_{ac,1} = \frac{1}{X}[V_s V_{pn} V_{\phi 1} - (V_s)^2] \tag{5.22}$$

Since no real power loss is assumed, the real power supplied to the grid is same as that ahead the interconnecting reactance. Taking into account the reactive power loss in the reactance, the reactive power behind the secondary transformer is calculated as

$$Q_{pn} = \frac{1}{X}[(V_{pn})^2 - V_{pn} V_s V_{\phi 1}] \tag{5.23}$$

Then the inverter dc current, I_d, can be found by equating the dc PV power and ac power behind the secondary transformer same, from which

$$I_d = \frac{1}{V_{pv}}[(P_{ac,1})^2 + (Q_{pn})^2]^{\frac{1}{2}} \tag{5.24}$$

The computer model of the MPPT control system developed in this section will be evaluated in Chapter 7 through a variety of simulations, which will cover every possible weather condition.

CHAPTER 6

REAL/REACTIVE POWER CONTROLLER (RRPC)

6.1 Real/Reactive Power Controller of the PV-Fuel Cell Hybrid System

Figure 6.1 shows voltage descriptions for the PV-fuel cell hybrid power plant connected to the power utility grid through interconnecting reactors. The currents injected into the utility grid from the PV power and the fuel cell power plants are $\underline{I}_{ps}$ and $\underline{I}_{fs}$ respectively.

$$\underline{I}_{ps} = \frac{V_{pn} \sin\phi_{pn}}{X_p} - j\frac{V_{pn}\cos\phi_{pn} - V_s}{X_p} \tag{6.1}$$

$$\underline{I}_{fs} = \frac{V_{fn} \sin\phi_{fn}}{X_f} - j\frac{V_{fn}\cos\phi_{fn} - V_s}{X_f} \tag{6.2}$$

The total real power supplied to the grid is the summation of the power from the PV array and that from the fuel cells.

$$P_{ac} = \frac{V_{pn}V_s \sin\phi_{pn}}{X_p} + \frac{V_{fn}V_s \sin\phi_{fn}}{X_f} \tag{6.3}$$

Similarly the total reactive power supplied to the grid is given as

$$Q_{ac} = \frac{V_{pn}V_s \cos\phi_{pn} - V_s^2}{X_p} + \frac{V_{fn}V_s \cos\phi_{fn} - V_s^2}{X_f} \tag{6.4}$$

If the interconnecting reactors, X_p and X_f, are assumed to be equal, the equations of (6.3) and (6.4) will be written as

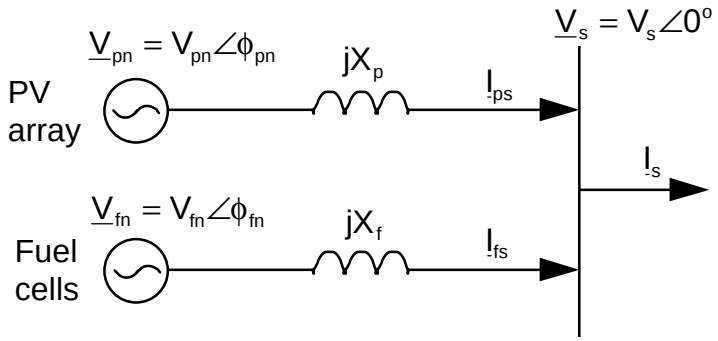

Figure 6.1. Voltage notations for the PV-fuel cell hybrid system.

$$P_{ac} = \frac{V_s}{X}(V_{pn}\sin\phi_{pn} + V_{fn}\sin\phi_{fn}) \tag{6.5}$$

$$Q_{ac} = \frac{V_s}{X}(V_{pn}\cos\phi_{pn} + V_{fn}\cos\phi_{fn}) - \frac{2V_s^2}{X} \tag{6.6}$$

Since the phase angle difference between the utility grid voltage and the inverter output voltage is small,

$$\sin\phi_{pn} \approx \phi_{pn} \tag{6.7}$$

$$\sin\phi_{fn} \approx \phi_{fn} \tag{6.8}$$

Therefore, the real power is generally controlled by variations of the phase angles. The reactive power control can be made by changes of the voltage magnitudes because the variation of $\cos\phi_{fn}$ is small.

V_{pn} and ϕ_{pn} were control variables in the PV power plant. The neural network controller for MPPT could change those control variables for maximum power point tracking of the PV array. So, those variables are regarded as non-controllable in this chapter for real and reactive power control. It is V_{fn} and ϕ_{fn} that remain the control variables in this situation.

A diagram of the real/reactive power controller in the fuel cell power plant is shown in Figure 6.2. If the RRPC operates in the reactive power control mode, the reactive power output of the PV generator, $Q_{ac,1}$, is added to $Q_{ac,2}$. The summation of those reactive power outputs is

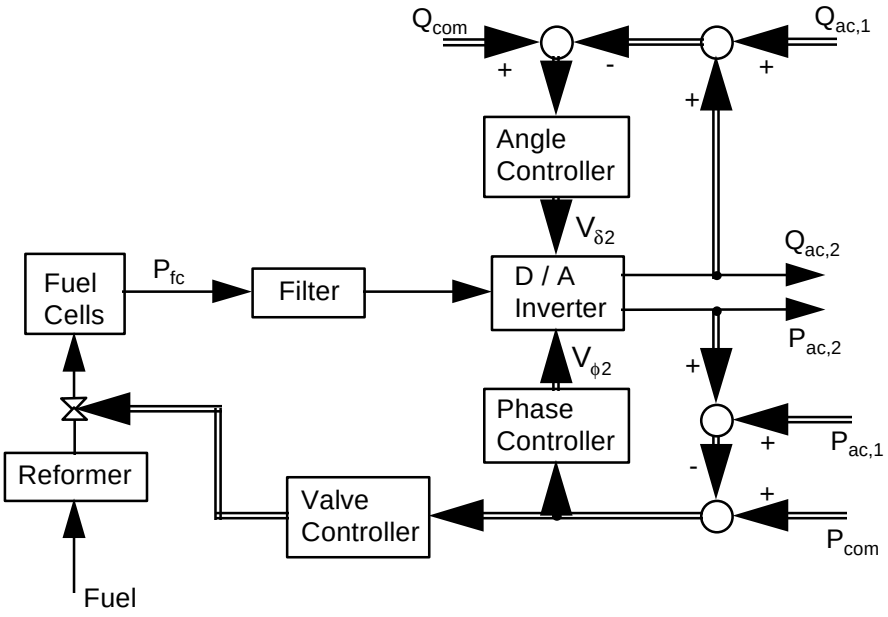

Figure 6.2 Real/reactive power control system of the fuel cell power plant.

compared to the reactive power command and the error is sent to the angle controller to generate appropriate control signals to the inverters.

If the RRPC operates in the real power control mode, the summation of $P_{ac,1}$ and $P_{ac,2}$ is compared to the real power command. Then, the error goes to the phase controller for generating the switching control signals to the inverters. The real power error is also supplied to the valve controller to control the fuel flow into the fuel cell stacks.

6.2 Computer Model of the RRPC System

Figure 6.3 illustrates a computer model of the fuel cell power and the RRPC system. The characteristic equations of a fuel cell were represented in Equation (2.12)-(2.13) in Chapter 2, which explains the important role of its electrode kinetics. Appropriate control signals for the inverters of the fuel cell power plant are generated through PI control loops to meet the system's demands for real and reactive powers. The real and reactive powers supplied to the utility grid can be calculated in the inverters using the control signals and the fuel cell voltage.

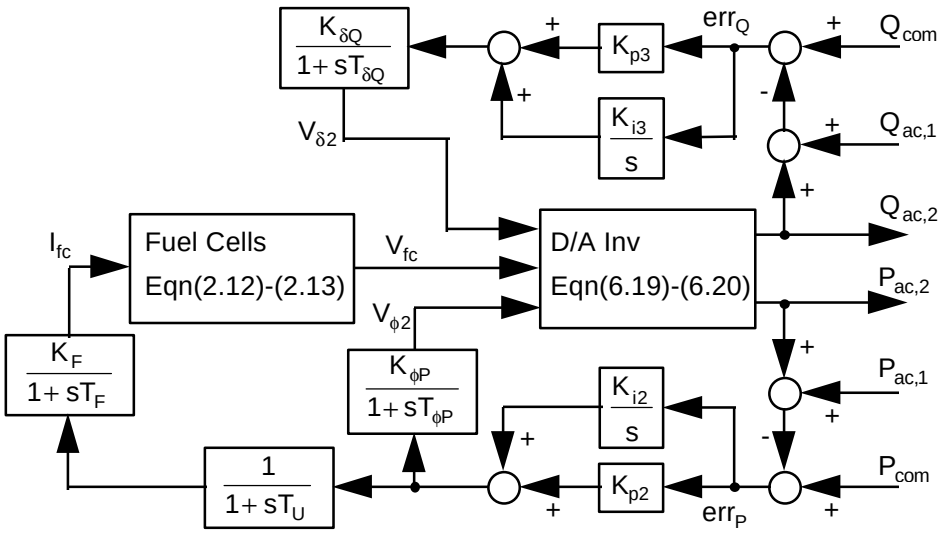

Figure 6.3 Computer model of the fuel cell plant and RRPC system.

The derivation of the power equations is mostly similar to that performed for the PV power plant in the previous chapter. The dc-ac inverters receive switching control signals from the angle controller and the phase controller, and provides the utility grid with a certain amount of real and reactive powers. The ac line-to-line voltage ahead the primary Y-connected transformer, $\underline{V}_{fo,A}$, and that ahead the primary Δ-connected transformer, $\underline{V}_{fo,B}$, in Figure 4.3 can be calculated as

$$\underline{V}_{fo,A} = \frac{4}{\sqrt{2}\pi} V_{fc} \cos\delta_2 \angle\phi_{f1} \tag{6.9}$$

$$\underline{V}_{fo,B} = \frac{4}{\sqrt{2}\pi} V_{fc} \cos\delta_2 \angle\phi_{f1} \tag{6.10}$$

where the angle δ_2 is able to control the magnitude of the above voltage and the angle ϕ_{f1} determines the phase between the above voltage and the grid reference voltage. Then, the ac line-to-line voltage behind the secondary transformer, $\underline{V}_{fn}$, can be derived as

$$\underline{V}_{fn} = V_{fn} \angle\phi_{fn} \tag{6.11}$$

where

$$V_{fn} = \frac{4\sqrt{2}}{\pi} N V_{fc} \cos\delta_2 \cos 15^o \tag{6.12}$$

$$\phi_{fn} = \phi_{f1} + 15^o \tag{6.13}$$

The angles of δ_2 and ϕ_{fn} are the control variables to the inverters behind the fuel cell stacks, and the control variables are generated from the angle controller and the phase controller. The outputs of the angle controller and the phase controller are defined, respectively, as

$$V_{\delta 2} = \cos\delta_2 \tag{6.14}$$

$$V_{\phi 2} = \cos\phi_{fn} \tag{6.15}$$

Next, the line current, $\underline{I}_{fs}$, injected into the utility grid is calculated as

$$\underline{I}_{fs} = \frac{\underline{V}_{fn} - \underline{V}_s}{jX} \tag{6.16}$$

$$= \frac{V_{fn}\sin(\phi_{fn} - 30^o) + V_s \sin 30^o}{\sqrt{3}X} - j\frac{V_{fn}\cos(\phi_{fn} - 30^o) - V_s \cos 30^o}{\sqrt{3}X} \tag{6.17}$$

From the following complex power equation, the real and reactive powers supplied to the grid from the fuel cell power plant can be derived as

$$P_{ac,2} + jQ_{ac,2} = 3\underline{V}_s \underline{I}_{fs}^{\,*} \tag{6.18}$$

$$P_{ac,2} = \frac{1}{X}[V_s V_{fn} \sin\{\cos^{-1}(V_{\phi 2})\}] \tag{6.19}$$

$$Q_{ac,2} = \frac{1}{X}[V_s V_{fn} V_{\phi 2} - (V_s)^2] \tag{6.20}$$

The computer model of the RRPC system developed in this section will be tested in Chapter 7 through a variety of simulation cases to evaluate the model's effectiveness.

CHAPTER 7

CASE STUDIES

In this chapter, the computer models of the MPPT and RRPC systems for the PV-fuel cell hybrid power plant are tested under various conditions of insolation, cell temperature, and real and reactive power commands in order to evaluate the accuracy of the models. The computer models of the MPPT control and RRPC system have been developed in Chapter 5 and Chapter 6, respectively. Computer simulations are performed on a variety of possible conditions, such as sudden decrease/increase of insolation with constant cell temperature, slow decrease/increase of insolation with constant cell temperature, variable insolation and cell temperature, and change of power commands with variable insolation and cell temperature. The first five conditions assume that real and reactive power commands are set to be constant as P_{com} = 2.3MW, Q_{com} = 0.5MVar. Simulation results show transient response of the following variables:

I_{pv} - PV array current,
V_{pv} - PV array voltage,
P_{pv} - DC power of the PV array,
$P_{ac,1}$ - PV real power supplied to the grid,
$Q_{ac,1}$ - PV reactive power supplied to the grid,
V_{fc} - fuel cell plant voltage,
I_{fc} - fuel cell plant current,
P_{fc} - DC power of the fuel cell plant,
$P_{ac,2}$ - fuel cell real power supplied to the grid,
$Q_{ac,2}$ - fuel cell reactive power supplied to the grid,
P_{ac} - total real power from the PV and fuel cell plants,
and Q_{ac} - total reactive power from the PV and fuel cell plants.

7.1 Sudden Decrease of Insolation with Constant Cell Temperature

This section shows simulation results for the computer models of the MPPT control and RRPC system under a disturbance that insolation drops suddenly with cell temperature maintained constant. Figure 7.1 illustrates that the insolation decreases from 100 mW/cm^2 to 30 mW/cm^2 in a short time. Figure 7.2 (a) - (i) show the hybrid system response subject to such a sudden change of insolation.

As the insolation decreases, the PV array current, I_{pv}, decreases correspondingly as shown in Figure 7.2 (b). Since the inverter current, I_d, in Equation (5.3) and Figure 5.2 cannot decrease instantaneously, the capacitor, C_d, in Figure 4.2 discharges to compensate for the two current difference (I_{pv} - I_d). It results in a decrease of the PV array voltage, V_{pv}. The neural network controller for MPPT responds to produce the maximum available solar power under the changed condition by generating appropriate switching signals to the inverter. Figure 7.2 (c) illustrates how well the NN controller controls the inverter for the PV array to track the peak power points. The switching signals make the ac real power, $P_{ac,1}$, of the PV plant decrease, which, then, produces a corresponding decrease of the inverter current, I_d. An equilibrium state is reached when the inverter current, I_d, is equal to the PV array current, I_{pv}.

When the insolation decreases, the PV array voltage, V_{pv}, also decreases as discussed above. Since the switching signals from the NN controller cannot be generated immediately, the magnitude of the inverter ac voltage decreases. This causes a decrease in the reactive power

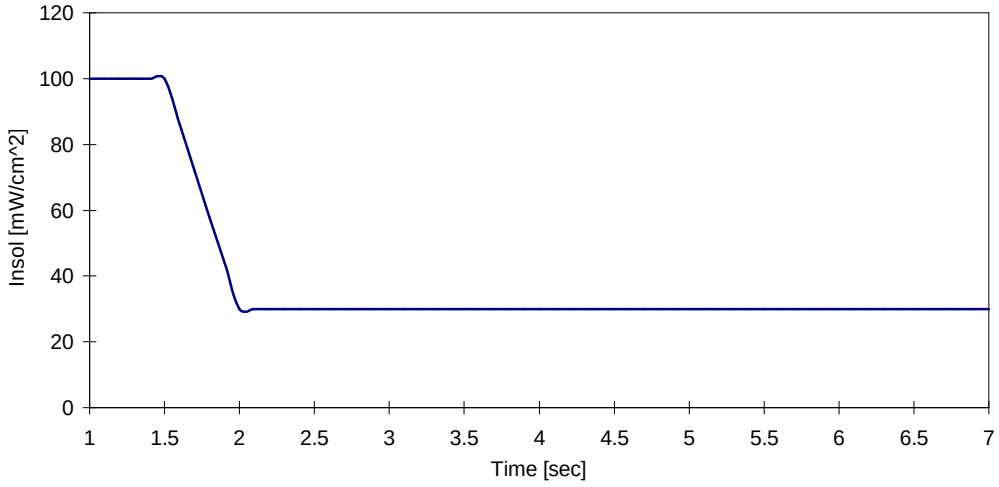

Figure 7.1 Sudden decrease of insolation from 100 mW/cm^2 to 30 mW/cm^2.

supplied to the grid from the PV power plant as shown in Figure 7.2 (d). The NN controller, then, operates to bring the reactive power back to zero, which is assumed to be the reactive power reference to the PV power station. This causes the PV array voltage, V_{pv}, to settle down to a new state. At equilibrium, the reactive power from the PV power plant is nearly equal to zero.

The changes of real and reactive powers of the PV power plant are inputs to the RRPC system of the fuel cell power plant. When the ac real power, $P_{ac,1}$, of the PV plant decreases as a result of the sharp insolation decrease, the real power error, err_P, increases. That error signal goes through the PI compensator to cause not only the fuel cell current, I_{fc}, to increase but also the output voltage of the phase controller to increase. Then the ac real power, $P_{ac,2}$, of the fuel cell plant increases to compensate for the down of the PV power. Since the response time of the fuel cell stacks is not able to follow such a sharp change of the PV power, the total ac real power, P_{ac}, from the PV and fuel cell plants experiences a great deal of changes for a short transient time as shown in Figure 7.2 (i). On the other hand, as the ac reactive power, $Q_{ac,1}$, of the PV plant decreases, the reactive power error, err_Q, increases. That error signal causes the output voltage of the angle controller to decrease so that an increase of the reactive power of the fuel cell plant can be achieved. Therefore, variations of the total ac reactive power, Q_{ac}, from the PV and fuel cell plants are small and Q_{ac} is well maintained at the reactive power command, Q_{com}.

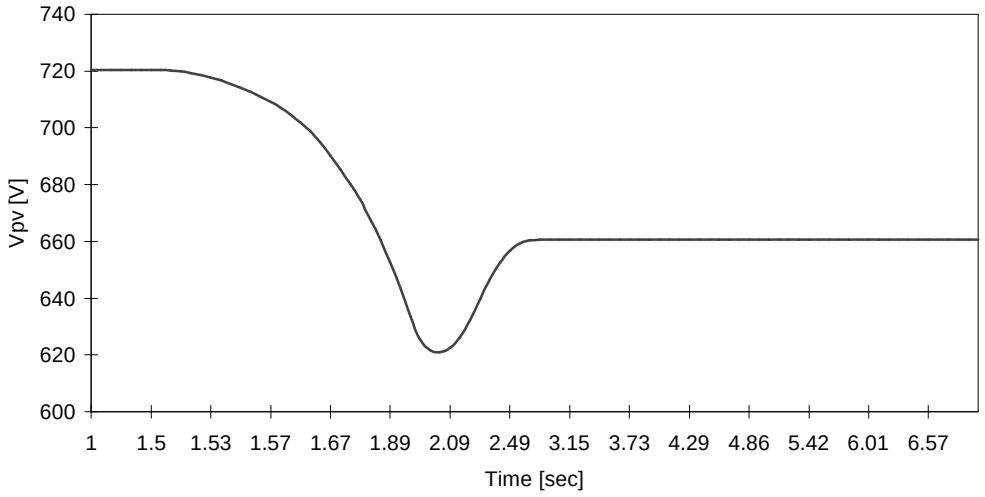

Figure 7.2 (a) Transient response of the PV array voltage (V_{pv}) for sudden insolation decrease from 100mW/cm^2 to 30mW/cm^2.

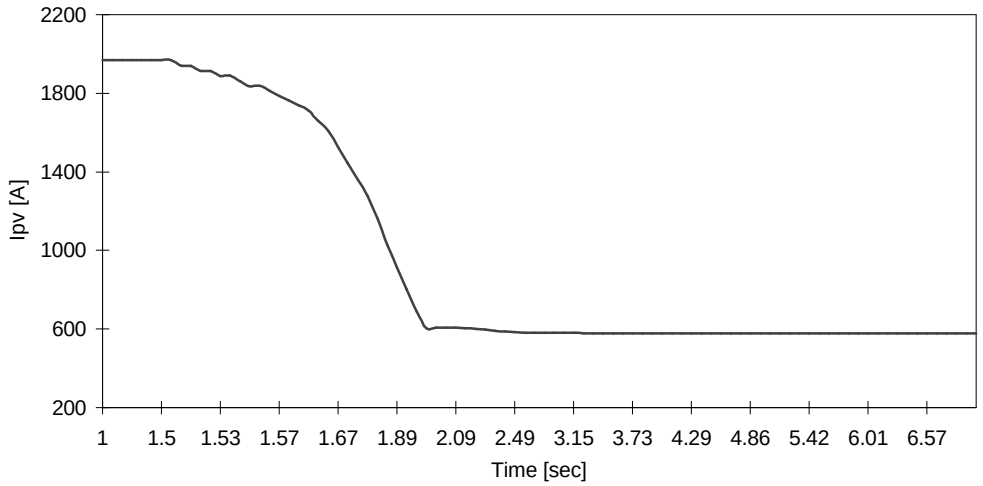

Figure 7.2 (b) Transient response of the PV array current (I_{pv}) for sudden insolation decrease from 100mW/cm^2 to 30mW/cm^2.

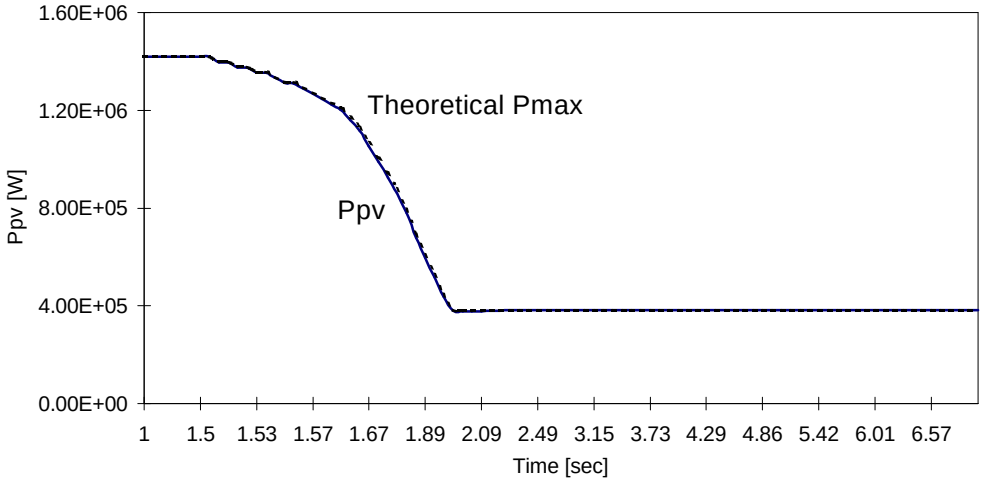

Figure 7.2 (c) Transient response of the PV array DC power (P_{pv}) for sudden insolation decrease from 100mW/cm^2 to 30mW/cm^2.

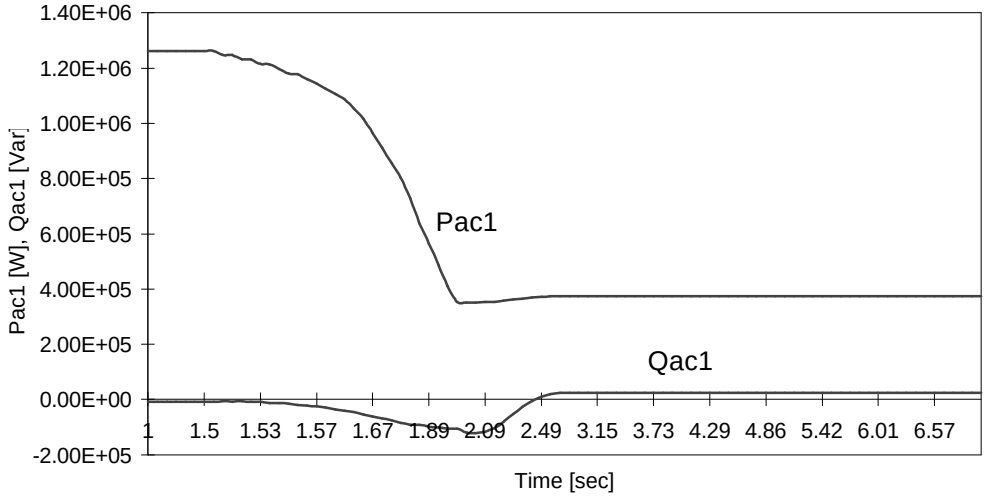

Figure 7.2 (d) Transient response of the PV array power (P_{ac1}, Q_{ac1}) supplied to the grid for sudden insolation decrease from 100mW/cm^2 to 30mW/cm^2.

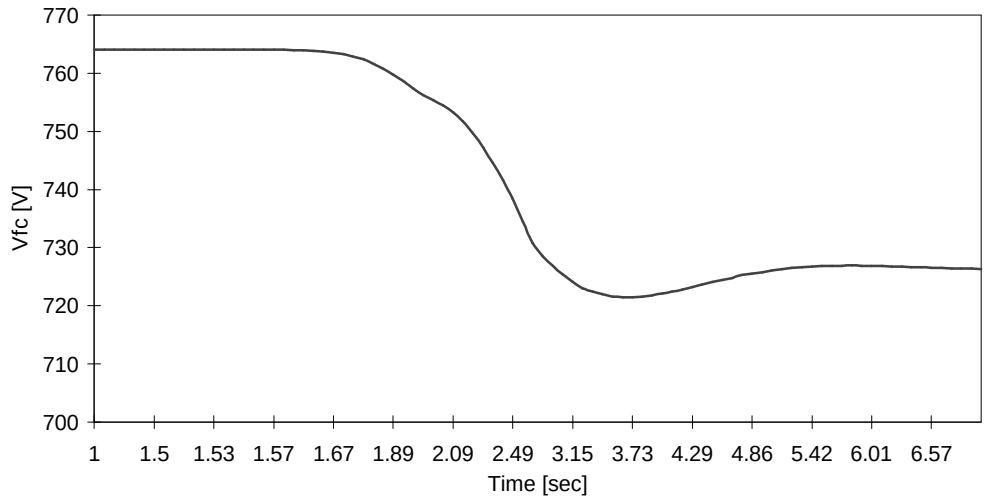

Figure 7.2 (e) Transient response of the fuel cell voltage (V_{fc}) for sudden insolation decrease from 100mW/cm^2 to 30mW/cm^2.

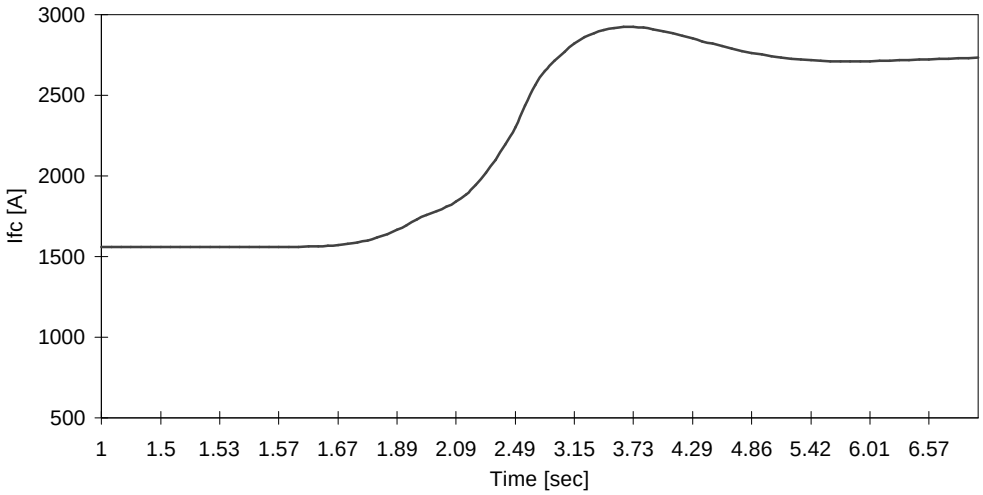

Figure 7.2 (f) Transient response of the fuel cell current (I_{fc}) for sudden insolation decrease from 100mW/cm^2 to 30mW/cm^2.

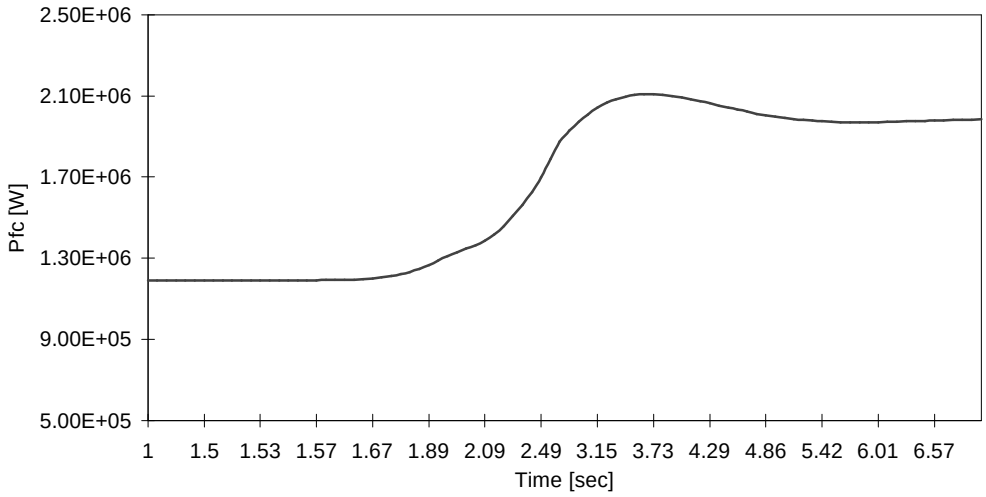

Figure 7.2 (g) Transient response of the fuel cell DC power (P_{fc}) for sudden insolation decrease from 100mW/cm^2 to 30mW/cm^2.

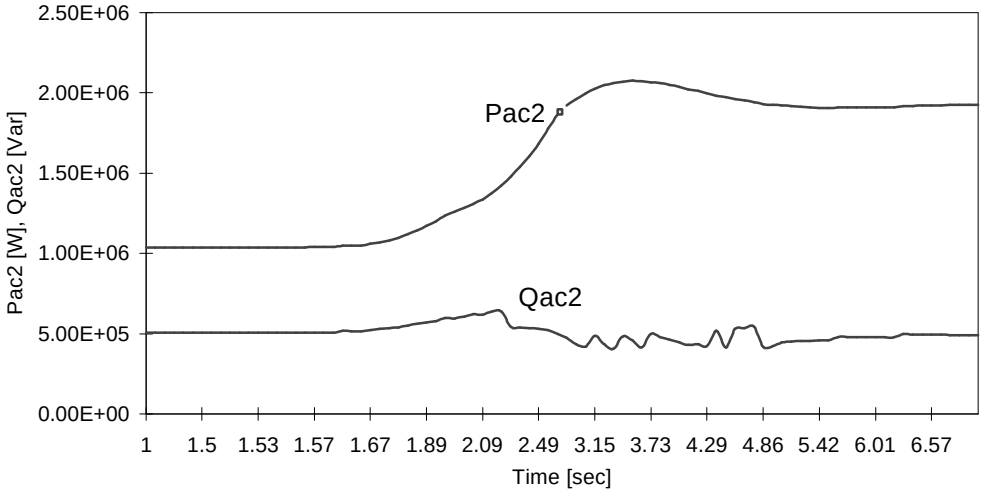

Figure 7.2 (h) Transient response of the fuel cell power (P_{ac2}, Q_{ac2}) supplied to the grid for sudden insolation decrease from 100mW/cm^2 to 30mW/cm^2.

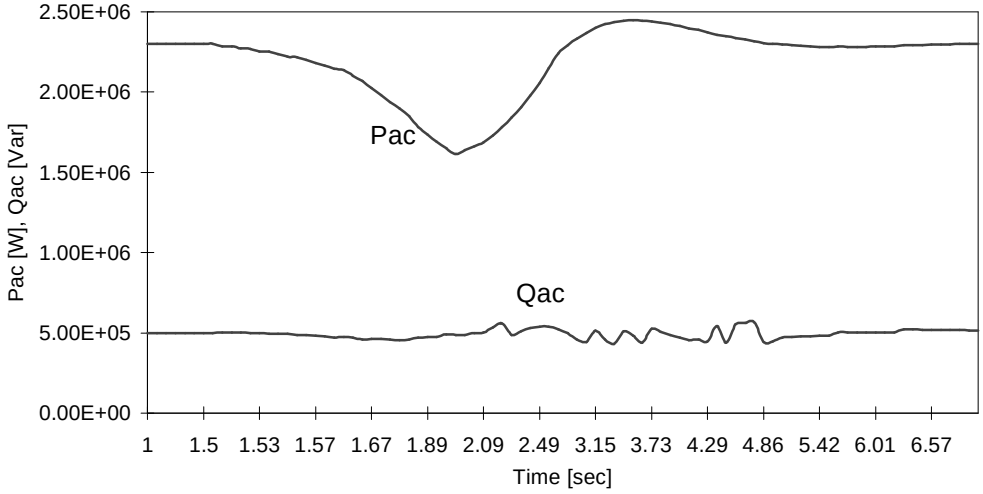

Figure 7.2 (i) Transient response of the total power (P_{ac}, Q_{ac}) supplied to the grid for sudden insolation decrease from 100mW/cm^2 to 30mW/cm^2.

7.2 Slow Decrease of Insolation with Constant Cell Temperature

This section shows simulation results for the developed computer models under a slow decrease of insolation while cell temperature is maintained constant. That slow insolation decrease from 100mW/cm^2 to 30mW/cm^2 is illustrated in Figure 7.3. Figure 7.4 (a) - (i) show the hybrid system response following such a slow change of insolation. Whole variables discussed in this section have the same trend of variations when compared with the results of the previous section, but the changes progress slowly owing to the slowly varying insolation.

As the insolation decreases slowly, the PV array current, I_{pv}, also decreases steadily. The capacitor, C_d, in Figure 4.2 discharges slowly because the difference between the array current, I_{pv}, and the PV inverter current, I_d, is small. Therefore, the PV array voltage decreases smoothly, so it does not shape undershoot while it did in Figure 7.2 (a), where it resulted from the sharp insolation decrease. The neural network controller for MPPT responds to produce the maximum available solar power by generating appropriate switching signals to the inverter. The switching signals make the ac real power, $P_{ac,1}$, of the PV plant decrease slowly, which produces a corresponding decrease of the inverter current, I_d. An equilibrium state is reached when the inverter current, I_d, is equal to the PV array current, I_{pv}.

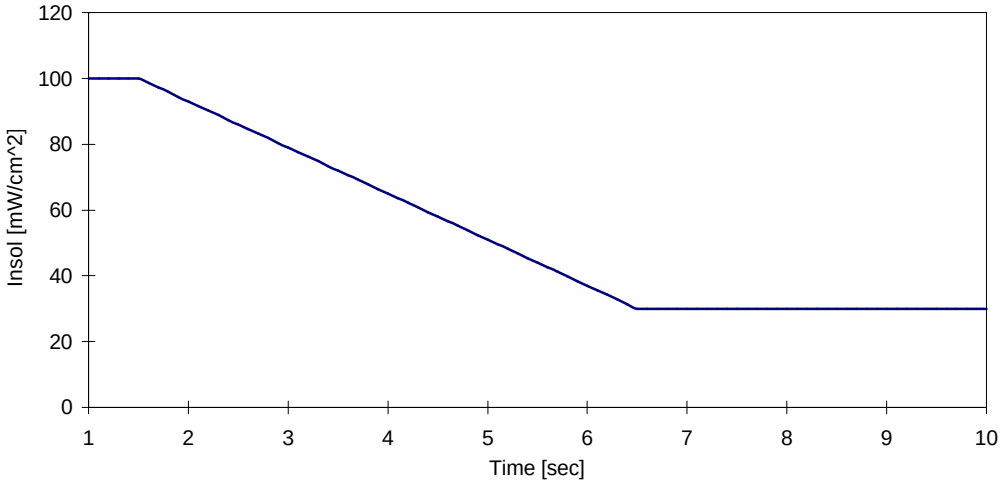

Figure 7.3 Slow decrease of insolation from 100 mW/cm^2 to 30 mW/cm^2.

When the insolation decreases slowly, the PV array voltage, V_{pv}, also decreases as discussed above. Since the switching signals from the NN controller can nearly catch up with the slowly varying insolation, the decrease of the inverter ac voltage is very small. This causes the PV reactive power supplied to the grid from the PV power plant to decrease a little as shown in Figure 7.4 (d) compared with Figure 7.2 (d). The NN controller operates to bring the reactive power back to zero, so equilibrium can be achieved.

When the ac real power, $P_{ac,1}$, of the PV plant decreases as a result of the slow insolation decrease, the real power error, err_p, increases. That error signal goes through the PI compensator to cause not only the fuel cell current, I_{fc}, to increase but also the output voltage of the phase controller to increase. Then the ac real power, $P_{ac,2}$, of the fuel cell plant increases slowly to compensate for the down of the PV power. Since the response time of the fuel cell stacks is short enough to follow such a slow change of the PV power, the fuel cell voltage does not shape undershoot and the fuel cell current does not shape overshoot. When the response of Figure 7.4 (i) is compared with that of Figure 7.2 (i), the former does not show a sharp variation of the total real power because the insolation changes slowly. Therefore, the fuel cell power plant can accurately compensate for the PV power variations. On the other hand, as the ac reactive power, $Q_{ac,1}$, of the PV plant decreases slowly, the reactive power error, err_Q, increases. That error signal causes the output voltage of the angle controller to decrease so that an increase of the reactive power of the fuel cell plant can be achieved. Therefore, variations of the total ac reactive power, Q_{ac}, from the PV and fuel cell plants are very small and Q_{ac} is well-maintained at the reactive power command, Q_{com}.

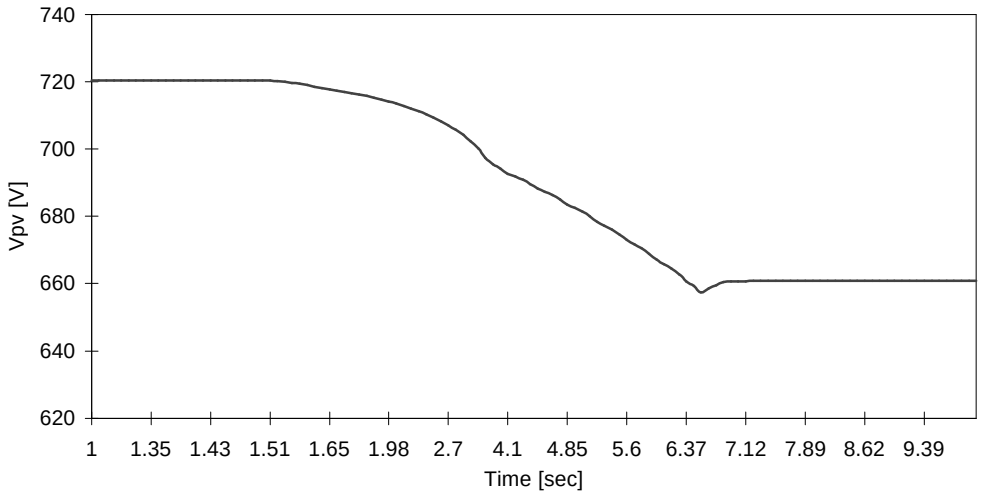

Figure 7.4 (a) Transient response of the PV array voltage (V_{pv}) for slow insolation decrease from 100mW/cm^2 to 30mW/cm^2.

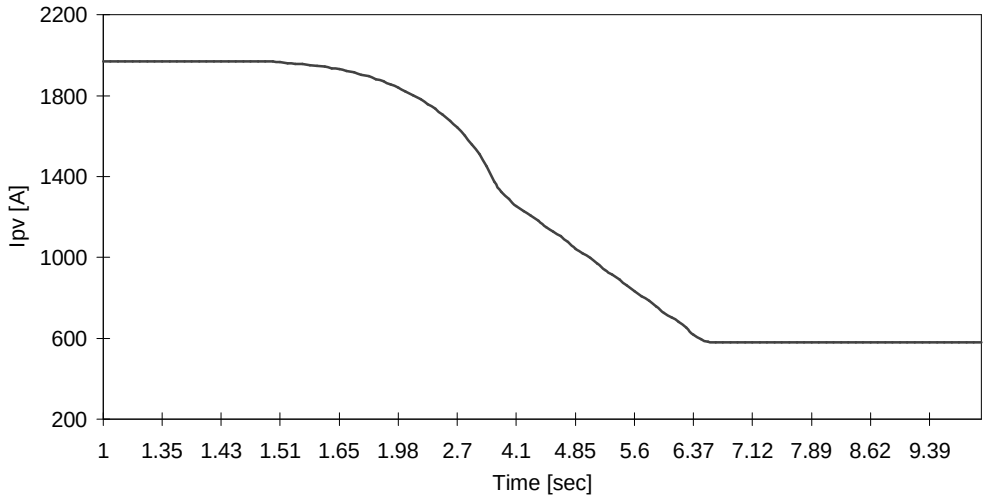

Figure 7.4 (b) Transient response of the PV array current (I_{pv}) for slow insolation decrease from 100mW/cm^2 to 30mW/cm^2.

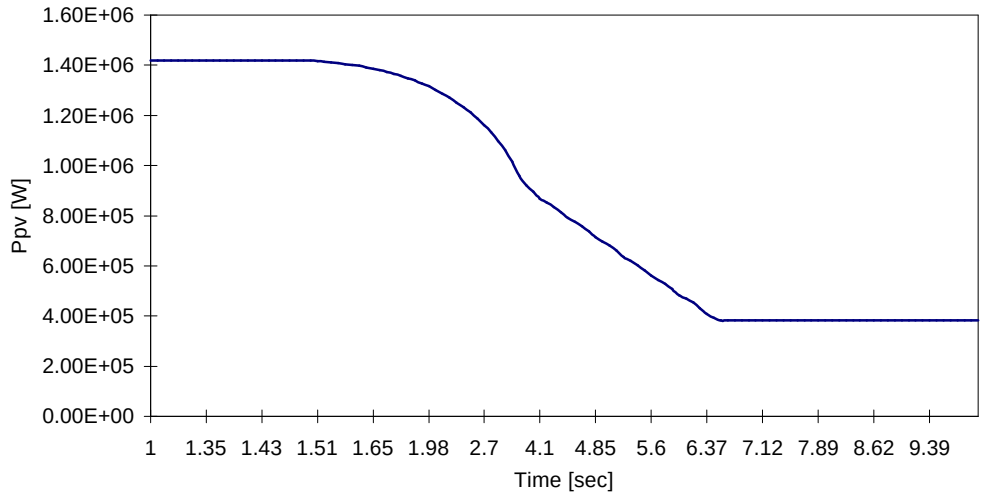

Figure 7.4 (c) Transient response of the PV array DC power (P_{pv}) for slow insolation decrease from 100mW/cm^2 to 30mW/cm^2.

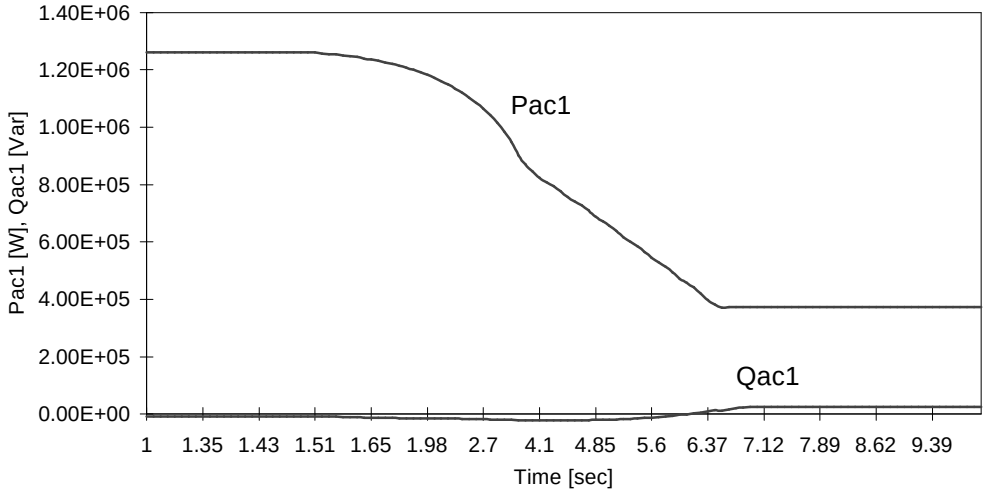

Figure 7.4 (d) Transient response of the PV array power (P_{ac1}, Q_{ac1}) supplied to the grid for slow insolation decrease from 100mW/cm^2 to 30mW/cm^2.

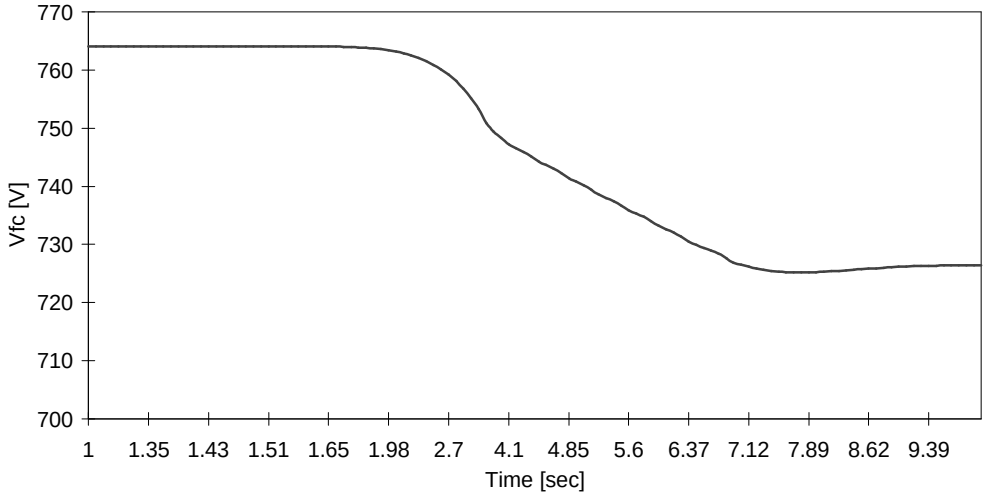

Figure 7.4 (e) Transient response of the fuel cell voltage (V_{fc}) for slow insolation decrease from 100mW/cm^2 to 30mW/cm^2.

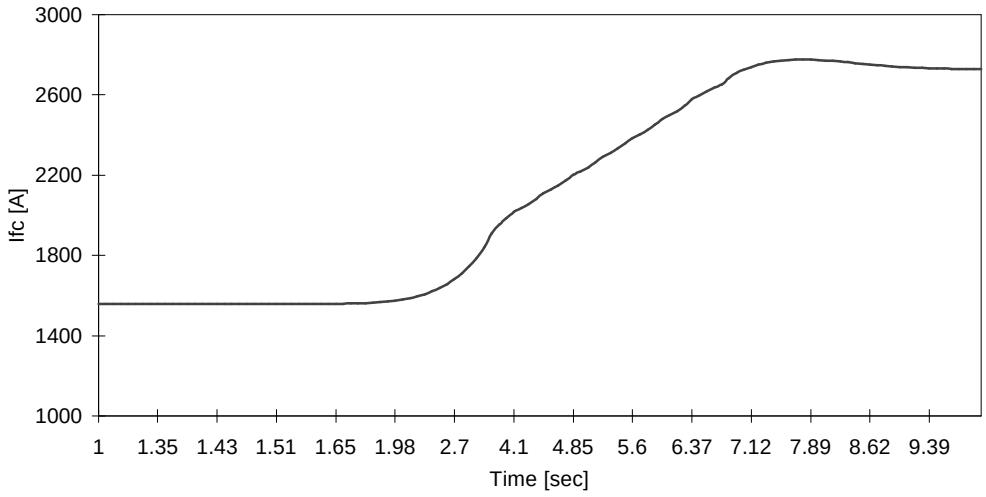

Figure 7.4 (f) Transient response of the fuel cell current (I_{fc}) for slow insolation decrease from 100mW/cm^2 to 30mW/cm^2.

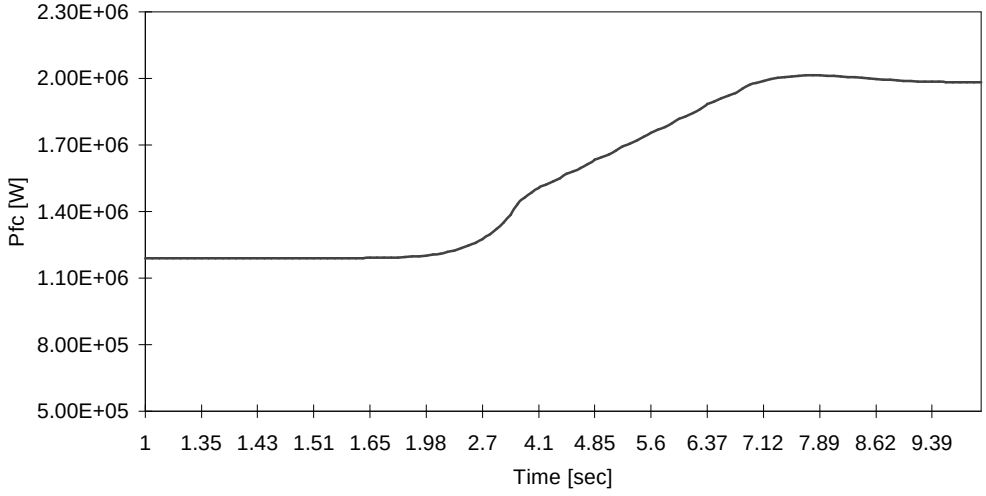

Figure 7.4 (g) Transient response of the fuel cell DC power (P_{fc}) for slow insolation decrease from 100mW/cm^2 to 30mW/cm^2.

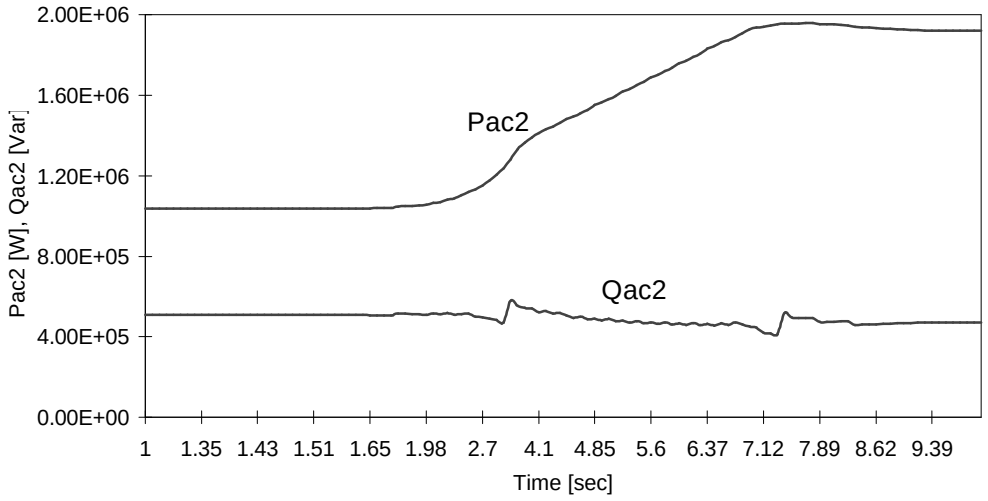

Figure 7.4 (h) Transient response of the fuel cell power (P_{ac2}, Q_{ac2}) supplied to the grid for slow insolation decrease from 100mW/cm^2 to 30mW/cm^2.

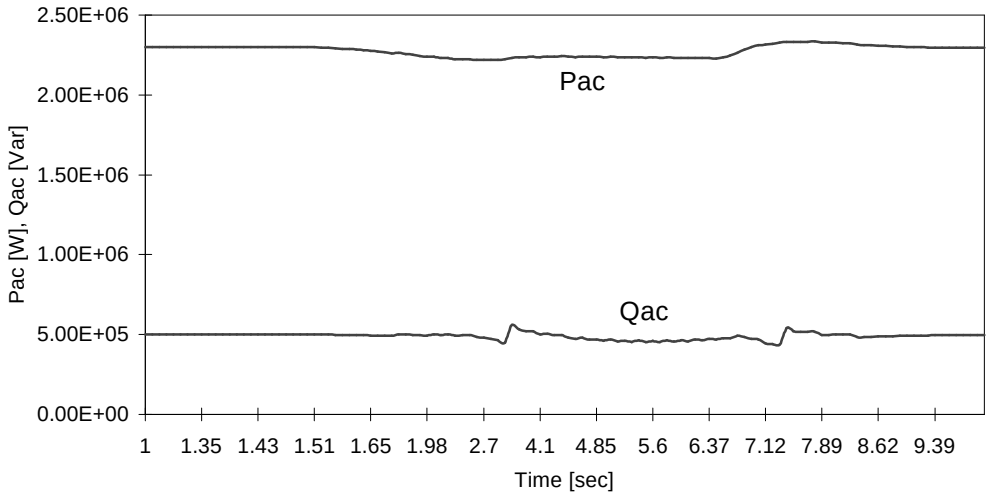

Figure 7.4 (i) Transient response of the total power (P_{ac}, Q_{ac}) supplied to the grid for slow insolation decrease from 100mW/cm^2 to 30mW/cm^2.

7.3 Sudden Increase of Insolation with Constant Cell Temperature

This section shows simulation results for the developed computer models of the MPPT control and RRPC system under a disturbance that insolation increases suddenly with cell temperature maintained constant. Figure 7.5 illustrates the insolation increase from 30mW/cm^2 to 100mW/cm^2 in a short period. Figure 7.6 (a) - (i) show the hybrid system response subject to such a sudden change of insolation.

As the insolation increases, the PV array current, I_{pv}, increases correspondingly as shown in Figure 7.6 (b). Since the inverter current, I_d, in Equation (5.3) and Figure 5.2 cannot increase instantaneously, the capacitor, C_d, in Equation 4.2 discharges to compensate for the two current difference (I_{pv} - I_d). It results in an increase of the PV array voltage, V_{pv}. The neural network controller for MPPT responds to produce the maximum available solar power under the changed condition by generating appropriate switching signals to the inverter. Figure 7.6 (c) illustrates how well the NN controller controls the inverter for the PV array to track the peak power points. The switching signals make the ac real power, $P_{ac,1}$, of the PV plant increase, which, then, produces a corresponding increase of the inverter current, I_d. An equilibrium state is reached when the inverter current, I_d, is equal to the PV array current, I_{pv}.

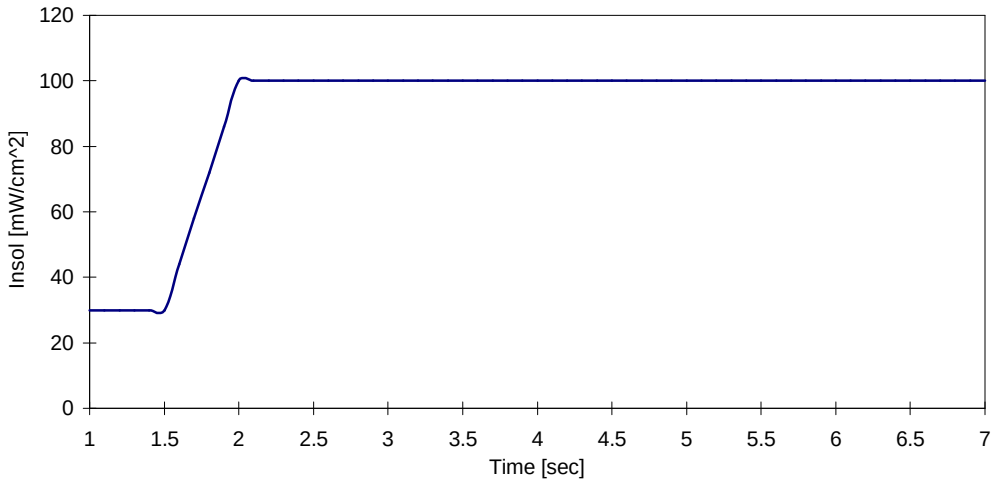

Figure 7.5 Sudden increase of insolation from 30 mW/cm^2 to 100 mW/cm^2.

When the insolation increases, the PV array voltage, V_{pv}, also increases as discussed above. Since the switching signals from the NN controller cannot be generated immediately, the magnitude of the inverter ac voltage increases. This causes an increase in the reactive power supplied to the grid from the PV power plant as shown in Figure 7.6 (d). The NN controller, then, operates to bring the reactive power back to zero. This causes the PV array voltage, V_{pv}, to settle down to a new state. At equilibrium, the reactive power from the PV power plant is nearly equal to zero.

The changes of real and reactive powers of the PV power plant are inputs to the RRPC system of the fuel cell power plant. When the ac real power, $P_{ac,1}$, of the PV plant increases as a result of the sharp insolation increase, the real power error, err_P, decreases. That error signal goes through the PI compensator to cause not only the fuel cell current, I_{fc}, to decrease but also the output voltage of the phase controller to decrease. Then the ac real power, $P_{ac,2}$, of the fuel cell plant decreases to compensate for the growth of the PV power. Since the response time of the fuel cell stacks is not able to follow such a sharp change of the PV power, the total ac real power, P_{ac}, from the PV and fuel cell plants experiences a great deal of changes for a short transient time as shown in Figure 7.6 (i). On the other hand, as the ac reactive power, $Q_{ac,1}$, of the PV plant increases, the reactive power error, err_Q, decreases. That error signal causes the output voltage of the angle controller to increase so that a decrease of the reactive power of the fuel cell plant can be achieved. Therefore, variations of the total ac reactive power, Q_{ac}, from the PV and fuel cell plants are small and Q_{ac} is well-maintained at the reactive power command, Q_{com}.

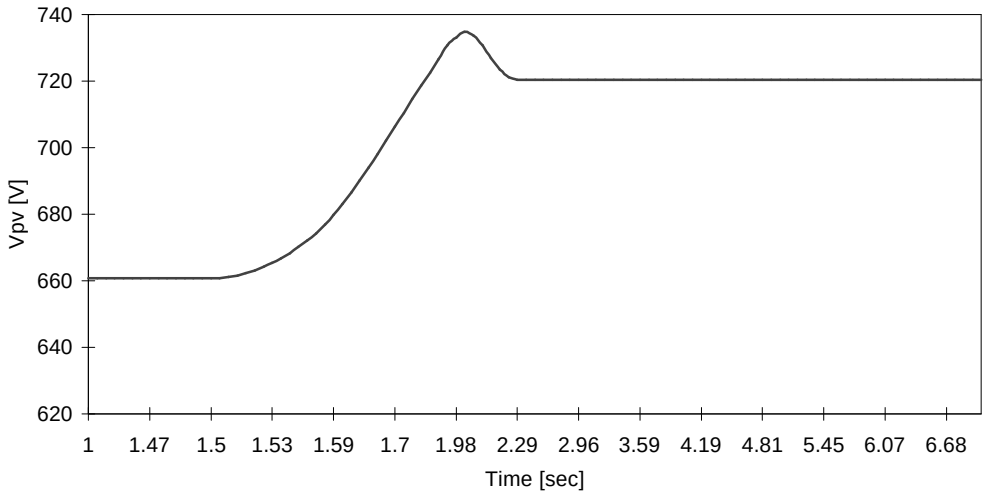

Figure 7.6 (a) Transient response of the PV array voltage (V_{pv}) for sudden insolation increase from 30mW/cm^2 to 100mW/cm^2.

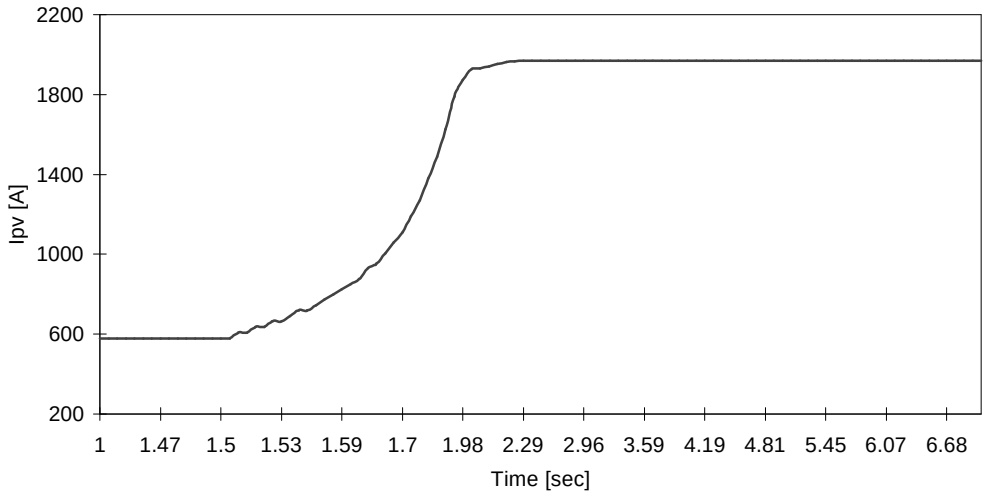

Figure 7.6 (b) Transient response of the PV array current (I_{pv}) for sudden insolation increase from 30mW/cm^2 to 100mW/cm^2.

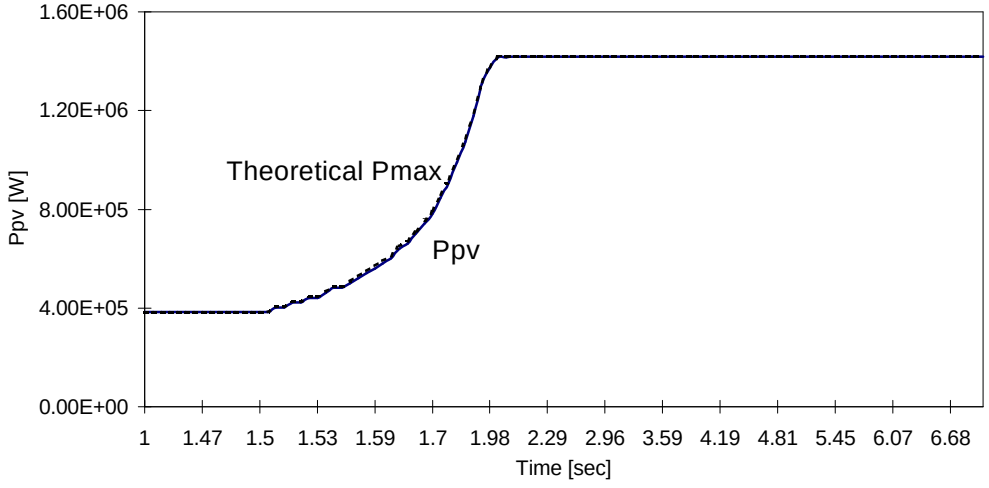

Figure 7.6 (c) Transient response of the PV array DC power (P_{pv}) for sudden insolation increase from 30mW/cm^2 to 100mW/cm^2.

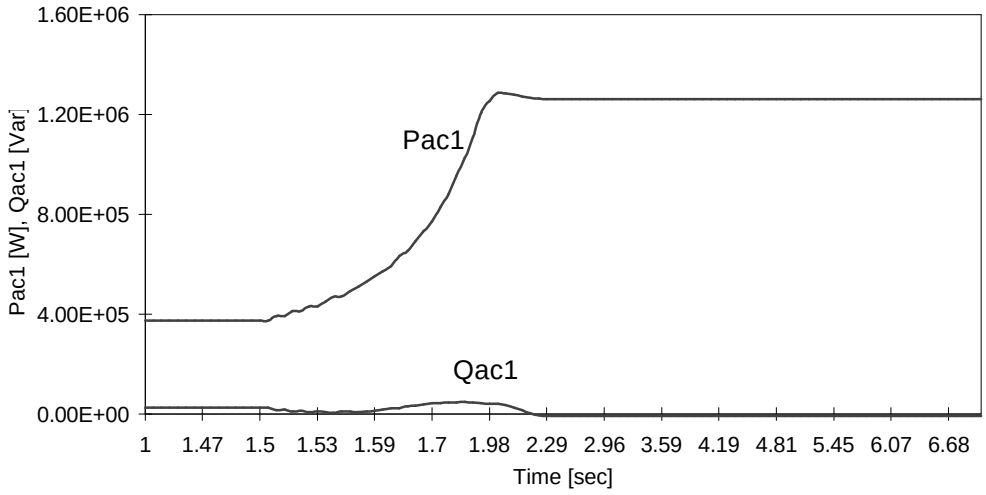

Figure 7.6 (d) Transient response of the PV array power (P_{ac1}, Q_{ac1}) supplied to the grid for sudden insolation increase from 30mW/cm^2 to 100mW/cm^2.

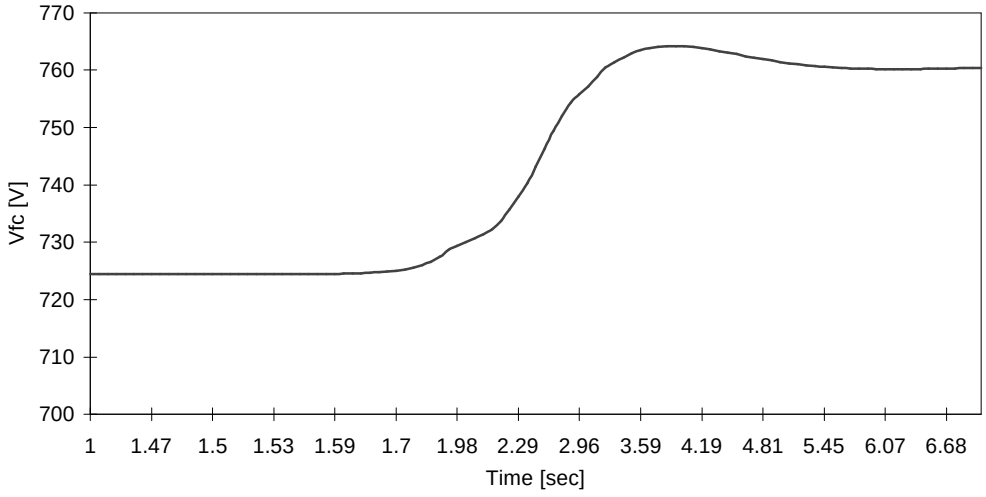

Figure 7.6 (e) Transient response of the fuel cell voltage (V_{fc}) for sudden insolation increase from 30mW/cm^2 to 100mW/cm^2.

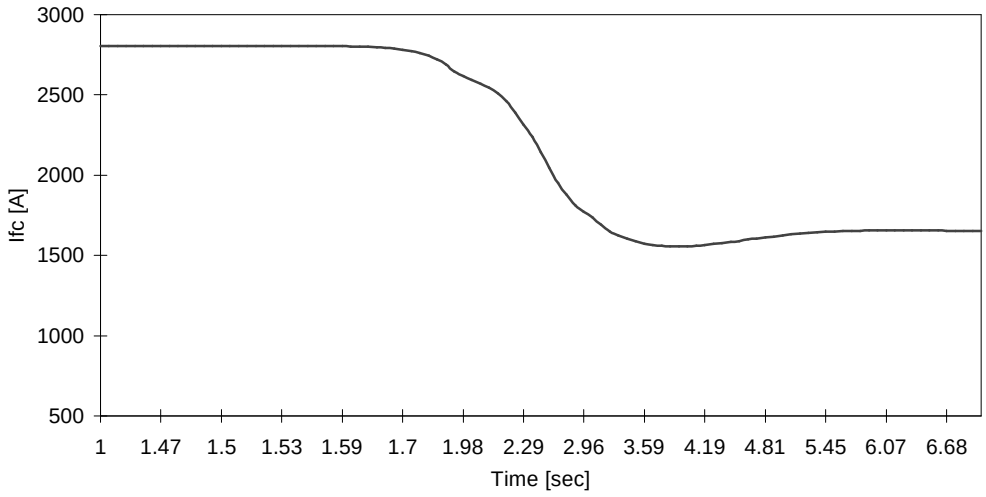

Figure 7.6 (f) Transient response of the fuel cell current (I_{fc}) for sudden insolation increase from 30mW/cm^2 to 100mW/cm^2.

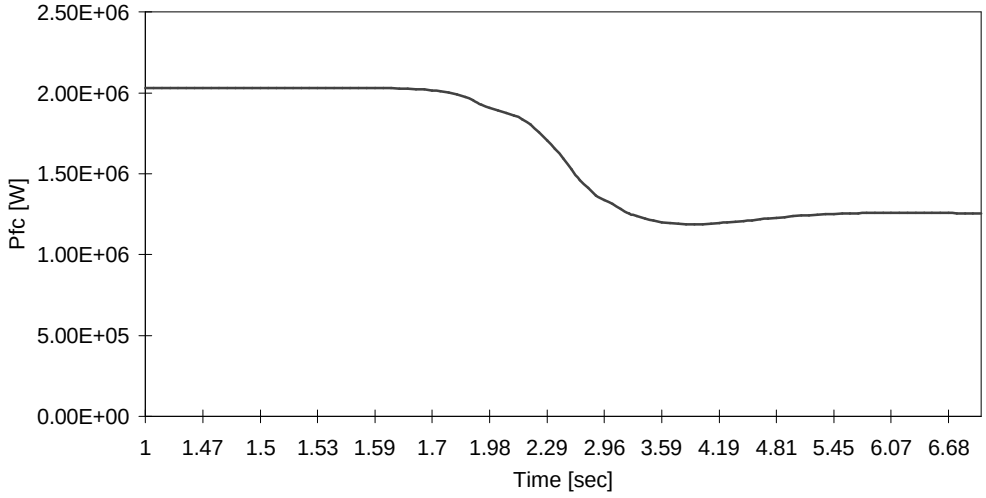

Figure 7.6 (g) Transient response of the fuel cell DC power (P_{fc}) for sudden insolation increase from 30mW/cm^2 to 100mW/cm^2.

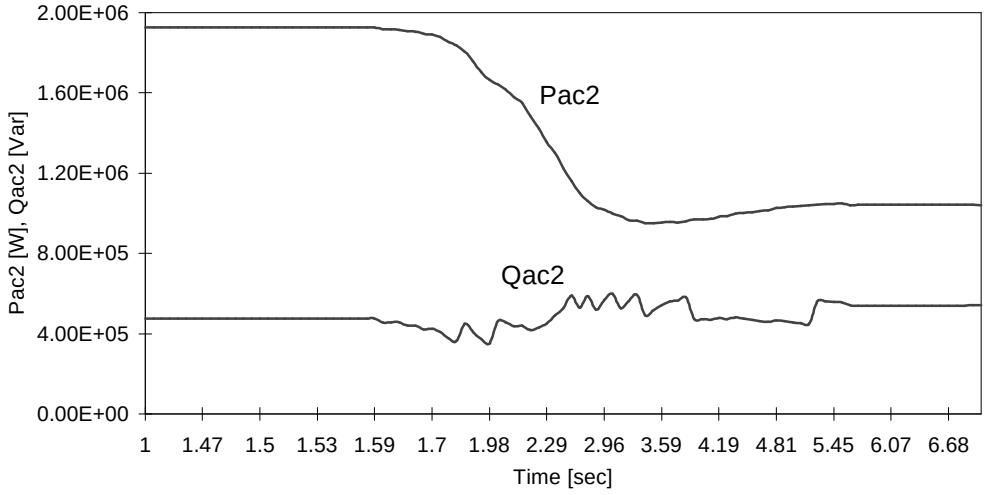

Figure 7.6 (h) Transient response of the fuel cell power (P_{ac2}, Q_{ac2}) supplied to the grid for sudden insolation increase from 30mW/cm^2 to 100mW/cm^2.

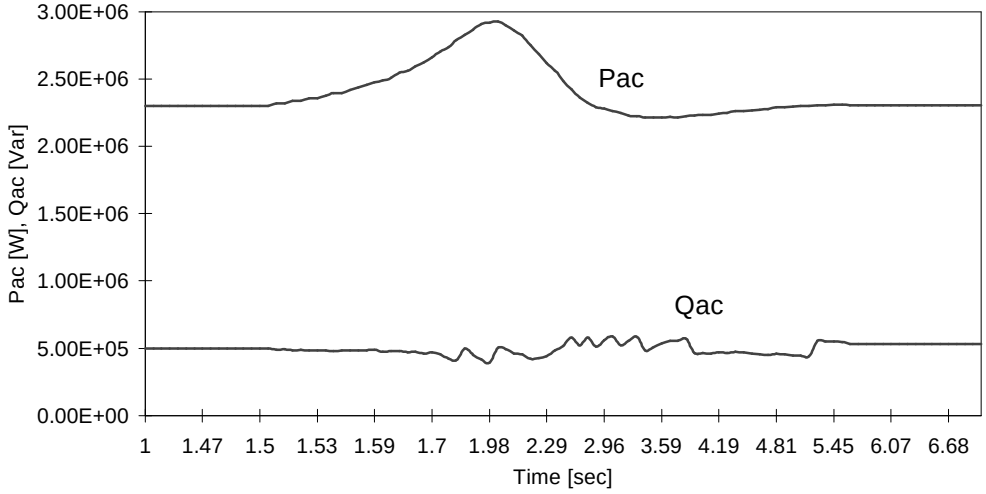

Figure 7.6 (i) Transient response of the total power (P_{ac}, Q_{ac}) supplied to the grid for sudden insolation increase from 30mW/cm^2 to 100mW/cm^2.

7.4 Slow Increase of Insolation with Constant Cell Temperature

This section shows simulation results for the developed computer models under a slow increase of insolation while cell temperature is maintained constant. That slow insolation increase from 30mW/cm^2 to 100mW/cm^2 is illustrated in Figure 7.7. Figure 7.8 (a) - (i) show the hybrid system response following such a slow change of insolation. Whole variables discussed in this section have the same trend of variations when compared with the results of the previous section, but the changes progress slowly owing to the slowly varying insolation.

As the insolation increases slowly, the PV array current, I_{pv}, also increases steadily. The capacitor, C_d, in Figure 4.2 discharges slowly because the difference between the array current, I_{pv}, and the PV inverter current, I_d, is small. Therefore, the PV array voltage increases smoothly, so it does not shape overshoot while it did in Figure 7.6 (a), where it resulted from the sharp insolation increase. The neural network controller for MPPT responds to produce the maximum available solar power by generating appropriate switching signals to the inverter. The switching signals make the ac real power, $P_{ac,1}$, of the PV plant decrease slowly, which produces a corresponding decrease of the inverter current, I_d. An equilibrium state is reached when the inverter current, I_d, is equal to the PV array current, I_{pv}.

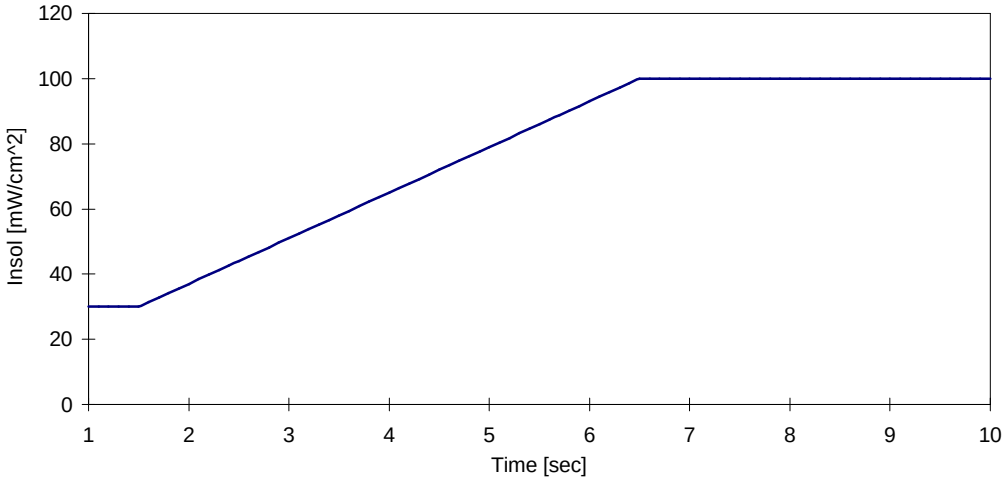

Figure 7.7 Slow increase of insolation from 30 mW/cm^2 to 100 mW/cm^2.

When the insolation increases slowly, the PV array voltage, V_{pv}, also increases as discussed above. Since the switching signals from the NN controller can nearly catch up with the slowly varying insolation, the increase of the inverter ac voltage is very small. This causes the PV reactive power supplied to the grid from the PV power plant to increase a little as shown in Figure 7.8 (d) compared with Figure 7.6 (d). The NN controller operates to bring the reactive power back to zero, so equilibrium can be achieved.

When the ac real power, $P_{ac,1}$, of the PV plant increases as a result of the slow insolation increase, the real power error, err_p, decreases. That error signal goes through the PI compensator to cause not only the fuel cell current, I_{fc}, to decrease but also the output voltage of the phase controller to decrease. Then the ac real power, $P_{ac,2}$, of the fuel cell plant decreases slowly to compensate for the growth of the PV power. Since the response time of the fuel cell stacks is short enough to follow such a slow change of the PV power, the fuel cell voltage does not shape overshoot and the fuel cell current does not shape undershoot. When the response of Figure 7.8 (i) is compared with that of Figure 7.6 (i), the former does not show a sharp variation of the total real power because the insolation changes slowly. Therefore, the fuel cell power plant can accurately compensate for the PV power variations. On the other hand, as the ac reactive power, $Q_{ac,1}$, of the PV plant increases slowly, the reactive power error, err_Q, decreases. That error signal causes the output voltage of the angle controller to increase so that a decrease of the reactive power of the fuel cell plant can be achieved. Therefore, variations of the total ac reactive power, Q_{ac}, from the PV and fuel cell plants are very small and Q_{ac} is well-maintained at the reactive power command, Q_{com}.

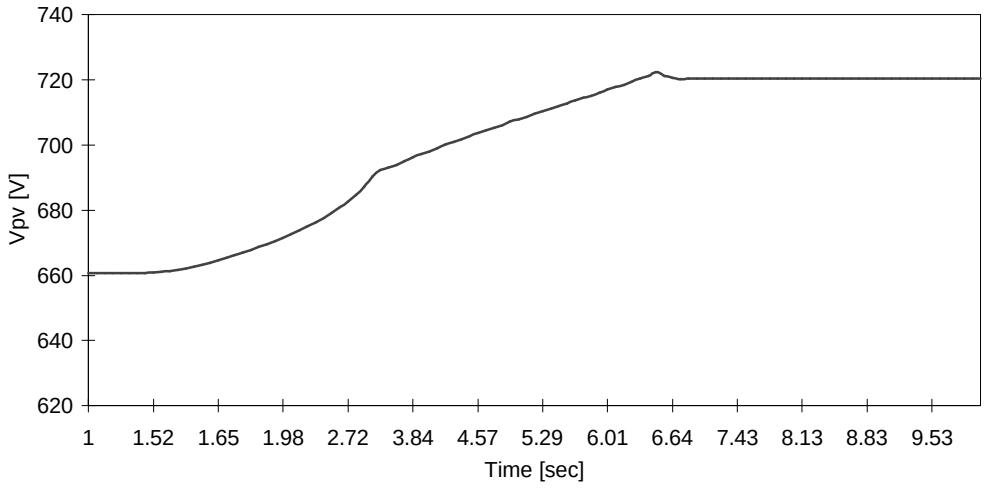

Figure 7.8 (a) Transient response of the PV array voltage (V_{pv}) for slow insolation increase from 30mW/cm^2 to 100mW/cm^2.

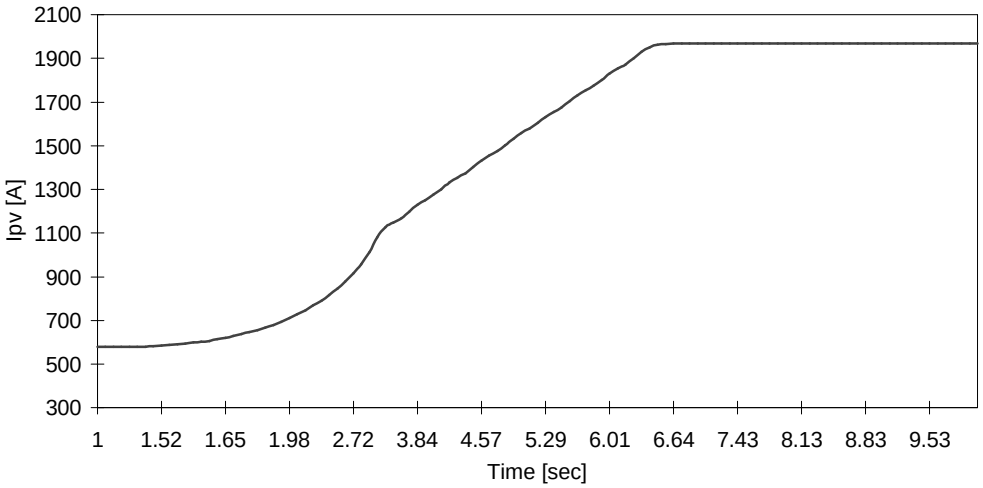

Figure 7.8 (b) Transient response of the PV array current (I_{pv}) for slow insolation increase from 30mW/cm^2 to 100mW/cm^2.

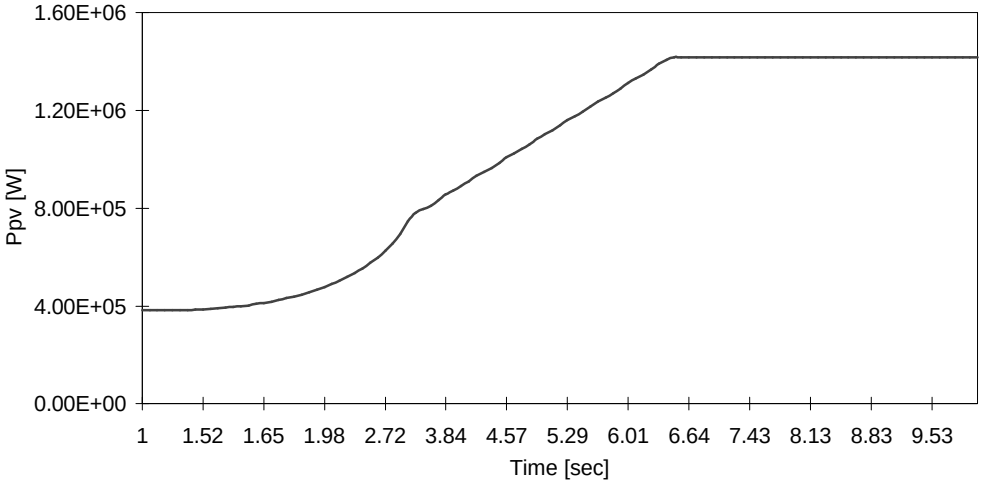

Figure 7.8 (c) Transient response of the PV array DC power (P_{pv}) for slow insolation increase from 30mW/cm^2 to 100mW/cm^2.

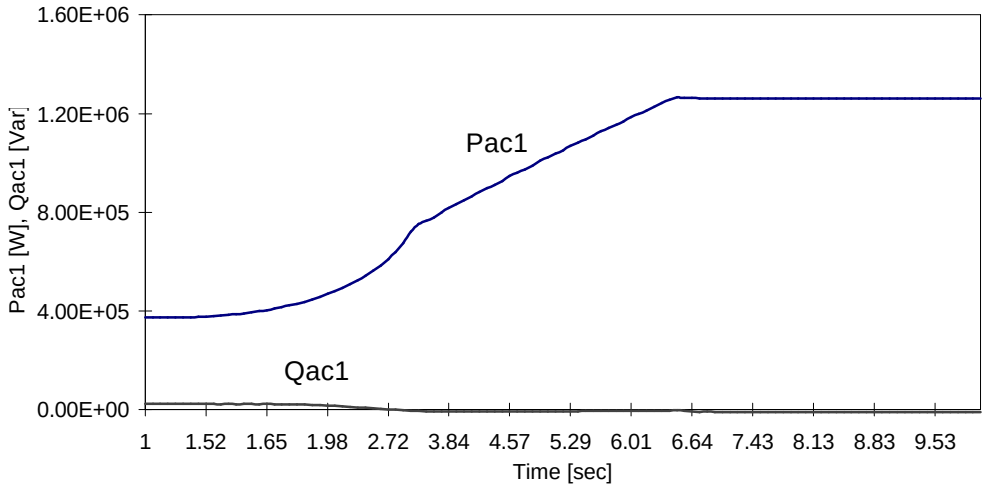

Figure 7.8 (d) Transient response of the PV array power (P_{ac1}, Q_{ac1}) supplied to the grid for slow insolation increase from 30mW/cm^2 to 100mW/cm^2.

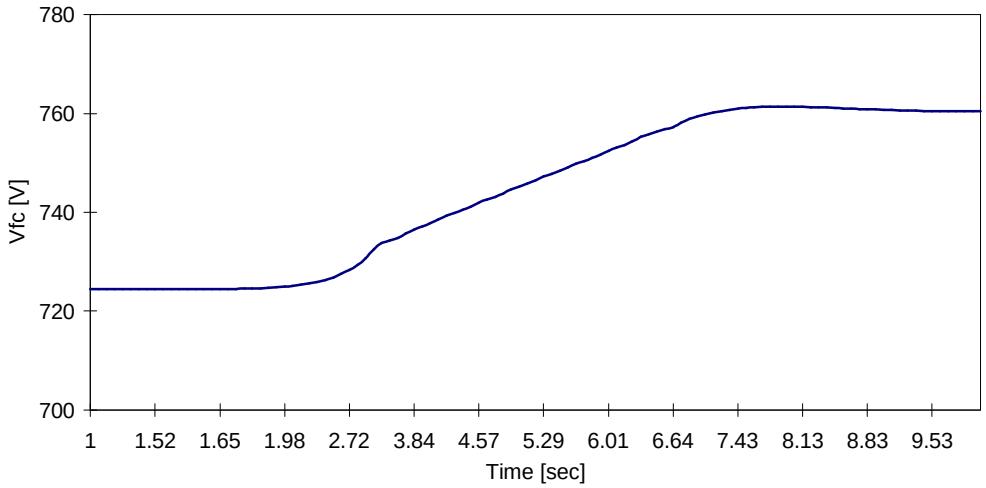

Figure 7.8 (e) Transient response of the fuel cell voltage (V_{fc}) for slow insolation increase from 30mW/cm^2 to 100mW/cm^2.

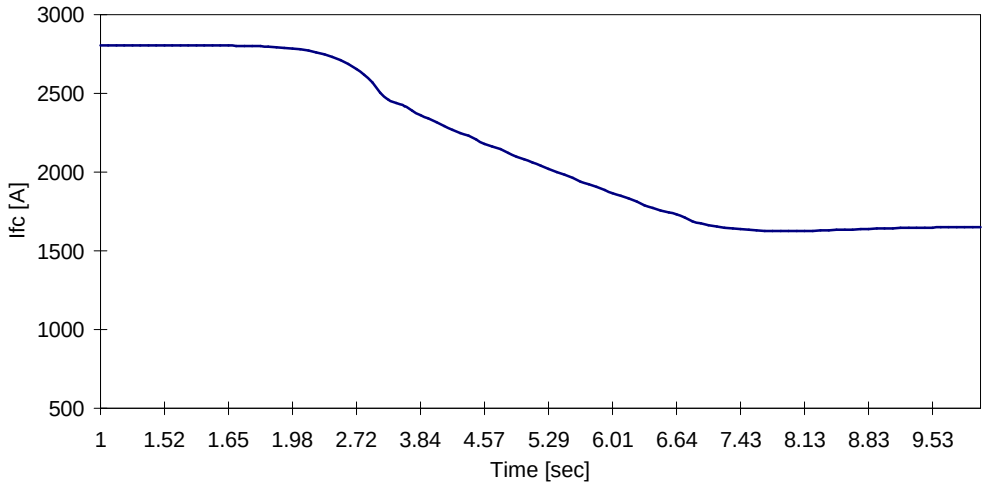

Figure 7.8 (f) Transient response of the fuel cell current (I_{fc}) for slow insolation increase from 30mW/cm^2 to 100mW/cm^2.

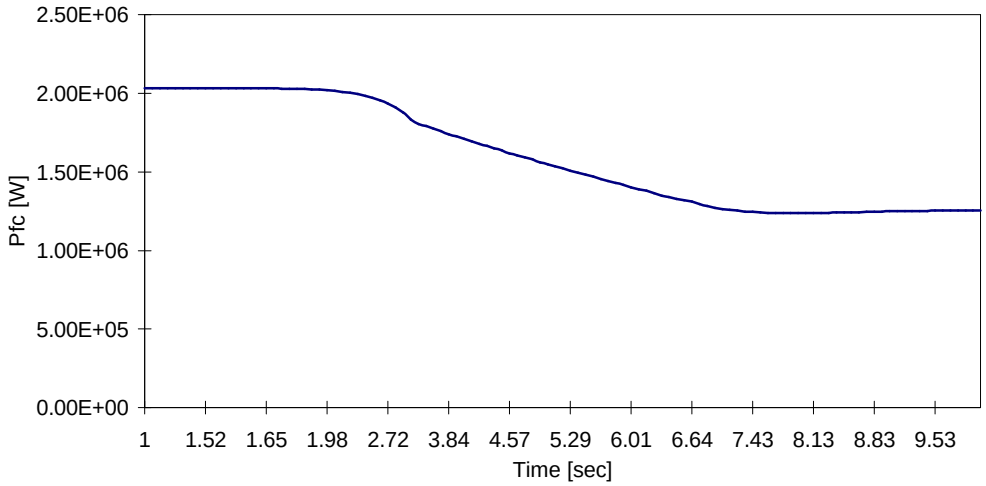

Figure 7.8 (g) Transient response of the fuel cell DC power (P_{fc}) for slow insolation increase from 30mW/cm^2 to 100mW/cm^2.

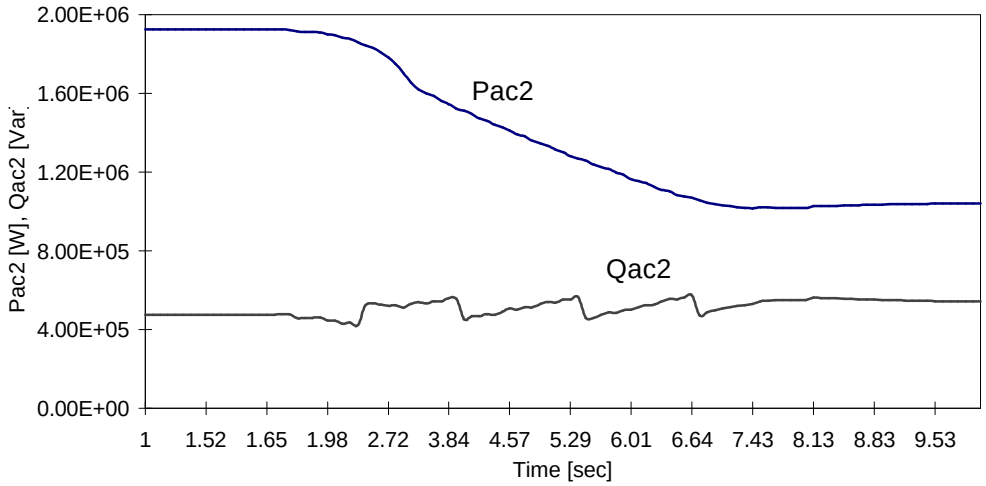

Figure 7.8 (h) Transient response of the fuel cell power (P_{ac2}, Q_{ac2}) supplied to the grid for slow insolation increase from 30mW/cm^2 to 100mW/cm^2.

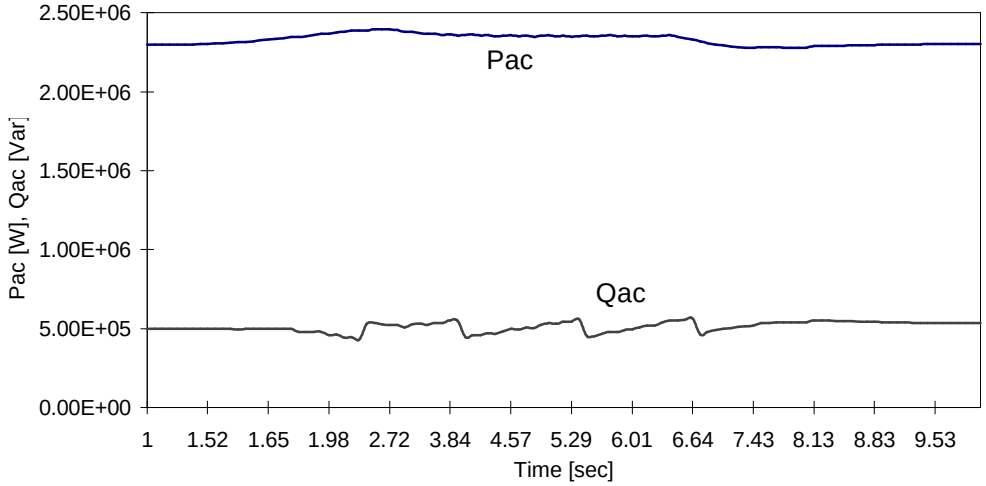

Figure 7.8 (i) Transient response of the total power (P_{ac}, Q_{ac}) supplied to the grid for slow insolation increase from 30mW/cm^2 to 100mW/cm^2.

7.5 Variable Insolation and Cell Temperature

This section shows simulation results for the developed computer models under disturbances that both insolation and cell temperature vary. Figure 7.9 illustrates actual changes of the insolation and cell temperature for 42 seconds. Those data were measured from the Virginia Tech Solar Test Facility (VTSTF) mounted on the roof of the Whittemore building in Virginia Tech campus on December 23, 1996. Figure 7.10 (a) - (i) show the hybrid system response following those weather changes.

As shown in Figure 7.10 (b), the PV array current, I_{pv}, exactly takes after the variations of insolation. Thus, it can be said that PV array currents rather than PV array voltages carry the close relationship with insolation changes. Figure 7.10 (c) indicates that the neural network controller for MPPT works so well that the PV array dc power accurately resembles the look of the insolation variations. As shown in Figure 7.10 (d), the ac reactive power, $Q_{ac,1}$, of the PV plant is always around zero, but it is a little apart from zero when the insolation varies suddenly. Figure 7.10 (h) and (i) reveal that the RRPC for the fuel cell power plant responds very well to the real and reactive power changes in the PV power plant. The power changes are due to the instant insolation changes. Therefore, the proposed two-loop controller for the PV-fuel cell hybrid system controls very effectively the inverters so that the PV power plant can always achieve maximum available solar power points. Moreover, the fuel cell power plant can satisfy the system-side requirement for real and reactive powers.

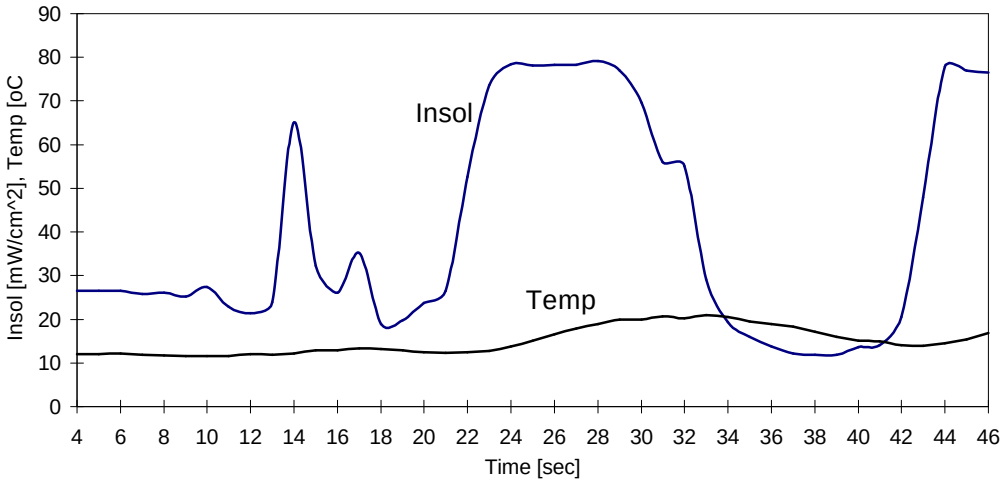

Figure 7.9 Variations of insolation and cell temperature.

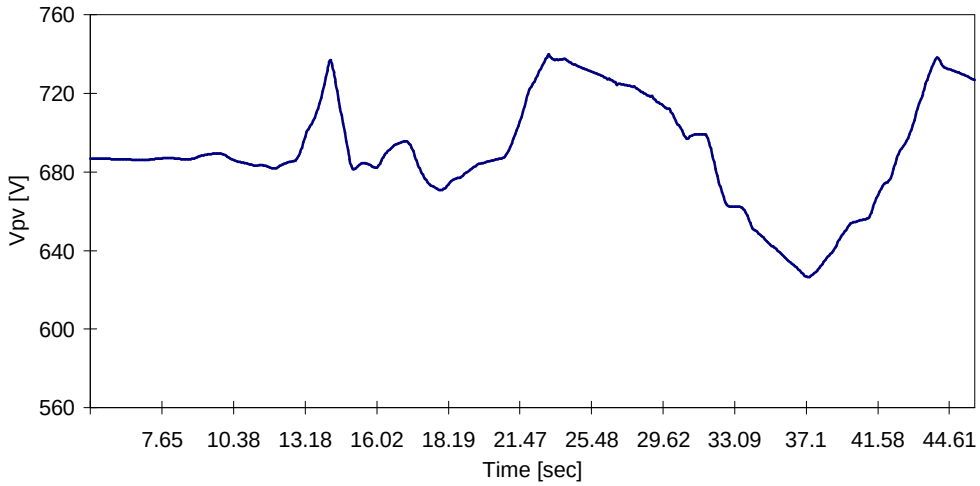

Figure 7.10 (a) Transient response of the PV array voltage (V_{pv}) for real-time variations of insolation and cell temperature.

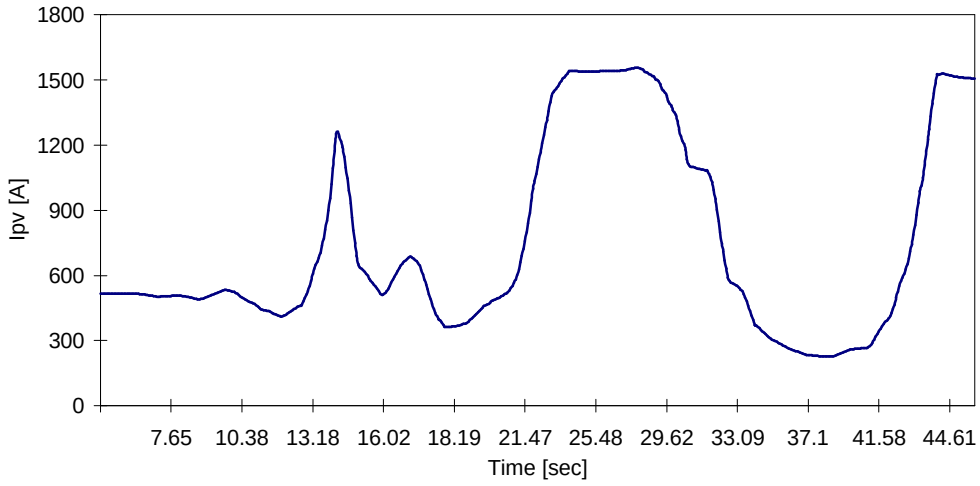

Figure 7.10 (b) Transient response of the PV array current (I_{pv}) for real-time variations of insolation and cell temperature.

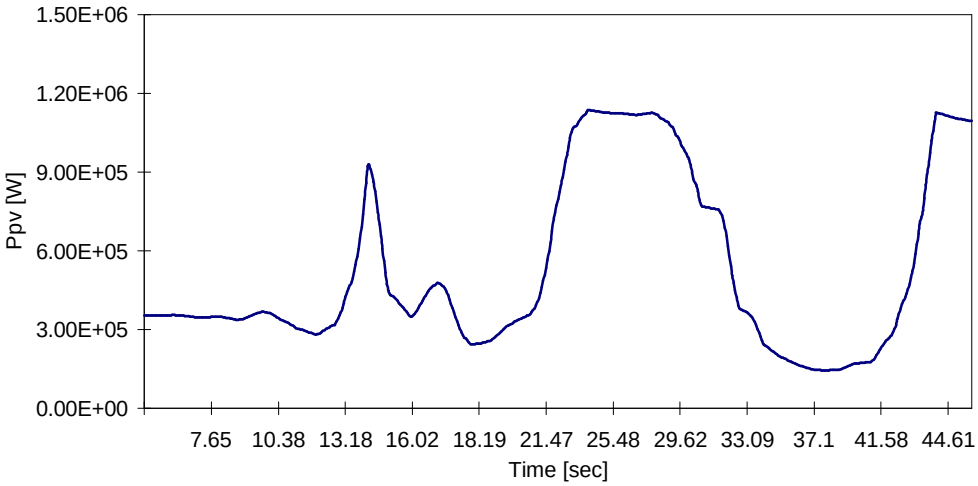

Figure 7.10 (c) Transient response of the PV array DC power (P_{pv}) for real-time variations of insolation and cell temperature.

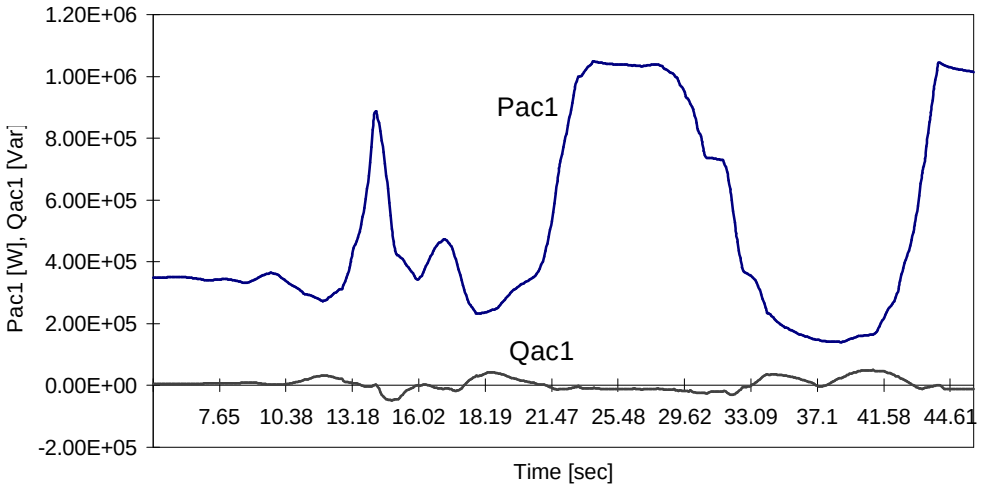

Figure 7.10 (d) Transient response of the PV array power (P_{ac1},Q_{ac1}) supplied to the grid for real-time variations of insolation and cell temperature.

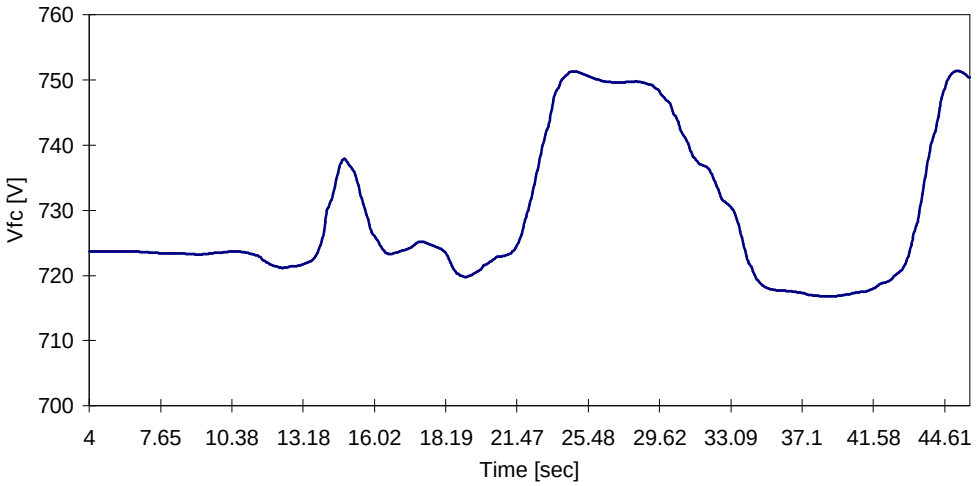

Figure 7.10 (e) Transient response of the fuel cell voltage (V_{fc}) for real-time variations of insolation and cell temperature.

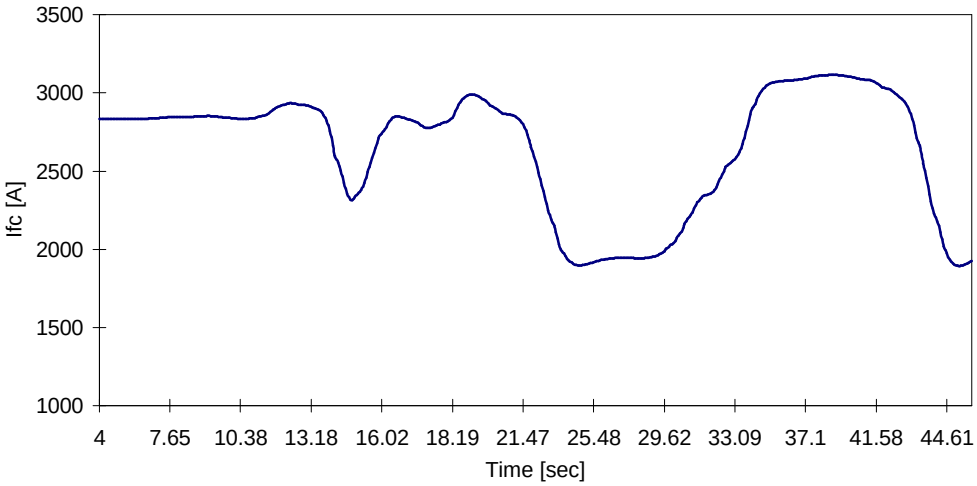

Figure 7.10 (f) Transient response of the fuel cell current (I_{fc}) for real-time variations of insolation and cell temperature.

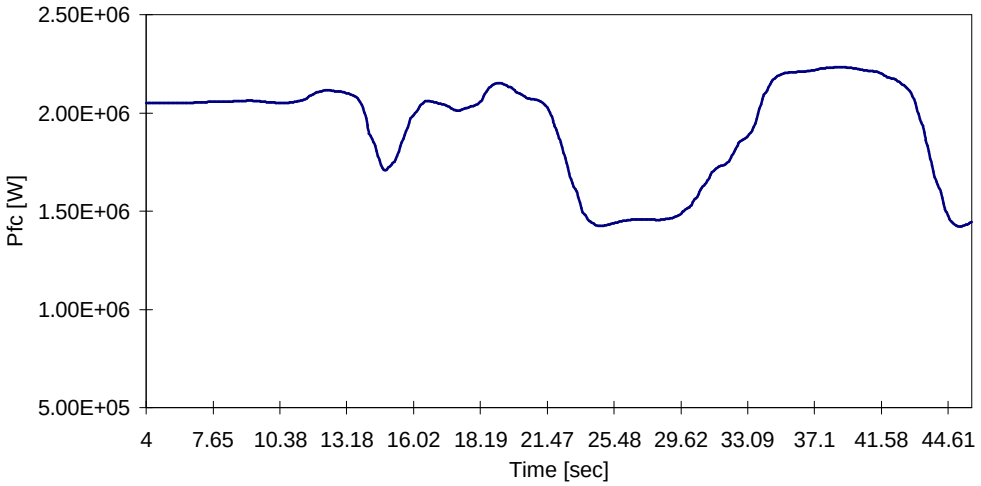

Figure 7.10 (g) Transient response of the fuel cell DC power (P_{fc}) for real-time variations of insolation and cell temperature.

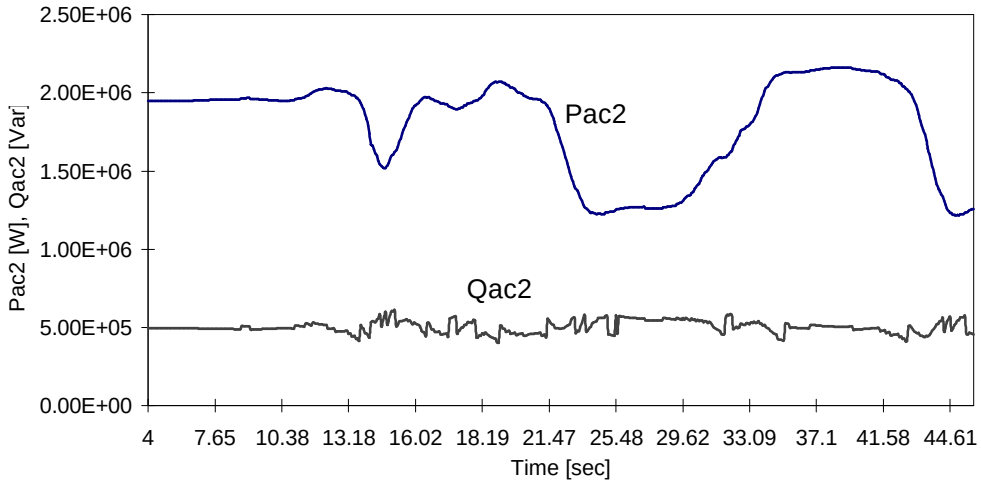

Figure 7.10 (h) Transient response of the fuel cell power (P_{ac2}, Q_{ac2}) supplied to the grid for real-time variations of insolation and cell temperature.

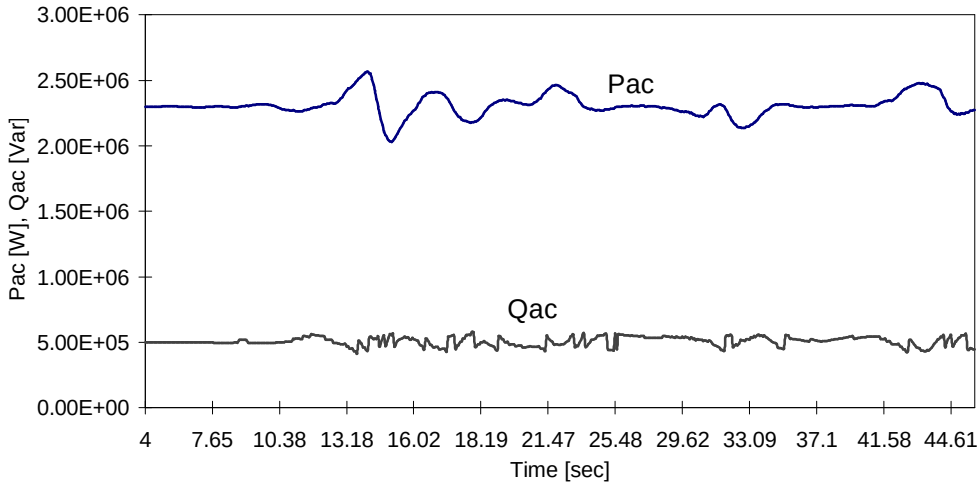

Figure 7.10 (i) Transient response of the total power (P_{ac}, Q_{ac}) supplied to the grid for real-time variations of insolation and cell temperature.

7.6 Change of Power Commands with Variable Insolation and Cell Temperature

This section shows simulation results for the developed computer models of the MPPT control and RRPC system under the same weather condition as in the previous section but with a change of power commands in the middle of time period. The real and reactive power commands are changed from 2.3MW, 0.5MVar to 1.5MW, 1.0MVar respectively at the instant of 20 second in time period. Figure 7.11 (a) - (i) show the hybrid system response following the changes of power commands.

As shown in Figure 7.11 (a), (b), (c) and (d), the variables belonging to the PV power plant such as V_{pv}, I_{pv}, P_{pv}, $P_{ac,1}$ and $Q_{ac,1}$ show exactly the same shapes as those in the previous section. It implies that a change of power commands in the middle of operation does not influence the operation of the PV power plant. Instead, the change of power commands is taken charge on by the fuel cell plant. The RRPC for the fuel cell power plant responds so well to the power command changes that the total real and reactive powers, P_{ac} and Q_{ac}, supplied to the utility grid show nice transitions to the new power commands, as shown in Figure 7.11 (i).

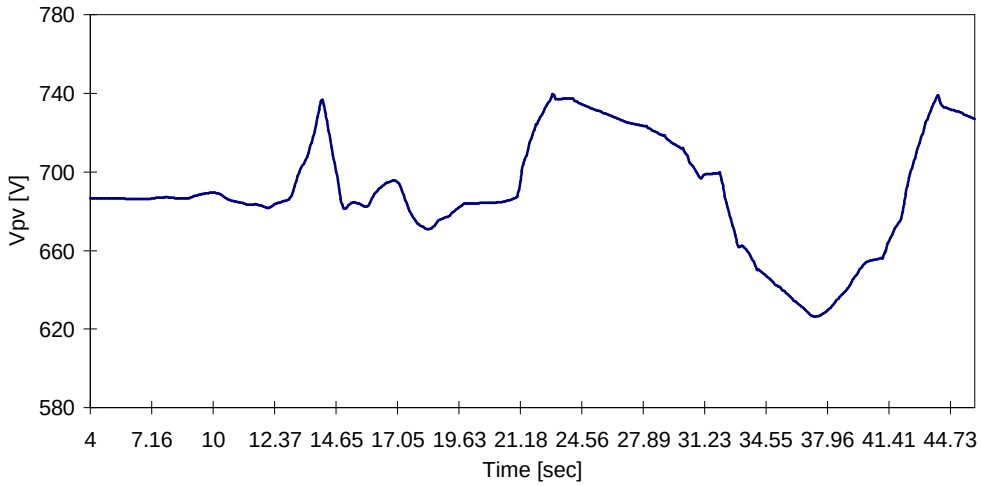

Figure 7.11 (a) Transient response of the PV array voltage (V_{pv}) for change of power commands with variable insolation and cell temperature.

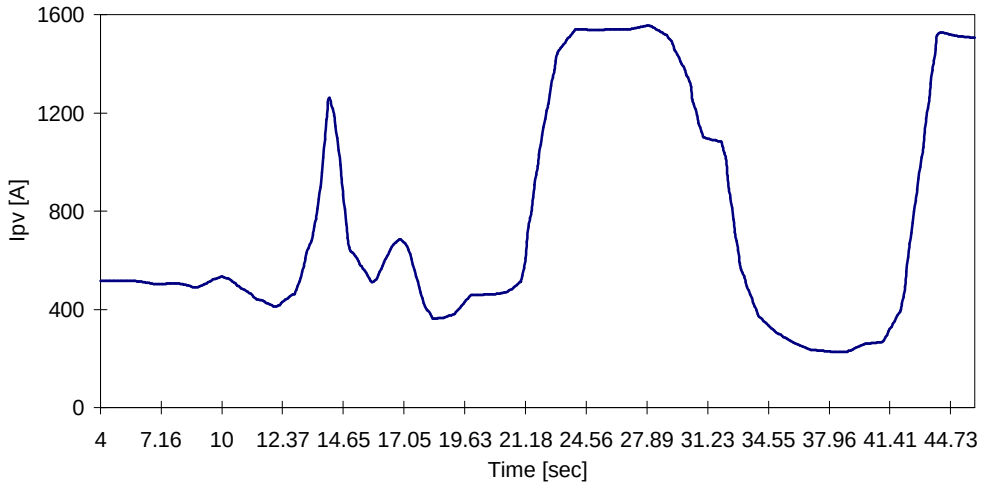

Figure 7.11 (b) Transient response of the PV array current (I_{pv}) for change of power commands with variable insolation and cell temperature.

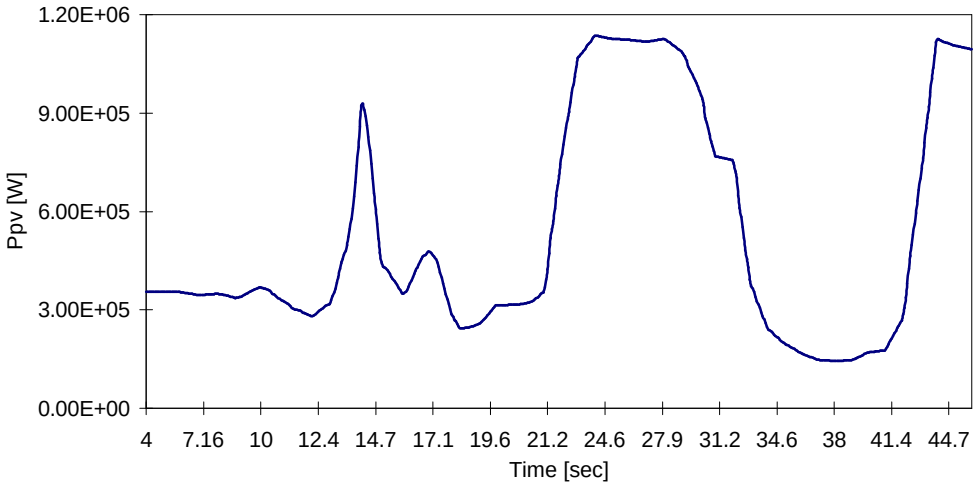

Figure 7.11 (c) Transient response of the PV array power (P_{pv}) for change of power commands with variable insolation and cell temperature.

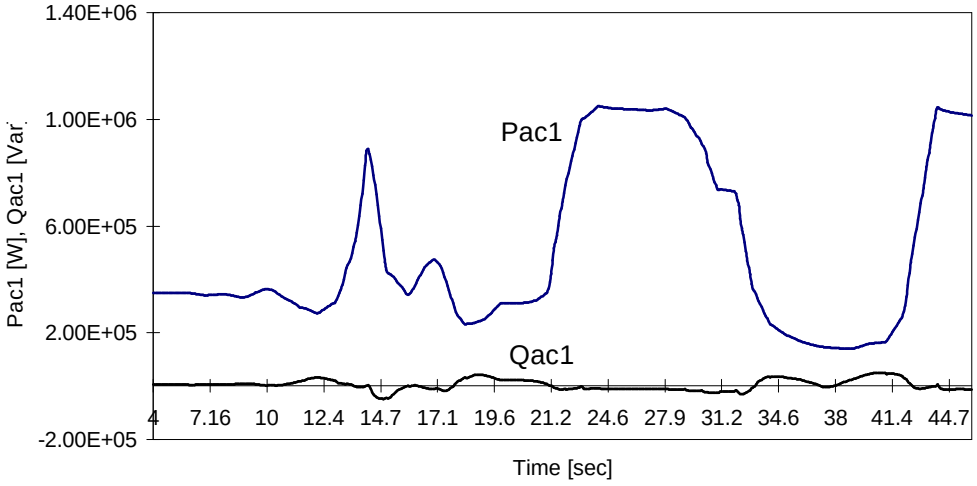

Figure 7.11 (d) Transient response of the PV array power (P_{ac1}, Q_{ac1}) supplied to the grid for change of power commands with variable insolation and cell temperature.

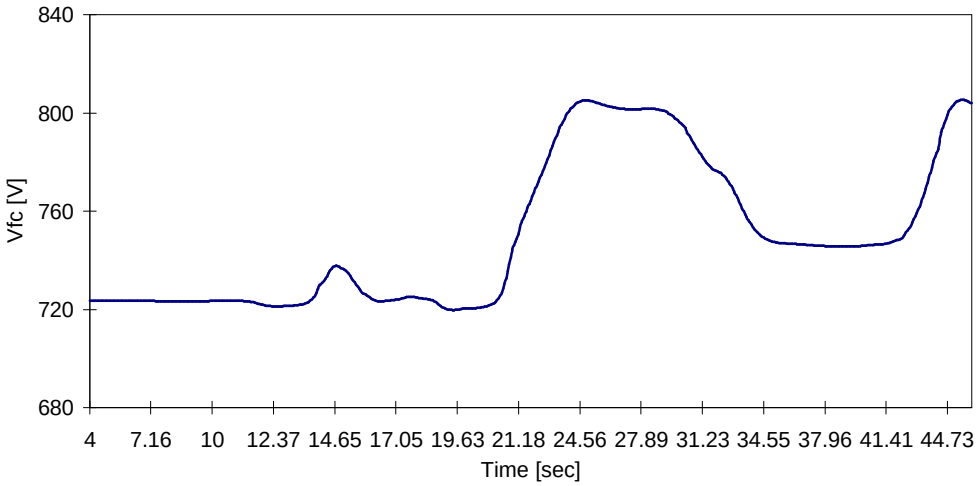

Figure 7.11 (e) Transient response of the fuel cell voltage (V_{fc}) for change of power commands with variable insolation and cell temperature.

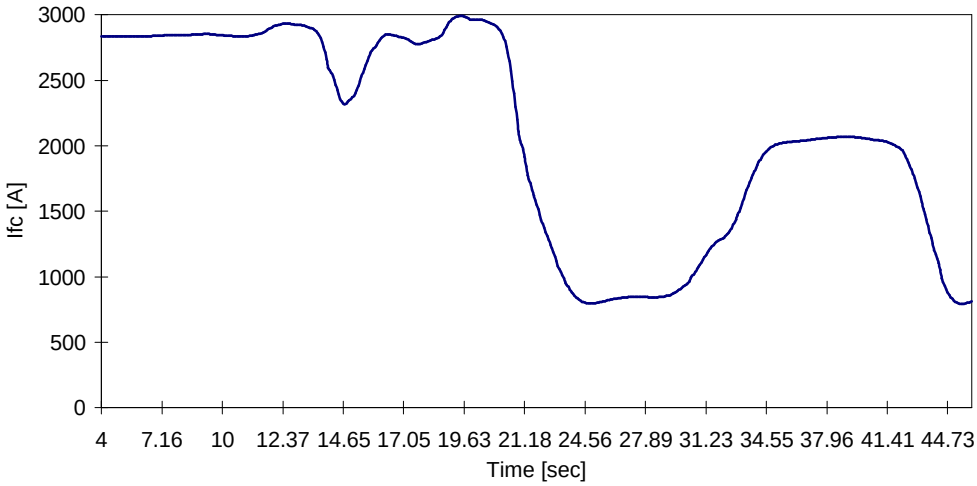

Figure 7.11 (f) Transient response of the fuel cell current (I_{fc}) for change of power commands with variable insolation and cell temperature.

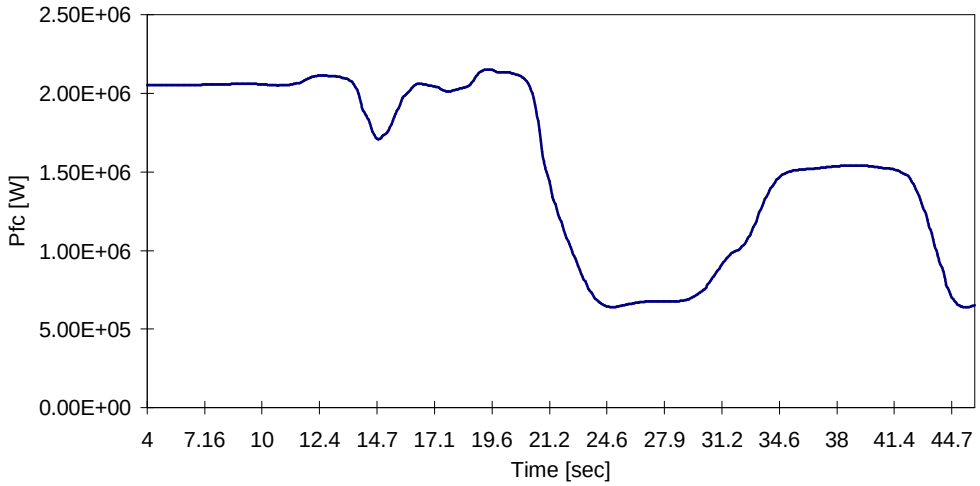

Figure 7.11 (g) Transient response of the fuel cell DC power (P_{fc}) for change of power commands with variable insolation and cell temperature.

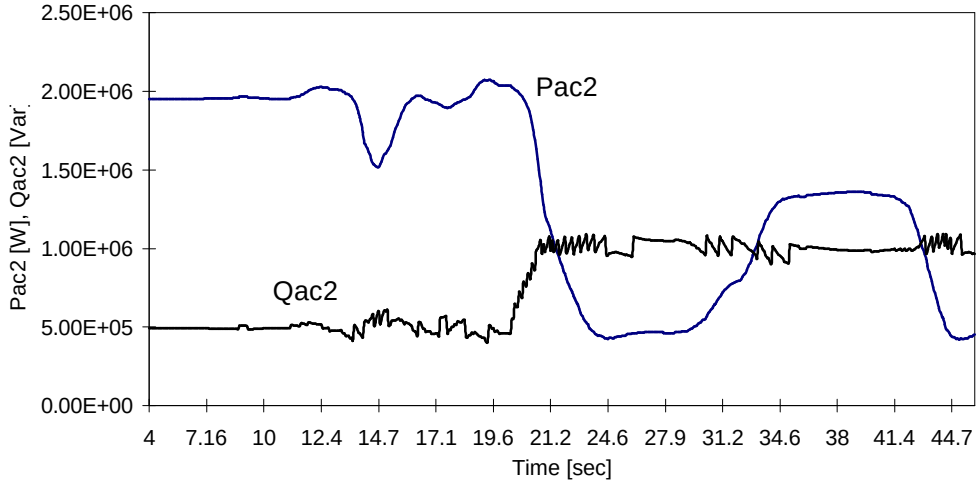

Figure 7.11 (h) Transient response of the fuel cell power (P_{ac2}, Q_{ac2}) supplied to the grid for change of power commands with variable insolation and cell temperature.

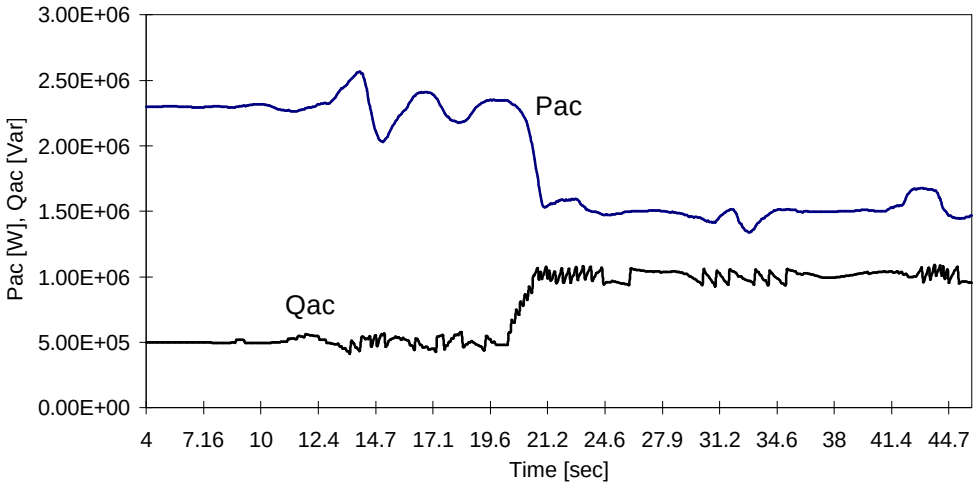

Figure 7.11 (i) Transient response of the total power (P_{ac}, Q_{ac}) supplied to the grid for change of power commands with variable insolation and cell temperature.

CHAPTER 8

ENVIRONMENTAL EVALUATION

8.1 Introduction

Solar photovoltaic and fuel cell power generations are not free from environmental impacts. One major disadvantage of PV power plants is that they require an extensive land for large-scale centralized power plant construction. Their indirect impacts on environment during production and disposal of the PV systems cannot be ignored since these materials contain some toxic elements. Fuel cell systems produce very little amounts of SO_2, NO_x and other particulates in the fuel reforming process and their low CO_2 emissions result from high energy conversion efficiency.

As two major criteria for calculating environmental impacts of the proposed PV-fuel cell hybrid system, land requirement for the power plant and its lifetime CO_2 emissions are considered. A requirement of land area would nearly soon be a crucial factor for power station construction in densely populated regions, particularly such as eastern U.S.A, Europe and East Asia. The world's rising concern about the increasing CO_2 concentration in the atmosphere and its potential impact on global warming gives a suggestion that CO_2 emission rates be considered in selecting electricity generating technologies.

Land area requirement and lifetime CO_2 emissions for PV, fuel cell, and conventional fossil fuel power plants are studied in the first and second part of this chapter, respectively. The next part deals with environmental evaluation of the proposed hybrid system. It is carried out in terms of land requirement for the plant construction and their lifetime CO_2 emissions.

8.2 Land Requirement

The land area required for each electric power plant varies over a significant range, depending upon factors such as individual utility design specifications, land costs, and the installed capacity. Photovoltaic modules that provide power for remote systems are useful with small land disturbance, but, when used for a grid-connected central power station, land requirement is a major consideration. A PV power plant requires the most extensive land due to the low energy density of solar radiation and low efficiencies of solar cells. It ranges from 20,000 to 35,000 m^2/MW [16].

The amount of land needed for the installation of a fuel cell power plant may be relatively small like 500 - 1,000 m^2/MW owing to the capability of its modular construction [19]. This feature, together with very low environmental impact, may allow fuel cell power plants to be located close to the point of use, where its waste heat can be used in cogeneration applications. This siting flexibility of the fuel cell power plants may not only permit a reduction in transmission and distribution loss but also provide for power control close to the load center. Therefore, it is able to make a utility defer transmission and distribution investments.

Table 8.1 summarizes the standard figures of land use for electricity generating power plants, including conventional fossil-fuel power sources [82]. For coal plants, land area required

Table 8.1 Land requirement for electric power plants.

Power sources	Land use [m^2/MW]
Photovoltaics	20,000
Fuel cells	700
Coal	3,700*
Oil	900
Natural gas	800

* Includes land needed for solid waste disposal.

for ash and flue gas desulfurization (FGD) waste disposal is included. Since oil and natural gas-fired power plants do not need ash disposal, the land required for their power plant construction is much lower than that of coal power plants.

8.3 CO_2 Emissions

This section calculates the lifetime CO_2 emissions from photovoltaics with polycrystalline silicon, phosphoric acid fuel cells, and three conventional fossil fuel (coal, oil and natural gas) power plants. The 30-year lifetime CO_2 emissions for those power plants are summarized in Table 8.2. The total CO_2 amount generated during a power plant's lifetime is calculated by adding the CO_2 produced during its construction to the CO_2 produced from burning fuels and from its operation and maintenance (O&M).

Table 8.2 CO_2 emissions for electric power plants with a 30-year lifetime.

Power sources	CO_2 from plant construction* [kg/MWh]	CO_2 from O & M [kg/MWh]	CO_2 from burning fuel [kg/MWh]	Total CO_2 emissions [kg/MWh]
Photovoltaics	81.8	9	-	90.8
Fuel cells	0.9	8	461.4	470.3
Coal	3.5	28	987.4	1018.9
Oil	6.4	16	738.5	760.9
Natural gas	2.7	10	551.4	564.1

* For the calculation, capacity factors for coal, oil, natural gas and fuel cell power plants are 65%, 25%, 25%, and 25%, respectively.

More than 95% of CO_2 produced from fossil fuel-burning power plants is generated during their operation as a consequence of fuel combustion. The CO_2 productions from coal, oil, and natural gas power plants by burning the fuels are calculated in Appendix A in detail. Those calculations are made by using carbon content and heating values for each of the fossil fuels, and electricity conversion efficiency of the power plant.

For a photovoltaic power plant, nearly 90% of CO_2 emissions from the PV power plant result from the CO_2 generated during the plant's construction stage. The CO_2 generated during the construction of a PV power plant is calculated by multiplying the primary energy consumed by the CO_2 emission factor of the primary energy. The detailed calculations are illustrated in Appendix B.

Almost all of CO_2 production from a fuel cell power plant occurs during a fuel reforming process that reforms natural gas into hydrogen-rich gas. Same as in the calculations of CO_2 emissions from the fossil-fuel power plants, the CO_2 amount emitted from the fuel cell plant is calculated using heating value of natural gas and the plant's electricity conversion efficiency. The whole calculations are shown in Appendix C.

Significant reduction of CO_2 emissions from energy generation could be achieved by improving the plant's efficiency or shifting fossil fuel to renewable energy sources. The PV system produces considerably less CO_2 over a 30-year lifetime than the fossil-fuel power plants. When natural gas power systems are substituted for coal power plants as a method of CO_2 reduction, it could reduce the CO_2 production by 45%. However, this reduction could not achieve a long-time solution to global warming. Substituting PV technologies for coal-fired power plants could reduce CO_2 production over time.

8.4 Evaluation of the PV-Fuel Cell Hybrid Power Plant

Environmental impacts of the proposed PV-fuel cell hybrid power plant are going to be evaluated in terms of land area requirement and life cycle CO_2 emissions. According to the Table 8.1, the land requirement for photovoltaic power stations is 6-25 times higher compared to the other forms of power generation. Fuel cell power plants need the least land area for plant construction. When these two power plants are integrated, land requirement for the hybrid plant would decrease so that the PV power could get an applicable position to be located near highly populated area.

From the Table 8.2, photovoltaic power plants produce 6-11 times less lifetime CO_2 gas than other power generating sources and the CO_2 emissions from fuel cell power plants also very little. So, the hybrid power plant has an excellent potential to reduce lifetime CO_2 emissions.

Figure 8.1 shows the comparison result of the proposed hybrid power plant with other power generation forms in terms of land surface requirement and lifetime CO_2 production.

Thus, fuel cell power generation, having the least land use, is able to alleviate the heavy burden for large surface requirement of the PV power plants. It also has a fast-ramping capability to smoothen the fluctuating PV power outputs as discussed in Chapter 3. Moreover, the hybrid power plant has a very little potential for lifetime CO_2 emissions because the PVs and fuel cells are the power sources that produce the least lifetime CO_2 emissions.

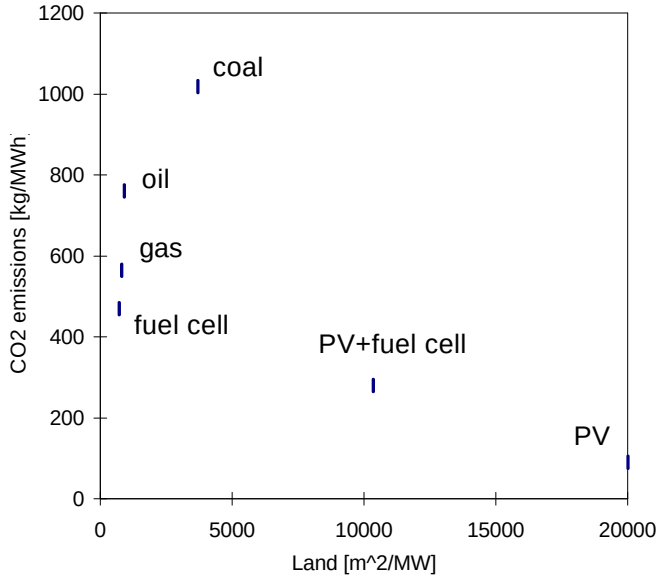

Figure 8.1 Land requirement and lifetime CO_2 emissions for electric power plants.

CHAPTER 9

CONCLUSIONS AND RECOMMENDATIONS

This dissertation is contributive to solving control problems of interconnecting a PV-fuel cell hybrid power plant to a utility grid by using a two-loop controller. Power generation from a PV power plant contains a positive aspect that it mostly takes after the utility system's peak demand. However, the PV power generation is less appealing due to the significant feature of its intermittent power output on a fluctuating weather condition. Thus, a PV power generation should be integrated with other power sources. Combining either a fuel cell or a battery power with a PV power plant had been proven to be a feasible technology for alleviating such a PV power's inherent problem [1, 2, 7, 13, 18].

This study compared in detail the above two technologies for the PV power backup. It was found that the fuel cell power has more beneficial effects over the battery power when operates with a utility-connected PV power station. Both the fuel cell and the battery power have nice characteristics in common such as fast load-response capability, modularity in production, highly reliable power sources and environmental acceptability. However, the two PV backup powers exhibit several different attributes with respect to efficiency, capacity variation, flexibility in operation, cost, and environmental externality.

The next thing to be encountered is to design an efficient controller for maximizing performance of the PV-fuel cell hybrid power plant and to present simplified computer models of the controller. A two-loop controller was proposed for this purpose. One loop is a neural network controller for MPPT, which tries to always extract maximum available solar power from the PV array under varying conditions of insolation, cell temperature and utility system load. Since the PV module's nonlinear I-V characteristics match well to a neural network application, the neural network approach was adopted in this study to keep track of maximum power points of the PV array.

A PID type real/reactive power controller (RRPC) in the fuel cell power plant is the other loop. The RRPC is going to achieve the utility system's requirement for real and reactive

powers by controlling the fuel cell stacks and the PCS. Real power is controlled by regulating both the incoming fuel to the fuel cell stacks and the switching signals to the PCS of the fuel cell power plant. Reactive power control is made by producing appropriate switching scheme to the PCS.

Time-domain simulation results showed effectiveness of the developed two-loop controller and its simplified computer models. The proposed neural network controller for MPPT produces accurately the switching signals to the dc-ac inverter for the PV array to keep track of the peak power points even when the insolation changes rapidly. The RRPC system responds well to the PV power changes so that the PV-fuel cell hybrid power plant can maintain the utility system's real and reactive power commands. The satisfactory dynamic responses may open the door for the two-loop controller to be applicable in transient stability analysis of the hybrid power plant. Conversion of dc power to ac in the hybrid power plant is made by controlling switching scheme of the inverters. Thus, the hybrid power system can achieve more versatile real and reactive power control than the conventional power sources because the former does not contain any rotating masses.

Environmental evaluation of the proposed PV-fuel cell hybrid power plant is made in terms of land requirement for the plant construction and lifetime CO_2 emissions. The CO_2 emissions of the hybrid power plant are caused by fuel consumption during its life-long period, and its construction and O&M work. Then, the environmental evaluation of the hybrid power plant is compared with those of the conventional fossil-fuel power generation forms. Fuel cell power and PV power have uniquely excellent characteristics in land requirement and CO_2 emissions, respectively. The PV power, however, requires extensive land for the plant construction. The fuel cell power plant emits moderate amount of CO_2 gas to the atmosphere during its operation. Therefore, the combination of the PV and the fuel cell power utilizes the merits of the two power sources and alleviates their disadvantages.

This dissertation tried to develop the two-loop controller for the PV-fuel cell hybrid power plant as a part of assisting renewable energy sources to be utilized more in the future. The photovoltaic and fuel cell powers are socially acceptable technologies by the people, who concern about a degradation of environment. The major impediment to expand photovoltaic power generation for a stand-alone or a utility-connected application is the high production cost of the PV modules. The price of PV modules dropped to less than \$6/W in 1983 and is projected to continue to decrease in the future.

The technology for manufacturing a phosphoric-acid fuel cell is mature today for commercial applications, but it is not much applied to electric power utilities because of cost. Its initial capital cost is a factor of 3 or higher than conventional alternative power sources. The research and development of advanced fuel cell technologies are under laboratory conditions. When the coal gasification technology is feasible economically, the fuel cell usage is projected to increase a lot. As the PV power penetration to the electric power utility increases, the demand for the fuel cell power application will grow as well to be integrated with the PV power. The

fuel cell power has a great capability to compensate for the PV power's inherent problem of intermittent power generation under inclement weather conditions, as proven in this dissertation. Then, the proposed two-loop controller would be adopted to maximize the performance of the PV-fuel cell hybrid power plant.

NOMENCLATURE

$A = B$	Ideality factor (1.60)
b	Tafel slope (0.11)
C_1	Internal capacitance of a fuel cell
C_d	Capacitance in parallel with the PV array
C_{ov}	Overvoltage capacitance of a battery cell
C_b	Battery capacitance
E_0	Open circuit voltage of a fuel cell
E_f	Terminal voltage of a fuel cell (V)
E_{G0}	Band gap for silicon (1.10eV)
E_r	Reversible potential of the cell (1.0 V)
I	PV cell output current (A)
I_0	PV cell saturation current (A)
I_d	Current flowing into the inverter from the PV array (A)
I_f	Cell current density (A/cm^2)
I_{fc}	Current from the fuel cell stacks (A)
I_{fo}	Exchange current density for oxygen reduction reaction (0.003)
I_{or}	Saturation current at T_r in a PV cell ($15793X10^{-6}$)
I_{ph}	light-generated current in a PV cell (A)
I_{scr}	PV cell short-circuit current at 25 ^oC and 100 mW/cm^2 (3.27)
K	Boltzmann's constant ($13805X10^{-23}$ $Nm/^oK$)
K_i	Short-circuit current temperature coefficient at I_{scr} (0.0017 $A/^oC$)
L_T	Internal equivalent inductance of a fuel cell
N	Turn ratio of the transformers in the PV and fuel cell power plant
P_{ac}	Total real power supplied to the grid (W)
$P_{ac,1}$	Output real power supplied to the grid from the PV power plant (W)
$P_{ac,2}$	Output real power supplied to the grid from the fuel cell power plant (W)
P_{pv}	Output power of the PV array (W)
q	Electron charge ($16X10^{-19}$ C)
Q_{ac}	Total reactive power supplied to the grid (Var)
$Q_{ac,1}$	Output reactive power supplied to the grid from the PV power plant (Var)
$Q_{ac,2}$	Output reactive power supplied to the grid from the fuel cell power plant (Var)

Q_{pn}	Reactive power behind the transformer in the PV power plant (Var)
R	External load resistance
R_1	Charge transfer resistance of a fuel cell
R_b	Self-discharge resistance of a battery cell
R_{bat}	Internal resistance of a battery cell
R_f	Internal resistance of a fuel cell (0.5)
R_{ov}	Overvoltage resistance of a battery cell
R_s	Series resistance of a PV cell (0.006)
R_{sh}	Internal shunt resistance of a PV cell
R_T	Electrolyte resistance of a fuel cell
T	PV cell temperature (^{o}K)
T_c	PV cell temperature (^{o}K)
T_r	Reference temperature (301.18 ^{o}K)
V	Terminal voltage for a PV cell, a battery cell, or a fuel cell (V)
V_{fc}	Terminal voltage of the fuel cell stacks (V)
V_{fn}	Voltage hehind the transfomer in the fuel cell power plant (V)
V_{oc}	Open circuit voltage of a battery cell
V_{pn}	Voltage hehind the transfomer in the PV power plant (V)
V_{pv}	Terminal voltage of the PV array (V)
V_s	Reference utility grid voltage (V)
$V_{\delta 1}$	One control variable to the inverter in the PV power plant (V)
$V_{\delta 2}$	One control variable to the inverter in the fuel cell power plant (V)
$V_{\phi 1}$	One control variable to the inverter in the PV power plant (V)
$V_{\phi 2}$	One control variable to the inverter in the fuel cell power plant (V)
λ	PV cell illumination (mW/cm^2)
ϕ_{pn}	Phase angle of the inverter voltage in the PV power plant
ϕ_{fn}	Phase angle of the inverter voltage in the fuel cell power plant

REFERENCES

[1] S. Rahman and K. Tam, "A Feasibility Study of Photovoltaic-Fuel Cell Hybrid Energy System", *IEEE Transactions on Energy Conversion*, Vol. 3, No. 1, March 1988, pp. 50-55.

[2] K. Tam and S. Rahman, "System Performance Improvement Provided by a Power Conditioning Subsystem for Central Station Photovoltaic-Fuel Cell Power Plant", *IEEE Transactions on Energy Conversion*, Vol. 3, No. 1, March 1988, pp. 64-70.

[3] B.K. Bose, P.M. Szczesny and R.L. Steigerwald, "Microcomputer Control of a Residential Photovoltaic Power Conditioning System", *IEEE Transactions on Industry Applications*, Vol. IA-21, No. 5, September/October 1985, pp. 1182-1191.

[4] H. Matsuda, "Interconnecting Dispersed Photovoltaic Power Generation Systems with Existing Utility Grid: A Study at ROKKO Inland Test Facility, Japan", *Int. J. Solar Energy*, 1992, Vol. 13, pp. 1-10.

[5] O. Wasynczuk, "Modeling and Dynamic Performance of a Line-Commutated Photovoltaic Inverter System", *IEEE Transactions on Energy Conversion*, Vol. 4, No. 3, September 1989, pp. 337-343.

[6] O. Wasynczuk and N.A. Anwah, "Modeling and Dynamic Performance of a Self-Commutated Photovoltaic Inverter System", *IEEE Transactions on Energy Conversion*, Vol. 4, No. 3, September 1989, pp. 322-328.

[7] K.C. Kalaitzakis and G.J. Vachtsevanos, "On the Control and Stability of Grid Connected Photovoltaic Sources", *IEEE Transactions on Energy Conversion*, Vol. 2, No. 4, December 1987, pp. 556-562.

[8] U. Boegli and R. Ulmi, "Realization of a New Inverter Circuit for Direct Photovoltaic Energy Feedback into the Public Grid", *IEEE Transactions on Industry Applications*, Vol. IA-22, No. 2, March/April 1986, pp. 255-258.

[9] E.J. Simburger and R.B. Fling, "Engineering Design for a Central Station Photovoltaic Power Plant", *IEEE Transactions on Power Apparatus and Systems*, Vol. PAS-102, No. 6, June 1983, pp. 1668-1677.

[10] S.M. Chalmers, P.M. Anderson and P.L. Vogt, "The Effect of Photovoltaic Power Generation on Utility Operation", *IEEE Transactions on Power Apparatus and Systems*, Vol. PAS-104, No. 3, March 1985, pp. 524-530.

[11] F. Lasnier and T.G. Ang, *Photovoltaic Engineering Handbook*, The Adam Hilger, 1990.

[12] Y. Hamakawa, "Recent Advances in Solar Photovoltaic Technology and Its New Role for Environmental Issue", *Renewable Energy*, Vol. 5, Part I, pp. 34-43, 1994.

[13] B.H. Chowdhury and S. Rahman, "Analysis of Interrelationships Between Photovoltaic Power and Battery Storage for Electric Utility Load Management", *IEEE Transactions on Power Systems*, Vol. 3, No. 3, August 1988, pp. 900-907.

[14] G. Smith, *Storage Batteries - Including Operation, Charging, Maintenance and Repair*, Pitman Advanced Publishing Program, 1980.

[15] K. Tam, P. Kumar and M. Foreman, "Enhancing the Utilization of Photovoltaic Power Generation by Superconductive Magnetic Energy Storage", *IEEE Transactions on Energy Conversion*, Vol. 4, No. 3, September 1989, pp. 314-321.

[16] H. Schaefer and G. Hagedorn, "Hidden Energy and Correlated Environmental Characteristics of PV Power Generation", *Renewable Energy*, Vol. 2, No. 2, pp. 159-166, 1992.

[17] M. Ohnishi and A. Takeoka, "Advanced Photovoltaic Technologies and Residential Applications", *Renewable Energy*, Vol. 6, No. 3, pp. 275-282, 1995.

[18] A. Chaurey and S. Deambi, "Battery Storage for PV Power Systems: An Overview", *Renewable Energy*, Vol. 2, No. 3, pp. 227-235, 1992.

[19] L.J. Blomen and M.N. Mugerwa, *Fuel Cell Systems*, Plenum Press, New York, 1993

[20] T.M. Calloway, "Autonomous Photovoltaic-Diesel Power System Design", *Proc. IEEE PV Specialists Conference*, Las Vegas, Nevada, October 1985, pp. 280-284.

[21] T. Hiyama, S. Kouzuma and T. Imakubo, "Identification of Optimal Operating Point of PV Modules using Neural Network for Real Time Maximum Power Tracking Control", *IEEE Transactions on Energy Conversion*, Vol. 10, No. 2, June 1995, pp. 360-367.

[22] T. Hiyama, S. Kouzuma and T. Imakubo, “Evaluation of Neural Network Based Real Time Maximum Power Tracking Controller for PV System”, *IEEE Transactions on Energy Conversion*, Vol. 10, No. 3, September 1995, pp. 543-548.

[23] W.J. Lueckel, L.G. Eklund and S.H. Law, “Fuel Cells for Dispersed Power Generation”, *IEEE Transactions on Power Apparatus and Systems*, Vol. PAS-92, No. 1, January 1973, pp. 230-236.

[24] R.A. Fernandes and H.D. Philipp, “Hydrogen Cycle Peak-Shaving on the New York State Grid Using Fuel Cells”, *IEEE Transactions on Power Apparatus and Systems*, Vol. PAS-96, No. 2, March 1977, pp. 467-477.

[25] R.M. Reinstrom, “Carbonate Fuel Cell Power Plant Systems”, *IEEE Transactions on Power Apparatus and Systems*, Vol. PAS-100, No. 12, December 1981, pp. 4752-4758.

[26] R.A. Bell and R.B. Hayman, “The Electric Utility 4.5 MW Fuel Cell Power Plant - An Urban Demonstration”, *IEEE Transactions on Power Apparatus and Systems*, Vol. PAS-100, No. 12, December 1981, pp. 4760-4764.

[27] D.M. Rigney et al., “Expansion Planning with Dispersed Fuel Cell Power Plants on Actual Utility Systems”, *IEEE Transactions on Power Apparatus and Systems*, Vol. PAS-103, No. 9, September 1984, pp. 2388-2393.

[28] S. Matsumoto et al., “Performance Model of Molten Carbonate Fuel Cell”, *IEEE Transactions on Energy Conversion*, Vol. EC-5, No. 2, June 1990, pp. 252-257.

[29] T. Shinoki, M. Matsumoto and A. Sasaki, “Development of an Internal Reforming Molten Carbonate Fuel Cell Stack”, *IEEE Transactions on Energy Conversion*, Vol. EC-10, No. 4, December 1995, pp. 722-728.

[30] J.W. Beck et al., “A Computer Study of Battery Energy Storage and Power Conversion Equipment Operation”, *IEEE Transactions on Power Apparatus and Systems*, Vol. PAS-95, No. 4, July 1976, pp. 1064-1072.

[31] H.J. Kunisch, K.G. Kramer and H. Dominik, “Battery Energy Storage: Another Option for Load-Frequency-Control and Instantaneous Reserve”, *IEEE Transactions on Energy Conversion*, Vol. EC-1, No. 3, September 1986, pp. 41-46.

[32] J. Abraham et al., “Balance of Plant Considerations for Load-Leveling Batteries”, *IEEE Transactions on Energy Conversion*, Vol. EC-1, No. 2, June 1986, pp. 131-136.

[33] M.W. Migliaro, “Installation Design for Valve-Regulated Sealed Lead-Acid Batteries in Generating Stations”, *IEEE Transactions on Energy Conversion*, Vol. 4, No. 1, March 1989, pp. 20-24.

[34] J.W. Hurwitch and C.A. Carpenter, “Technology and Application Options for Future Battery Power Regulation”, *IEEE Transactions on Energy Conversion*, Vol. 6, No. 1, March 1991, pp. 216-223.

[35] G.M. Cook, W.C. Spindler and G.Grefe, “Overview of Battery Power Regulation and Storage”, *IEEE Transactions on Energy Conversion*, Vol. 6, No. 1, March 1991, pp. 204-211.

[36] M.A. Casacca and Z.M. Salameh, “Determination of Lead-Acid Battery Capacity via Mathematical Modeling Techniques”, *IEEE Transactions on Energy Conversion*, Vol. 7, No. 3, September 1992, pp. 442-446.

[37] Z.M. Salameh, M.A. Casacca and W.A. Lynch, “A Mathematical Model for Lead-Acid Batteries”, *IEEE Transactions on Energy Conversion*, Vol. 7, No. 1, March 1992, pp. 93-97.

[38] D. Kottick, M. Blau and D. Edelstein, “Battery Energy Storage for Frequency Regulation in an Island Power System”, *IEEE Transactions on Energy Conversion*, Vol. 8, No. 3, September 1993, pp. 455-458.

[39] G.J. Ball, G. Corey and B.L. Norris, “Government, Industry, and Utility Development and Evaluation of a Modular Utility Battery Energy Storage System”, *IEEE Transactions on Energy Conversion*, Vol. 10, No. 3, September 1995, pp. 549-554.

[40] C. Lu, C. Liu and C. Wu, “Effect of Battery Energy Storage System on Load Frequency Control Considering Governor Deadband and Generation Rate Constraint”, *IEEE Transactions on Energy Conversion*, Vol. 10, No. 3, September 1995, pp. 555-561.

[41] R. Ramakumar, H.J. Allison and W.L. Hughes, “Solar Energy Conversion and Storage Systems for the Future”, *IEEE Transactions on Power Apparatus and Systems*, Vol. PAS-94, No. 6, November 1975. pp 1926-1934.

[42] G.L. Campen, “An Analysis of the Harmonics and Power Factor Effects at a Utility Intertied Photovoltaic System”, *IEEE Transactions on Power Apparatus and Systems*, Vol. PAS-101, No. 12, December 1982, pp. 4632-4639.

[43] O. Wasynczuk, “Dynamic Behavior of a Class of Photovoltaic Power Systems”, *IEEE Transactions on Power Apparatus and Systems*, Vol. PAS-102, No. 9, September 1983, pp. 3031-3037.

[44] R.C. Dugan, W.T. Jewell and D.J. Roesler, “Harmonics and Reactive Power from Line-Commutated Inverters in Proposed Photovoltaic Subdivision”, *IEEE Transactions on Power Apparatus and Systems*, Vol. PAS-102, No. 9, September 1983, pp. 3205-3210.

[45] B.W. McNeill and M.A. Mirza, “Estimated Power Quality for Line Commutated Photovoltaic Residential System”, *IEEE Transactions on Power Apparatus and Systems*, Vol. PAS-102, No. 10, October 1983, pp. 3288-3295.

[46] C.M. Ong, “Operational Behavior of Line-Commutated Photovoltaic Systems on a Distribution Feeder”, *IEEE Transactions on Power Apparatus and Systems*, Vol. PAS-103, No. 8, August 1984, pp. 2262-2268.

[47] P.P. Groumpos, R.C. Cull and A.F. Ratajczak, “An Overview of Control Aspects of a Village Stand-Alone Photovoltaic Power System”, *IEEE Transactions on Power Apparatus and Systems*, Vol. PAS-103, No. 10, October 1984, pp. 2845-2853.

[48] M.A. Khallat and S. Rahman, “A Probabilistic Approach to Photovoltaic Generator Performance Prediction”, *IEEE Transactions on Energy Conversion*, Vol. EC-1, No. 3, September 1986, pp. 34-40.

[49] M.A. Khallat and S. Rahman, “A Model for Capacity Credit Evaluation of Grid-Connected Photovoltaic Systems with Fuel Cell Support”, *IEEE Transactions on Power Systems*, Vol. 3, No. 3, August 1988, pp. 1270-1276.

[50] S. Rahman, “Economic Impact of Integrating Photovoltaics with Conventional Electric Utility Operation”, *IEEE Transactions on Energy Conversion*, Vol. 5, No. 3, September 1990, pp. 422-428.

[51] M.G. Jaboori, M.M. Saied and A.A. Hanafy, “A Contribution to the Simulation and Design Optimization of Photovoltaic Systems”, *IEEE Transactions on Energy Conversion*, Vol. 6, No. 3, September 1991, pp. 401-406.

[52] S. Rahman and B.D. Kroposki, “Photovoltaics and Demand Side Management Performance Analysis at a University Building”, *IEEE Transactions on Energy Conversion*, Vol. 8, No. 3, September 1993, pp. 491-498.

[53] S. Rahman and M. Bouzguenda, “A Model to Determine the Degree of Penetration and Energy Cost of Large Scale Utility Interactive Photovoltaic Systems”, *IEEE Transactions on Energy Conversion*, Vol. 9, No. 2, June 1994, pp. 224-230.

[54] N. Mohan, T.M. Undeland and W.P. Robbins, *Power Electronics: Converters, Applications, and Design*, John Willey & Sons, 1989.

[55] L.H. Michaels, B.T. Fairchild and S.T. Kohn, “Hybrid Simulation of Fuel Cell Power Conversion Systems”, *IEEE Transactions on Power Apparatus and Systems*, Vol. PAS-96, No. 4, July 1977, pp. 1329-1336.

[56] G.E. Gareis et al., “The Interactionof Batteries and Fuel Cells with Electrical Distribution Systems: Force Commutated Converter Interface”, *IEEE Transactions on Power Apparatus and Systems*, Vol. PAS-96, No. 4, July 1977, pp. 1242-1250.

[57] D.P. Carroll et al., “The Interactionof Batteries and Fuel Cells with Electrical Distribution Systems: Line Commutated Converter Interface”, *IEEE Transactions on Power Apparatus and Systems*, Vol. PAS-96, No. 4, July 1977, pp.1202-1210.

[58] G.A. Phillips, J.W. Walton and F.J. Kornbrust, “Progress in Self-Commutated Inverters for Fuel Cells and Batteries”, *IEEE Transactions on Power Apparatus and Systems*, Vol. PAS-98, No. 4, July 1979, pp. 1466-1475.

[59] P.K. Simpson, “Foundations of Neural Networks”, *Proceedings of the Adaptive Control Systems Technology Symposium*, October 24-25, 1994, pp. 16-37.

[60] D.J. Sobajic and Y.H. Pao, “Artificial Neural-Net Based Dynamic Security Assessment for Electric Power Systems”, *IEEE Transactions on Power Systems*, Vol. 4, No. 1, February 1989, pp. 220-226.

[61] C.R. Chen and Y.Y. Hsu, “Synchronous Machine Steady-State Stability Analysis using an Artificial Neural Network”, *IEEE Transactions on Energy Conversion*, Vol. 6, No. 1, March 1991, pp. 12-20.

[62] Y.Y. Hsu and C.R. Chen, “Tuning of Power System Stabilizers using an Artificial Neural Network”, *IEEE Transactions on Energy Conversion*, Vol. 6, No. 4, December 1991, pp. 612-619.

[63] M. Aggoune et al., “Preliminary Results on Using Artificial Neural Networks for Security Assessment”, *IEEE Transactions on Power Systems*, Vol. 6, No. 2, May 1991, pp. 890-896.

[64] K. Ikenono and S. Iwamoto, “Generalization of Transient Stability Solution Using Neural Network Theory”, *Electrical Engineering in Japan*, Vol. 112, No. 3, 1992, pp. 72-79.

[65] M. Djukanovic, D.J. Sobajic and Y.H. Pao, “Neural Net Based Determination of Generator-Shedding Requirements in Electric Power Systems”, *IEE Proceedings -C*, Vol. 139, No. 5, September 1992, pp. 427-436.

[66] N. Kandil et al., “Fault Identification in an AC-DC Transmission System Using Neural Networks”, *IEEE Transactions on Power Systems*, Vol. 7, No. 2, May 1992, pp. 812-818.

[67] H. Mori, Y. Tamaru and S. Tsuzuki, “An Artificial Neural-Net Based Technique for Power System Dynamic Stability with the Kohonen Model”, *IEEE Transactions on Power Systems*, Vol. 7, No. 2, May 1992, pp. 856-864.

[68] D. Niebur and A.J. Germond, “Power System Static Security Assessment Using the Kohonen Neural Network Classifier”, *IEEE Transactions on Power Systems*, Vol. 7, No. 2, May 1992, pp. 865-872.

[69] H. Sasaki, M. Watanabe and R. Yokoyama, “A Solution Method of Unit Commitment by Artificial Neural Networks”, *IEEE Transactions on Power Systems*, Vol. 7, No. 3, August 1992, pp. 974-980.

[70] Y.Y. Hsu and L.H. Jeng, “Analysis of Torsional Oscillations Using an Artificial Neural Network”, *IEEE Transactions on Energy Conversion*, Vol. 7, No. 4, December 1992, pp. 684-690.

[71] T. Sorsa and H.N. Koivo, “Application of Artificial Neural Networks in Process Fault Diagnosis”, *Automatica*, Vol. 29, No. 4, 1993, pp. 843-849.

[72] Y. Zhang, O.P. Malik and G.P. Chen, “Artificial Neural Network Power System Stabilizers in Multi-Machine Power System Environment”, *IEEE Transactions on Energy Conversion*, Vol. 10, No. 1, March 1995, pp. 147-153.

[73] K.H. Abdul-Rahman, S.M. Shahidhpour and M. Daneshdoost, “AI Approach to Optimal VAR Control with Fuzzy Reactive Loads”, *IEEE Transactions on Power Systems*, Vol. 10, No. 1, February 1995, pp. 88-97.

[74] A.G. Bakirtzis et al., “Short Term Load Forecasting Using Fuzzy Neural Networks”, *IEEE Transactions on Power Systems*, Vol. 10, No. 3, August 1995, pp. 1518-1524.

[75] T. Denise King, M.E. El-Hawary and F. El-Hawary, “Optimal Environmental Dispatching of Electric Power Systems via an Improved Hopfield Neural Network Model”, *IEEE Transactions on Power Systems*, Vol. 10, No. 3, August 1995, pp. 1559-1564.

[76] A.A. El-Keib and X. Ma, “Application of Artificial Neural Networks in Voltage Stability Assessment”, *IEEE Transactions on Power Systems*, Vol. 10, No. 4, November 1995, pp. 1890-1896.

[77] T.S. Sidhu and Z. Ao, "On-Line Evaluation of Capacity and Energy Losses in Power Transmission Systems by Using Artificial Neural Networks", *IEEE Transactions on Power Delivery*, Vol.107, No. 4, October 1995, pp. 1913-1919.

[78] R. Noyes (ed.), *Fuel Cells for Public Utility and Industrial Power*, Noyes Data Corporation, 1977.

[79] M. Hsu, "Ztek's Ultra-High Efficiency Fuel Cell/Gas Turbine System for Distributed Generation", *1996 Fuel Cell Seminar*, Nov. 17-20, 1996, Orlando, Florida, pp. 183-186.

[80] R.C. Ruhl, M.A. Petrik and T.L. Cable, "Status of the TMI Systems", *1996 Fuel Cell Seminar*, Nov. 17-20, 1996, Orlando, Florida, pp. 187-189.

[81] G. Marland, "Carbon Dioxide Emission Rates for Conventional and Synthetic Fuels", *Energy*, Vol. 8, No. 12, 1983, pp. 981-992.

[82] OECD, *Environmental Effects of Electricity Generation*, OECD Publications Office, 1985.

[83] F. Kreith, P. Norton and D. Brown, "A Comparison of CO2 Emissions from Fossil and Solar Power Plants in the United States", *Energy*, Vol. 15, No. 12, 1990, pp. 1181-1198.

[84] "Fedral Technology Alert - Natural Gas Fuel Cells", 1996, http://w3.pnl.gov:2080/fta/5_nat.htm.

[85] Technology Transition Corporation, "The Entry Market for Fuel Cells", 1996, http://www. ttcorp.com/fccg/fcmabstr.htm.

[86] K. Jung, H. Kim and D. Rho, "Determination of the Installation Site and Optimal Capacity of the Battery Energy Storage System for Load Leveling", *IEEE Transactions on Energy Conversion*, Vol. 11, No. 1, March 1996, pp. 162-167.

[87] J.G. Kassakian, M.F. Schlecht and G.C. Verghese, *Principles of Power Electronics*, Addison-Wesley Publishing Company, 1991.

[88] N. Argaw, "Optimization of Photovoltaic Water Pumps Coupled with an Interfacing Pulse Width Modulated DC/AC Inverter Power Conditioning Device", *1994 IEEE First World Conference on Photovoltaic Energy Conversion*, Dec. 5-9, 1994, Hawii, pp. 1165-1168.

[89] R. Naik et al., "A Novel Grid Interface, Optimized for Utility-Scale Applications of Photovoltaic, Wind-Electric, and Fuel-Cell Systems", ", *IEEE Transactions on Power Delivery*, Vol. 10, No. 4, October 1995, pp. 1920-1926.

[90] W. Shireen and M.S. Arefeen, “An Utility Interactive Power Electronics Interface for Alternate/Renewable Energy Systems”, ”, *IEEE Transactions on Energy Conversion*, Vol. 11, No. 3, September 1996, pp. 643-648.

[91] A.J. Appleby, Fuel Cells: Trends in Research and Applications, Hemisphere Publishing Corporation, 1987.

APPENDIX. A

CO_2 EMISSIONS FROM CONVENTIONAL FOSSIL FUEL POWER PLANTS

CO_2 emission rates in terms of $kgCO_2/MWh$ for three conventional fossil fuel (coal, oil, and natural gas) power plants during their operations are computed. The following reactions may represent the complete combustion of fossil fuel at power plants.

$$C + O_2 \rightarrow CO_2 + \Delta \qquad \text{(A.1)}$$

$$\text{or} \quad CH_4 + 2O_2 \rightarrow CO_2 + 2H_2O + \Delta \qquad \text{(A.2)}$$

where Δ represents heat evolved. The CO_2 emissions shown in Equation (A.1) - (A.2) are considered as an undesirable side effect of burning fossil fuel to get useful energy.

For the CO_2 emission rate of coal combustion, Appalachian bituminous coal with 72% carbon content and 12,600 Btu/lb (29.347×10^9 J/ton) of heating value is taken as a representative. The CO_2 emission rate for complete combustion of the coal is computed as

$$\frac{0.72 \times 10^3 kgC}{29.347 \times 10^9 J} = 24.534 kgC / 10^9 J = 323.823 kgCO_2 / MWh$$

When the power plant has a 34% of electricity conversion efficiency, the CO_2 release rate would be 952.42 $kgCO_2/MWh$.

An emission rate for crude oil can be calculated from its composition, heating value, and efficiency of a power plant. The United Nations uses 1.4543 ton of coal equivalent to define a ton of oil equivalent and average crude oil is characterized as having $85.0 \pm 1.0\%$ carbon content. The CO_2 emission rate for complete combustion of crude oil is computed as follows

$$\frac{0.85\times10^{3}\,kgC}{1.4543\times29.347\times10^{9}\,J}=19.916\,kgC/10^{9}\,J=262.87\,kgCO_2/\,MWh$$

Then assuming 37% of electricity conversion efficiency, the CO_2 release rate would be 710.46 $kgCO_2$/MWh.

When natural gas is roughly assumed to contain 100% methane (CH_4), whose heating value is 23,861 Btu/lb (55.5756x10^9 J/ton), the CO_2 emission rate for methane is calculated as

$$\frac{0.75\times10^{3}\,kgC}{55.5756\times10^{9}\,J}=13.50\,kgC/10^{9}\,J$$

However, the average natural gas used in power plants contains 92.88% methane, 3.91% ethane (C_2H_6), a small amount of propane (C_3H_8) and other non-hydrocarbon gases, for a heating value of 9103 kcal/m^3. Considering the kinds of variability, the relation between carbon content and heating value of natural gas is approximated by the following equation

$$kgC/10^9J = 13.71 + [(kcal/m^3) \times 0.1124 - 1000] \times 3.083\times10^{-3}$$

For the average natural gas, this value is 13.78 kgC/10^9J (181.88 kg CO_2/MWh). Taking 39% as the efficiency of the natural gas power plant, the CO_2 emission rate would be 466.36 $kgCO_2$/MWh.

On the other hand, before each fuel is combusted at power plants, it is required to be processed at a fuel treatment stage. The fuel treatment processes usually consist of mining, transportation and refining of fossil fuel. Taking the CO_2 generation from the fuel treatment into account, Table A.1 summarizes the overall CO_2 emissions of the three fossil fuel power plants.

Table A.1 CO_2 productions from fossil fuel power plants with fuel treatment.

Fuel type	Power plant operation [$kgCO_2/MWh$]	Fuel treatment [$kgCO_2/MWh$]	Overall CO_2 production [$kgCO_2/MWh$]
Coal	952.42	35	987.42
Oil	710.46	28	738.46
Natural gas	466.36	85	551.36

APPENDIX. B

CO_2 EMISSIONS FROM PV POWER PLANTS

This section calculates estimates of the CO_2 emissions from both PV module fabrication and construction of the PV power plant, based on consumed energy analysis.

Accumulated energy requirements for construction of PV power plants are shown in Table B.1 [16]. The energy consumed for the photovoltaic modules and that for the remaining components such as supporting structures, cabling, power conditioning system, etc. constitute the accumulated energy for a PV power plant. The percentages by which electrical energy and raw fuel take charge out of the total energy consumption are 68.2% and 28.8%, respectively.

Table B.1 Accumulated energy requirements for PV power plants [16].

Cell structure	η [%]	PV Modules [kWh/kW_p]	Remaining components [kWh/kW_p]	Power station total [kWh/kW_p]
Single-crystalline	15.5	11,000	1,200	12,200
Poly-crystalline	13.5	7,500	1,500	9,000
Amorphous	8.0	5,500	2,000	7,500

- Size of power station = 1,500 kW_p
- Annual production capacity = 25 MW_p/yr

CO_2 emissions, involved in the construction process of the PV power plant by the consumption of electricity and fuels, can be estimated using the specific emission factors within an energy supply network. For the United States, 0.5984 kg/kWh for electrical energy and 0.48 kg/kWh for fossil fuels are calculated for their CO_2 emission factors. These calculations are based on the data that the percentage of electricity generated by coal is 54.6%, by oil 3.9%, and by natural gas 11.9%. The emission factors for coal, oil and natural gas power plants are 952.42 kg/MWh, 710.46 kg/MWh, and 466.36 kg/MWh, respectively, as calculated in Appendix A. Table B.2 shows the amount of CO_2 emitted during the construction of the PV power plant and equivalent CO_2 emissions during the system's working life cycle.

Table B.2. CO_2 emissions of PV power plants.

Cell structure	CO_2 emissions [kg CO_2/kW_p]	Equivalent CO_2 emissions [kg CO_2/MWh]
Single-crystalline	6,654.5	110.9
Poly-crystalline	4,909.1	81.8
Amorphous	4090.9	68.2

- Working life cycle = 30 yrs
- Annual load duration = 2,000 hrs

APPENDIX. C

CO_2 EMISSIONS FROM FUEL CELL POWER PLANTS

This section calculates CO_2 emissions during operation of phosphoric acid fuel cell (PAFC) power plants, which use natural gas as a fuel. Because the actual fuel of fuel cell stacks is hydrogen (H_2) gas rather than methane (CH_4), fuel reforming process is required to process CH_4 into H_2.

The fuel reforming system comprises three processes such as desulfurization, steam reforming, and CO shift. The reaction formula for those processes are written as

Steam reforming: $CH_4 + H_2O \rightarrow CO + 3H_2$ (C.1)

CO shift: $CO + H_2O \rightarrow CO_2 + H_2$ (C.2)

$$CH_4 + 2H_2O \rightarrow CO_2 + 4H_2 \quad \text{(C.3)}$$

Therefore, about 80% H_2 and 20% CO_2 are supplied to the fuel cell stacks, assuming the fuel is reformed completely.

When the natural gas contains 100% CH_4 with a heating value of 23,861 Btu/lb, the CO_2 emission rate for fuel cell power plants is calculated as

$$\frac{2.75lb \times 0.95}{23861Btu \times 0.45} = \frac{1.18346kg}{3.1439 \times 10^{-3} MWh} = 376.43kgCO_2 / MWh$$

assuming that the efficiencies of the reforming process and fuel cell power plant are 95% and 45%, respectively.

VITA

Kyoungsoo Ro

He was born on March 27, 1963, in Changnyung, Korea. He obtained his B.S. and M.S. degrees in Electrical Engineering from the Seoul National University, Korea in 1985 and 1987, respectively. He had finished course-works for his Ph.D. study at the Seoul National University in 1990. In the Fall of 1993, he joined the Virginia Polytechnic Institute and State University (Virginia Tech) to pursue his Ph.D. He has worked as a teaching assistant since 1994 and has taught the Power Engineering Laboratory since the Fall of 1995. He is supposed to obtain his doctorate degree on May 9, 1997. His interest areas are power system operation, control and stability, renewable energy systems (photovoltaics, fuel cells and batteries) and applications of artificial intelligence to power systems. He has been a member of Institute of Electrical and Electronics Engineers (IEEE) since 1995.

April 14, 1997